ESCOLA
SUPERIOR
DE SAÚDE
POLITÉCNICO
DO PORTO

M

MESTRADO
DESIGNAÇÃO DO MESTRADO

Proteomic profiling of the B cell immune synapse

Diogo Francisco Martins Cunha

07/2021

ESCOLA
SUPERIOR
DE SAÚDE

Proteomic Profiling of the B cell immune synapse

Author

Diogo Francisco Martins Cunha

Supervisor

Pieta Mattila, PhD (Scientific Supervisor)

Sara Hernández Pérez, MSc (Scientific Supervisor)

Mónica Vieira, PhD (Institutional Supervisor)

Dissertation presented to fulfil the necessary requirements to obtain the Master's degree in **Biochemistry in Health – Clinical and Metabolic Biochemistry** by the Escola Superior de Saúde do Instituto Politécnico do Porto.

This research work was only possible with the support of Erasmus+, which funded my internship abroad, Sigrid Juselius Foundation, with a grant for a partial period of my internship, and the Finnish National Agency for Education with another grant for continuing my master internship.

Agradecimentos

Era o sonho de menino, um dia, vestir uma bata branca e ajudar pessoas. Uma viagem com tantas aventuras e experiências que nunca deixaram desvanecer o sentimento, o entusiamo e emoção que esse menino sentia sempre que colocava uma bata. Devo esta dissertação a esse menino que sonhou e trabalhou para concretizar os seus objectivos.

Ao longo da realização da dissertação e de todo o meu percurso académico tive a sorte de contar com o apoio incondicional de várias pessoas e instituições que estarei para sempre eternamente grato.

À Doutora Pieta Mattila, orientadora da minha dissertação, deixo a maior palavra de agradecimento. As palavras não chegam para expressar todo o apoio e confiança depositada em mim ao longo deste ciclo, e espero que um dia seja merecedor da mesma. Muito obrigado pela orientação, pela confiança e por me impulsionar a ser sempre a melhor versão de mim mesmo.

À Sara Hernández-Pérez, co-orientadora da minha dissertação, por toda a ajuda, dedicação e empenho com que me orientou durante a dissertação, um eterno obrigado. Posso dizer que se um dia for um investigador como tu és e ensinaste a ser, serei uma pessoa realizada.

A todo o grupo "Lymphocyte Cytoskeleton Group", pela partilha, auxílio e acolhimento fazendo com que nunca me sentisse sozinho.

À instituição, Escola Superior de Saúde e todo o corpo docente, em especial destaque para a Professora Doutora Mónica Vieira e Professor Doutor Ricardo Ferraz, que sempre estiveram presentes e disponíveis no que fosse preciso.

À minha família, agradeço por tudo o que sou. Ao meu pai, Manuel Cunha e à minha mãe Maria Cunha por nunca me ter faltado nada. Fui um mimado e por vezes não vos soube dar o devido valor. Obrigado por nunca terem desistido de mim e espero que um dia consiga ser tão bom para os meus como vocês foram para mim. Ao meu avô Manuel Cunha e avós Helena e Maria Fernanda, que sempre cuidaram de mim e me educaram na pessoa que sou hoje. Espero que sintam orgulho em mim.

Finalmente, à Beatriz, Miguel, Marco, Bárbara, Joana, Maria, Ricardo, Sandra e a todos os meus amigos e conhecidos que me acompanharam nesta viagem e a tornaram inesquecível. Estou certo de que ainda teremos muito mais episódios pela frente!

Muito Obrigado a todos!

Resumo

O sistema imunitário é responsável por eliminar potenciais organismos tóxicos e perigosos. Mais ainda, tem como função evitar respostas auto-imunes que ponham em risco a integridade dos tecidos humanos. As características inerentes das células do sistema imunitário, medeiam a resposta imune adequando-a a cada situação específica.

Linfócitos B, ou células B, são consideradas uma parte fulcral da resposta imune adaptativa. Estas ao reconhecer os antigénios presentes nos microorganismos, conseguem activar e diferenciar em plasmócitos havendo produção e libertação de anticorpos contra os antigénios reconhecidos. Em última instância, conduz à opsonização e destruição dos microorganismos e toxinas. Para que o reconhecimento de antigénios seja possível, as células B estão equipadas com os receptores de células B. Estes ao ligarem-se aos antigénios desencadeiam uma variedade de vias de sinalização responsáveis por vários processos celulares como internalização do antigénio e reorganização do citoesqueleto de actina. Apesar da elevada importância destas células na resposta imunitária, ainda muito se desconhece sobre as proteínas envolvidas na regulação das vias de sinalização dos receptores das células B e a sua associação com outros processos biológicos e metabólicos.

Com isto em mente, o objectivo desta tese é estabelecer um método que permita isolar as proteínas recrutadas para o local onde ocorre a sinapse imunológica. Por análise de espectrofotometria de massa, poderá ser possível identificar proteínas que estejam a actuar na regulação da sinapse imunológica, e de uma forma mais geral, na resposta imune.

Palavras-chave: sistema imunitário; sinapse imunológica; células B; activação do receptor de células B; espectrometria de massa

Abstract

The immune system is responsible for eliminating threatening organisms and toxins, as well as for avoiding autoimmune responses that could be potentially harmful to the human tissues. Through special features of the immune cells, which can detect a massive variety of structures specific to pathogens, the immune system can mediate the adequate response to each specific situation.

B cells are considered focal elements of the adaptative immune response since the recognition of pathogen's antigens, and consequently activation and differentiation of B cells, results in the capture and elimination of the hazardous microbes and toxins. In order to successfully recognize potential threats, B cells are equipped with B cell receptors or BCRs. Antigen binding to the BCRs triggers an enormous number of downstream events in the cells, orchestrating numerous processes such as antigen internalization and actin reorganization.

Despite the importance of B cell responses for the immune system, many molecular players behind the regulation of the BCR signalling complexes and its interplay with other cellular processes such as antigen internalization and cytoskeletal rearrangements are still unknown or poorly understood.

Therefore, this work aims to set up and optimize a new pull-down method for the isolation of proteins recruited to the immune synapse site following BCR activation. Mass spectrometry (MS) protein analysis will reveal potential candidates to regulate the immunological synapse formation and, ultimately, the immune response.

Keywords: immune system; immune synapse; B cells; BCR proteome; BCR activation; mass spectrometry

Index

List of abbreviations

ACN – acetonitrile

ADP – adenosine diphosphate

AF488 – AlexaFluor 488

AF546 – AlexaFluor 546

APC – allophycocyanin

APC – antigen-presenting cell

ATP – adenosine triphosphate

BCAP – B cell adaptor for PI3K

BCR – B cell receptor

BLNK – B cell linker

BS3 - bis(sulfosuccinimidyl)suberate

BSA – bovine serum albumin

Btk – Bruton's tyrosine kinase

CIOM – conformation-induced oligomerization model

CSK – cytoskeletal buffer

cSMAC – central supramolecular activation cluster

DAG – diacylglycerol

DAPI - 4',6-Diamidino-2-Phenylindole, Dihydrochloride

DAVID - database for annotation, visualization and integrated discovery

DDA - data-dependent acquisition method

DTBP – Di-*tert*-butyl peroxide

DTT –dithiothreitol

EDTA - ethylenediaminetetraacetic acid

ERK1/2 – extracellular signal-regulated kinases 1 and 2

ESI – electrospray ionization

Fc region - fragment crystallizable region

GFP – green fluorescent protein

Grb2 – growth factor receptor-bound protein 2

HBsAg – hepatitis B surface antigen

HCOOH – formic acid

HCV – hepatitis C virus

HIV – human immunodeficiency virus

HPLC – high-performance liquid chromatography

HRP – horseradish peroxidase

IAA – iodoacetamide

Ig – immunoglobulin

IP3 – inositol 1,4,5-trisphosphate

IQGAP1 – IQ Motif Containing GTPase Activating Protein 1

IS – immune synapse

ITAM – immunoreceptor tyrosine-based activation motif

LC – liquid chromatography

LC-MS – liquid chromatography – mass spectrometry

m/z – mass over charge

MAPK – mitogen-activated protein kinase

MAPKK – mitogen-activated protein kinase kinase

MHCII – major histocompatibility complex class II

mIg – membrane-bound immunoglobulin

MS – mass spectrometry

MS/MS – tandem MS analysis

MTOC – microtubule-organizing centre

NH_4HCO_3 - ammonium bicarbonate

NK cell – natural killer cell

PAMP – pathogen-associated molecular pattern

PBMC - peripheral blood mononuclear cells

PBS - phosphate-buffered saline

PFA – paraformaldehyde

PI3K – phosphoinositide 3-kinase

PIP2 – phosphatidylinositol 4,5-bisphosphate

PIP3 – phosphatidylinositol (3,4,5)-trisphosphate

PLC-γ2 – phosphoinositide phospholipase C

PPR – pattern recognition receptor

pSMAC – peripheral supramolecular activation cluster

PTM - post-translational modifications

PVDF – polyvinylidene fluoride

RFP – red fluorescent protein

RT – room temperature

SA – surrogate antigen

SILAC – stable isotope labelling by amino acids

SPPLAT – selective proteomic proximity labelling using tyramide

Syk – spleen tyrosine kinase

TBS – tris-buffered saline

TCR – T cell receptor

TfR – transferrin receptor protein 1

Th cell – T helper cell

WASP – Wiskott Aldrich Syndrome protein

WB – western blot

WCL – whole cell lysate

Index of tables

Index of figures

1. Introduction

1.1. The innate and adaptive immunity

The immune system is a deep and intertwined network of biological processes, cells, soluble factors, and other chemicals working towards one common goal: protecting the host against various pathogens, such as microbes and viruses, toxins and even cancer cells. The immune system features two lines of defence – the innate immunity and the adaptive immunity. These two responses complement each other and provide the balance needed for an appropriate

immune response (Chaplin, 2010; Marshall et al., 2018). Innate immunity is an antigen-independent (non-specific) defence mechanism responsible for a fast and wide response to pathogen infection, buying time for a more precise and effective response. Innate strategies include anatomic and physiological barriers (skin and mucous membranes, inflammation, low stomach pH, lysozymes in tears and saliva), the innate immune cells: neutrophils, macrophages, basophils, dendritic cells, eosinophils, mast cells, monocytes, natural killer (NK) cells and the complement system that targets pathogens for destruction (Burrell et al., 2017; Chaplin, 2010; Gasteiger et al., 2017; Marshall et al., 2018; Turvey et al., 2009). Pattern recognition receptors (PPR) belong to a family of receptors that survey molecules intrinsically linked to pathogens, called pathogen-associated molecular patterns (PAMP). These receptors can be found both inside and outside of phagocytic cells or NK cells, and are regarded as mediators of the innate response (Amarante-Mendes et al., 2018; Mogensen, 2009). Although the innate response is fast, it is not durable and specific (Marshall et al., 2018; Warrington et al., 2011).

The adaptive response is a more complex and delayed response allowing the host to obtain immunological memory to a specific antigen so that, in a later exposure, the host can mount a rapid and efficient immune response. T lymphocytes and B lymphocytes are the central part of the adaptive responses, organizing the cell-mediated immune response and the humoral immune response, respectively (Alberts et al., 2002; Nicholson, 2016; Varadé et al., 2020). The immune response recruits a variety of lymphocytes subsets towards the pin-pointed stimulus. Upon activation, T cells start multiplying and differentiate in four different T cell main subsets targeting the pathogens or infected cells: helper T cells, memory T cells, regulatory T cells and cytotoxic T cells. On the other hand, B cells proliferate and differentiate into two main subsets: plasma B cells, responsible for antibody production, or memory B cells, that ensure immunological memory (Chaplin, 2010; Freitas et al., 2000; LaRosa et al., 2008).

1.2. The role of B lymphocytes

Among the different lymphocytes, B lymphocytes assume important functions in the production of high-specificity antibodies that can neutralize toxins and target infected cells for destruction (Carrasco, 2020; Kuokkanen et al., 2015). Moreover, B cells play vital roles in discriminating harmful pathogens from self and vaccines production for diseases prevention (Gonzalez et al., 2011; Siegrist et al., 2009). Notwithstanding, B cells and T cells developmental miscues may result in extremely harmful ailments for the host, such as autoimmune diseases, immunodeficiencies or cancer (Vale et al., 2010).

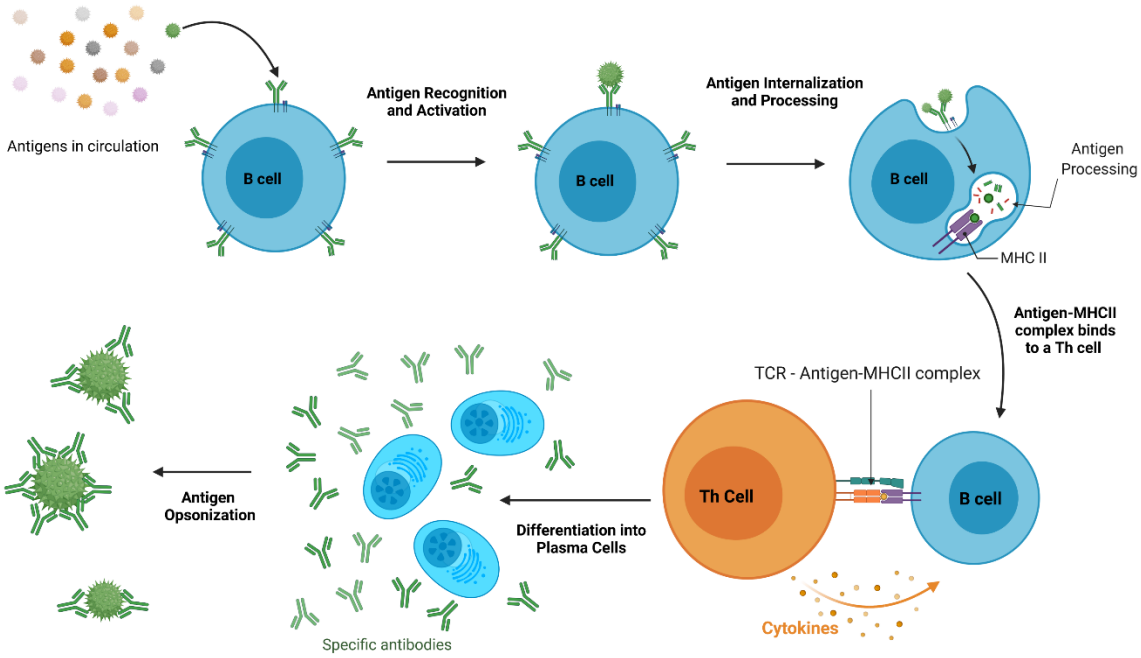

Figure 1. B cell activation and specific antibody output. Distinct antigens circulate throughout the body. When an antigen encounters a matching BCR, it triggers B cell activation. This leads to antigen-BCR internalization followed by antigen processing. The peptide-MHCII complex is presented on the cell surface to Th cells. The formation of the T cell receptor-MHCII-antigen peptide complex coupled with CD40 signalling triggers cytokines secretion that ultimately helps B cells to develop and mature into antibody-producing plasma cells. Secreted antibodies will then bind to antigens in order to start opsonization.

B cells are able to recognize and bind specific antigens, triggering intracellular signalling cascades that result in cell activation and differentiation into antibody-secreting plasma cells (Figure 1) or memory cells. Immunoglobulins (Ig) participate in the immune response as soluble antibodies or as part of the BCR. On one hand, soluble secreted antibodies bind to antigens in a process called opsonization, targeting these pathogens for phagocytosis or complement-directed destruction. On the other hand, the BCR binds to the soluble or presented antigen, starting internalization and processing. This process concludes with the presentation of the

peptide-MHCII (major histocompatibility complex class II) complex on the B cell plasma membrane, and successful presentation will lead to T helper cell (Th cell) activation, which will improve the humoral response (Marshall et al., 2018; Nicholson, 2016).

1.2.1. Structure of BCR

B cell receptor, or BCR, is a transmembrane protein composed of two parts: the correspondent membrane-bound Ig (mIg) that recognises the antigen and the CD79a/CD79b (Igα/Igβ) heterodimer. Igs are a Y-shaped protein complex with a heterotetrameric quaternary structure consisting of two identical heavy chains and two identical light chains. The variable regions of both light and heavy chains are regions susceptible of somatic recombination, or rearrangement, originating a large and diverse repertoire of antibody molecules, theoretically recognizing every single possible antigen. In addition, due to somatic hypermutation during the germinal centre reaction, expressed proteins in the variable region are even more diverse and display higher affinity and specificity to encountered antibodies (Feng et al., 2020; Wang, 2020). The mIg is divided into three distinct domains: an extracellular domain, a transmembrane domain and a cytoplasmic domain. The Ig membrane anchorage is provided by the C-terminal ends of the heavy chains. The mIg associates non-covalently with the transmembrane CD79a/CD79b heterodimer, assembling the fully functional BCR complex. The CD79a/CD79b heterodimer contains a conserved cytoplasmic domain containing several immunoreceptor tyrosine-based activation motif (ITAM) (Figure 2). ITAMs are phosphorylated by tyrosine-kinase family proteins ensuring the initiation of B-cell signalling cascade events (Feng et al., 2020; Friess et al., 2018; Wang, 2020). After B cell maturation and differentiation into plasma cells, the antibodies produced and secreted are almost identical to the BCRs that first encountered and interacted with that unique antigen. BCRs differ from the secreted antibodies by possessing a tail in C-terminal region of the heavy chains that crosses through the membrane and CD79a/CD79b signalling complex (Alberts et al., 2002; Goding, 1996).

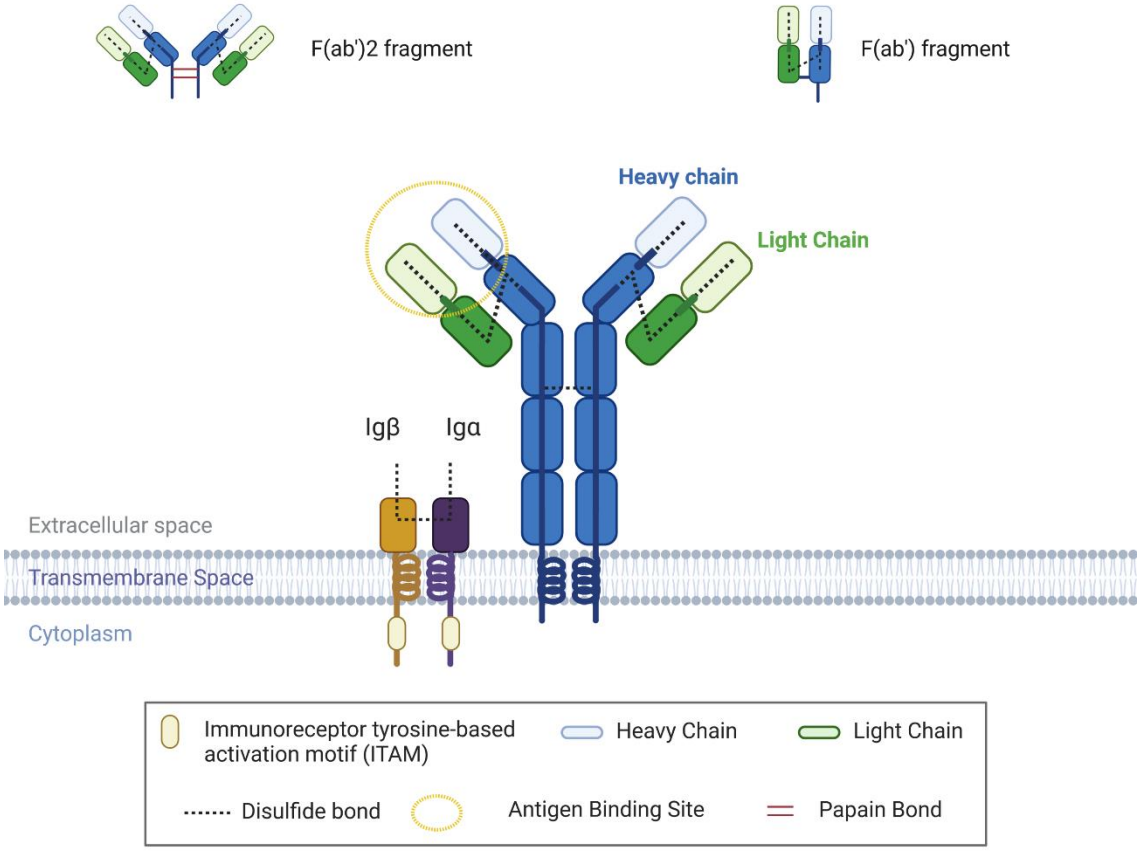

Figure 2. B cell receptor (BCR) structure. BCR is composed of a mIg associated with the CD79a/CD79b (Igα/Igβ) heterodimer. The mIg is composed of two identical heavy chains and two identical light chains. Igα/Igβ heterodimer comprises a cytoplasmatic domain containing a immunoreceptor tyrosine-based activation motif (ITAM) that enables the initiation of b cell signalling cascades. Heavy Chains are represented in shades of blue (darker for the constant region and lighter for the variable region). Light chains are represented in shades of green (darker for the constant region and lighter for the variable region).

1.2.2. BCR and the immune synapse

Classical *in vitro* studies (Lanzavecchia, 1987; Melchers et al., 1983; Batista et al., 1998) report that BCR signalling is triggered by the recognition of soluble antigens. However, later studies acknowledge a different and more prominent *in vivo* form of activation by antigens bound to the surface of the antigen-presenting cells (APCs), such as dendritic cells, follicular dendritic cells and macrophages, in the secondary lymphoid tissues. The recognition of the antigen in surface-bound form has been shown to lower the threshold for B cell activation, and it is emerging as the most typical form of antigen encounter *in vivo* (Batista et al., 2001; Carrasco et al., 2007).

The interaction between the APC-bound antigen and the BCR results in the formation of an activation platform, a specific cell-cell interaction structure named immune synapse (IS) (Batista et al., 2009). The IS is a site for both recognition and internalization of the antigen as well as a

starting point of the cascade that leads to processing, maturation and loading of antigens to MHCII for their presentation on the surface of B cells to activate and receive help from their T cell counterparts (Batista et al., 2009; Shaheen et al., 2019). It has been suggested that, even though these two separate functions ensue simultaneously, each BCR molecule can only perform one of the two: B cell signalling or antigen endocytosis (Avalos et al., 2014; Hou et al., 2006). The pathway each BCR follows could be determined by the crosslinking potential of the antigen (Caballero et al., 2006; Drake, 2018; Putnam et al., 2003).

1.2.3. BCR signalling pathways

APC-bound antigen coupling to the extracellular region of BCR triggers signalling pathways and antigen internalisation, relaying on a conformational change in the cytoplasmic domain of the CD79a/CD79b heterodimer from a closed to an open conformation position, thus allowing access for ITAMs phosphorylation (Hae et al., 2008; Kuokkanen et al., 2015). The tyrosine residues of the ITAMs are then phosphorylated by the Src-family tyrosine kinase Lyn (DeFranco, 1997), leading to the recruitment of other kinases and mediators (Dykstra et al., 2003; Sohn et al., 2008). A vital recruited kinase is the spleen tyrosine kinase (Syk) which, in turn, is phosphorylated and activated by the ITAMs. Syk/BCR complex is main the mediator of the signalling cascade and controls the three main signalling pathways: Phosphoinositide phospholipase C (PLC-ɣ2), Phosphoinositide 3-kinase (PI3K) and mitogen-activated protein kinase (MAPK) pathway (Geahlen, 2009).

PLC- ɣ2 pathway: In the PLC- ɣ2 pathway, Syk recruits B cell linker (BLNK), PLC-ɣ2. Growth factor receptor-bound protein 2 (Grb2) and Bruton's tyrosine kinase (Btk) are organised in a multiprotein complex that is sequentially phosphorylated to activate phosphatidylinositol 4,5-bisphosphate (PIP2). PIP2 produces diacylglycerol (DAG) and inositol 1,4,5-trisphosphate (IP3). IP3 is essential for releasing intracellular Ca^{2+} stores and the entry of extracellular Ca^{2+}, resulting in calmodulin and calcineurin activation. Lastly, Ca^{2+} influx allows NFAT activation, which leads to nuclear translocation and transcriptional activation. DAG is essential for NF-κB dimer production and translocation to nuclear and transcripts targeting genes (Baba et al., 2015; Kurosaki et al., 2000) In sum, in PLC- ɣ2 pathway, second messengers critical for calcium influx and protein kinase C activation are recruited that, ultimately, lead to the transcription of genes related to proliferation and survival (Figure 3) .

PI3K pathway: Recruitment of the co-receptor CD19 and B cell adaptor for PI3K (BCAP) enhances BCR activation, and are crucial for the PI3K pathway activation (Kurosaki, 2011). Both

BCAP and CD19 phosphorylation recruit the phosphorylated Rac1 and Vav complex in order to activate PI3K. These proteins are phosphorylated by the BLNK-Grb2 complex. Activated PI3K can phosphorylate PIP2 to phosphatidylinositol (3,4,5)-trisphosphate (PIP3). PIP3 recruits Akt to the membrane, where PI3K/PIP3 activates Akt signalling. Hence, it translocates to the nucleus, where activates transcription factors involved in cell survival. Moreover, PIP3 recruits BTK to the membrane to activate Wiskott Aldrich Syndrome protein (WASP), an actin nucleation promoting factor essential for B cell spreading and microcluster formation during B cell activation (Figure 3) (Nunes-Santos et al., 2019; Okkenhaug et al., 2015).

MAPK pathway: In the MAPK pathway, DAG produced via PLC- ɣ2 pathway, indirectly phosphorylates and activates mitogen-activated protein kinase kinase (MAPKK) and extracellular signal-regulated kinases 1 and 2 (ERK1/2) through Ras GTPase activation. Activated ERK-proteins are responsible for the nuclear translocation and activation of transcription factors mediating cell proliferation and differentiation, metabolic reprogramming and survival after antigen recognition (Figure 3) (Hamoudi et al., 2010; Yasuda, 2015). The signalling proteins recruited will modulate the gene expression to produce functional antibodies capable of recognizing the foreign antigen.

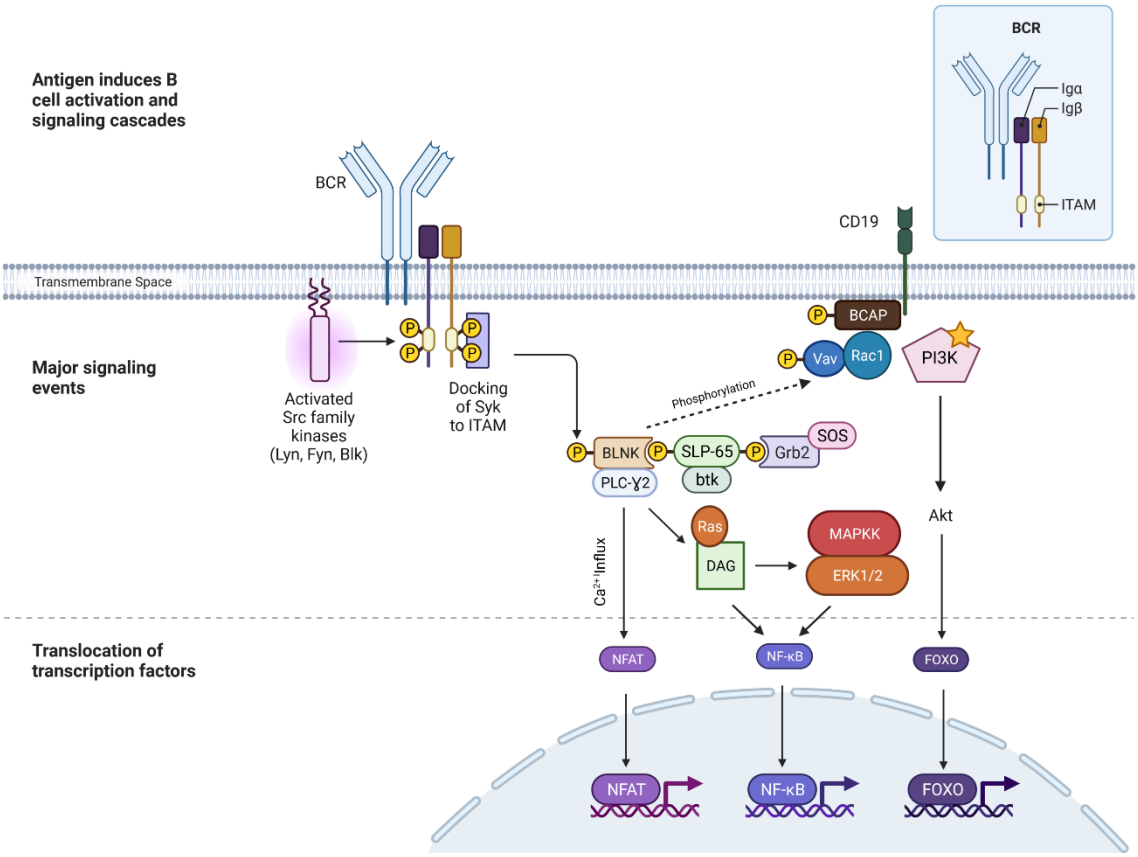

Figure 3. BCR downstream signalling pathways. Three major signalling pathways are triggered following BCR activation: PLC-γ2, PI3K and MAPK pathways. All pathways are in tight cooperation in order to translocate and activate transcription factors vital for cell proliferation and differentiation, metabolic reprogramming and survival after antigen recognition.

1.2.4. BCR mobility upon antigen presentation

The formation of the IS is orchestrated by a spatial reorganization of the BCR and membrane-bound antigen where BCR molecules need to be in close proximity. The radius of BCR clusters is estimated to be around 70 nm (Figure 4A) (Mattila et al., 2013; Mattila et al., 2016). The formation of the IS is a two-phase process. The first phase, or spreading phase, involves the spreading of the B cell onto the APC membrane in order to scavenge and assemble more BCR-antigen complexes (Figure 4B). The second phase, or contraction phase, involves the contraction of the cell, assembling the BCR-antigen complexes in one supracluster (Figure 4C). The spreading phase lasts a few minutes, matching with an increase in BCR mobility due to the disruption of the cortical actin cytoskeleton.

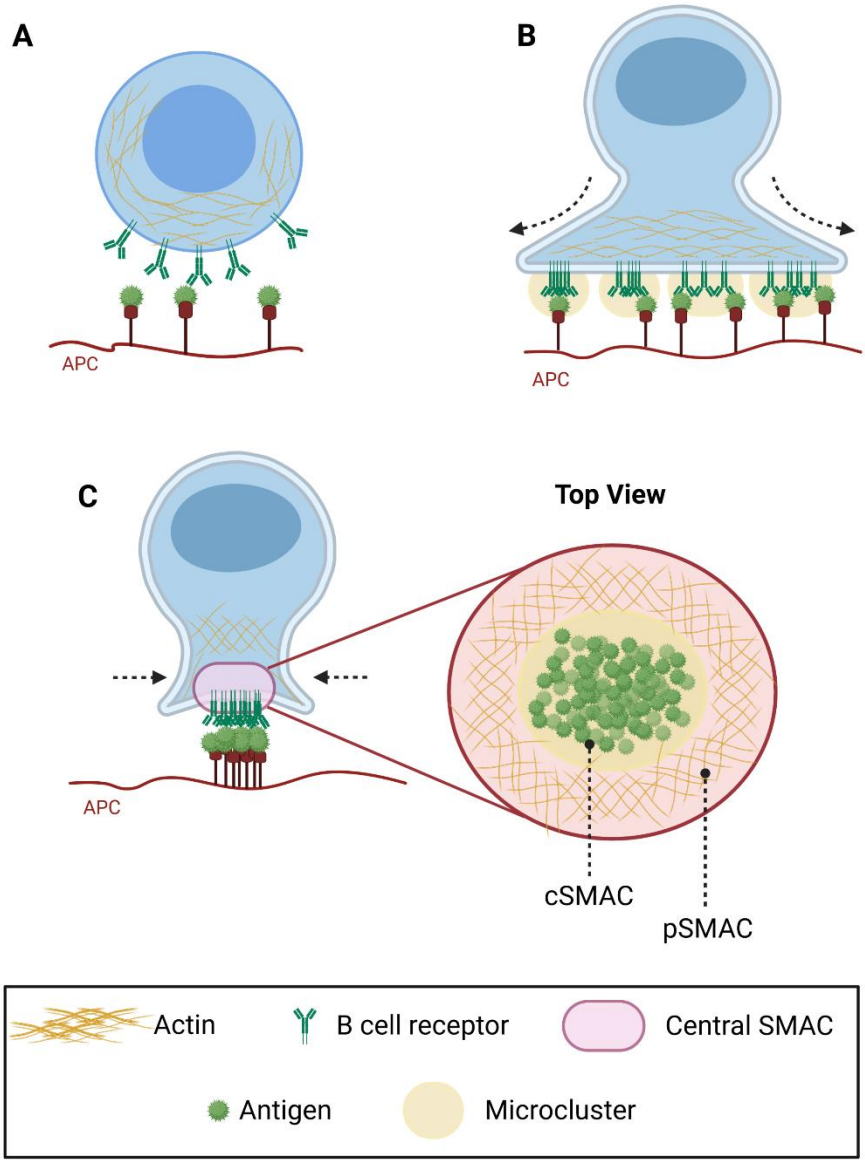

Figure 4. B cell immune synapse formation. (A) APC membrane-bound antigen encounters matching BCR and triggers activation. (B) Initialization of activation drives B cell spreading phase over the APC in search of more antigens. At the same time, BCR-antigen microclusters are being formed. (C) After synapse maturation, the cell begins the contraction phase to gather all microclusters in one big central cluster, cSMAC. A top view scheme of the IS is provided for better tracking of biological changes.

BCR mobility coupled with alterations in the actin cytoskeleton allows the combination of the BCR nanoclusters into microclusters in the membrane surface, which are considered signalling hotspots (Fleire et al., 2006; Mattila et al., 2016; Tolar et al., 2005). At the same time, while more and more BCR cluster, the microclusters continue to grow, and a contraction phase begins as the microclusters migrate to the centre of the IS. The mature synapse can be divided into the antigen-rich central supramolecular activation cluster (cSMAC) and the surrounding actin and adhesion

molecule-rich peripheral supramolecular activation cluster (pSMAC) (Carrasco et al., 2004)(Figure 4C). Another essential feature of the BCR-antigen complex is that the nature of the antigen - different affinity, avidity, structure or composition - can influence the B cell activation. Studies have stated that, not only B cells have a higher sensitivity to bound antigens in presenting cells, but also to particles with a higher density of antigenic epitopes. This feature seems even more important than the affinity of each epitope. Nonetheless, the affinity of the antigen influences the threshold for BCR activation (Batista et al., 2000; Fleire et al., 2006).

It becomes of the utmost importance to understand the organization of the BCR in the cell membrane in a transition from an inactive state to a signalling state as it may shed some light on the molecular mechanisms underlying BCR activation.

1.2.5. Models for BCR activation

Currently, three main models have been proposed to explain the organization of BCR in the cell membrane before and after the ligand is bound: the crosslinking model, the dissociation model and the conformation-induced oligomerization model (CIOM).

The crosslinking model first presented by Worthis and colleagues, postulates that receptors exist as monomers in the resting state. Immediately BCRs crosslink with multivalent antigens, it triggers the formation of microclusters (Figure 5A)(Liu et al., 2010; Tolar et al., 2005; Wortis et al., 1995). The model does not come without flaws, as several researchers pointed out inaccurate experimental results and the only confirmation coming with soluble antigens. The model does not offer molecular answers to how activation proceeds when BCR clusters are still observed in unstimulated cells or, different sized antigens are able to crosslink the BCR into a configuration that would allow the cytoplasmic domain to be in close proximity (Treanor, 2012; Yang et al., 2010).

In light of these limitation, a new model called the dissociation activation model was proposed by Reth and associates. This model postulates that majority of unstimulated receptors exist in auto-inhibitory oligomers. Upon antigen binding, a conformational change is responsible for separating these oligomers and creating access to the ITAM regions, hence allowing BCR activation and recruitment of signalling molecules (Figure 5B). This model displays some limitations as the techniques used cannot distinguish between dimers and higher order oligomers or does not provide information on how large or dynamic BCR structures are. (Schamel et al., 2000; Tolar et al., 2010; Yang et al., 2010).

The CIOM proposed by Tolar and colleagues presents similarities with the crosslinking activation model as states BCRs exist as monomers in the cell surface. Once antigen binds to the BCR, it promotes a conformational unmasking of the clustering interface in the Cμ4 domain, thus allowing signalization. Albeit, the conformational changes suggested have still to be confirmed by structural studies of the fragment crystallizable region (Fc region) of IgM (Figure 5C) (Tolar et al., 2009; Treanor, 2012; Treanor et al., 2010).

1.2.6. BCR clusters diffusion during BCR activation

The formation of the signalosomes and their displacement along the membrane to a central supracluster is not entirely understood, although advances in super-resolution microscopy have started to elucidate the mechanisms and molecules operating in the spatiotemporal dynamics of BCR activation (Castro et al., 2019; Li et al., 2019; Mattila et al., 2013, 2016; Treanor et al., 2010; Schnyder et al., 2011).

BCR cannot diffuse freely on the membrane surface. Instead, they are restricted in nanoclusters with a radius ranging around 70 nm (Mattila et al., 2013). In the resting state, the average diffusion coefficient of BCR (IgM isotype) is slow. Even more, in the resting state, IgM and IgD BCRs are segregated in different clusters and, IgD nanoclusters are higher in number and density of molecules (Mattila et al., 2016; Maity et al., 2015). Upon membrane-bound antigen encounter, BCR nanoclusters tend to merge in order to form signalling microclusters (Lee et al., 2017; Liu et al., 2010).

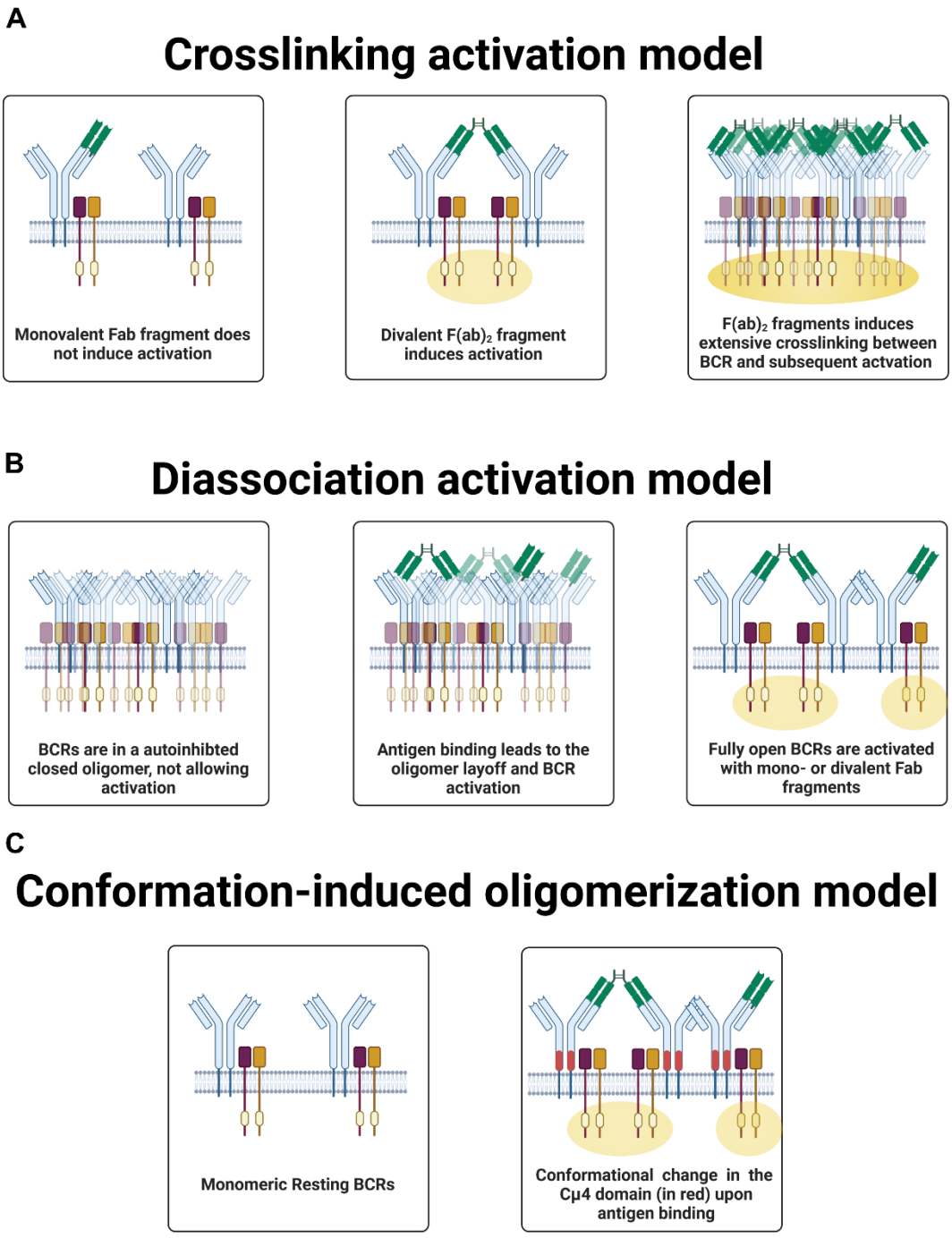

Figure 5. Different models for BCR activation. (A) Crosslinking Activation model postulates monovalent antigen, or surrogate antigen monovalent F(ab'), cannot induce BCR activation. For BCR activation, divalent Fab, $F(ab')_2$ has to crosslink BCR molecules, and signalling is as strong as the more extensive the crosslinking is. (B) Disassociation Activation Model postulates BCR molecules exist as an auto-inhibitory oligomer that can loosen up if the antigen is present. After BCR opening, it can be further activated by mono- or divalent antigen or Fab fragments. (C) BCRs are presented as monomers in the membrane with a closed conformation. Upon antigen binding, a force induces a conformational change in the Cμ4 domain of the BCR exposing the cytoplasmic domains for internal signalling.

Moreover, BCR diffusion increases, leading to collisions between BCRs (Tolar et al., 2009; Treanor et al., 2011). The result is the arrangement of microclusters, which can be IgM or IgD-only or with both isotypes (Mattila et al., 2013, 2016) At the same time that BCR microclusters form and translocate to the centre of the contact area (Fleire et al., 2006), B cell spreads on the antigen-associated membrane (Hae et al., 2008). Following along the contraction phase, cSMAC is established, BCR diffusion coefficient regresses to the levels before activation and the synapse maturation takes place (Treanor et al., 2011).

BCR activation is an exceptionally dynamic and complex process that needs strict coordination between receptors, co-receptors, membrane lipids. The actin cytoskeleton is responsible for adjusting the membrane diffusion landscape and regulating BCR – co-receptor dynamics and the respective signalling (Mattila et al., 2013; Treanor et al., 2010).

1.3. The actin cytoskeleton

The cytoskeleton was first discovered around the 1970s and 1980s, and it was thought to be present only in eukaryotes. It was not until 1992 that its existence was also discovered in prokaryotic organisms (Bork et al., 1992; Erickson, 2007; Wickstead et al., 2011). The actin cytoskeleton has been a subject of intense research since it engages in biological processes essential for various housekeeping functions of the cell. It enables the cell to maintain a stable shape and internal organization whilst providing the mechanical forces to execute morphological changes, cell movement, or even nucleus relocation when needed. The main polymers of the cytoskeleton are actin filaments, microtubules and intermediate filaments – each with a distinct functional profile depending on the physical and biological properties of their respective filaments (Fletcher et al., 2010).

Actin, a ubiquitous and highly abundant protein, exists in filamentous (F-actin) and monomeric (G-actin) form. The actin filaments are polar and dynamic polymeric structures, that have two structurally and biochemically different ends. The actin filaments are typically associated with the cellular membranes and are enabled to grow and shrink using two robust mechanisms (actin filament treadmill and myosin-based motility), allowing actin to be the central force in cell structural changes, motility, endocytosis and phagocytosis (Blanchoin et al., 2014; Dominguez et al., 2011). The barbed end, also known as the plus end, is where filament assembly occurs, and the filament disassembly occurs and the pointed end, or minus end. The actin assembly or disassembly are affected by the adenosine triphosphate/adenosine diphosphate

(ADP/ATP) status (Narita et al., 2011). The actin filament treadmill is a simple mechanism where the ATP-actin monomers are assembled to the filament barbed end, and through time suffer ATP hydrolysis and Pi release in actin filament. ADP-actin monomers are dissociated from the filament pointed end. The ADP-actin monomer is re-charged through ATP phosphorylation, and as a result, ATP-actin monomers are ready to be assembled again in the barbed end of the actin filaments (Pantaloni et al., 2001; Wiesner et al., 2003). The other recognized mechanism is myosin-based motility. Myosins are composed of a globular motor domain – binding the actin and ATP/ADP – and a neck domain involved in dimerization. Myosin movement along the actin filament is possible through the ATP-hydrolysis and ADP-release in the motor domain. Different classes of myosin will have different assignments: vesicle transport (myosin V), contractility of actin filament structures (myosin II), and movement of actin filaments (myosin VI), for example (Kneussel et al., 2013; Pollard et al., 2009; Strzyz, 2018).

In B lymphocytes, the dominating actin structures are distributed just beneath the plasma membrane as an actin-based cortex. Through dynamic connections to the plasma membrane, actin filaments form a barrier that confines BCRs and restricts their mobility. BCR diffusion is then negatively proportional to the F-actin density in the plasma membrane (Treanor et al., 2010). More precisely, previous studies using high-resolution microscopy techniques revealed that the cooperation between actin and ezrin is responsible for BCRs confinement in nanoscale domains (Gupta et al., 2006; Treanor et al., 2011).

Upon BCR activation through antigen binding, the actin depolymerizes for approximately 10 seconds, allowing BCR diffusion for maximal antigen uptake, activation, and endocytosis (Avalos et al., 2014; Li et al., 2019; Mattila et al., 2016; Tolar, 2017). The disassembly of actin is mediated by cofilin and ezrin-dephosphorylation, the last one inducing dissociation between actin and the plasma membrane. Both free BCRs and antigen-bound BCRs nanoclusters have the respective diffusion restrictions lifted and can interact with each other forming the microclusters (Freeman et al., 2011; Treanor et al., 2010, 2011). Increased BCR mobility also frees the BCR for interaction with its co-receptor CD19 and, thus, initiating signalling pathways. (Gasparrini et al., 2016; Mattila et al., 2013).

Before long, there is actin reassembly in the cell-cell interface, and the myosin-driven action can further promote BCR microclusters formation (Chaudhuri et al., 2011). Even more, branched F-actin starts assembling around this interface (Fleire et al., 2006; Freeman et al., 2011). The development of filopodia and lamellipodia promotes the spreading of B cell into the antigen-

associated membrane of the APC. As B cell continues to expand more, it also promotes microclusters formation at the tip of these actin structures. Later on, microclusters will be pushed towards the cSMAC. The extent of B cell spreading is coherent with antigen nature (Liu et al., 2010) and the spreading allows B cells to capture the maximum antigen possible for a more powerful activation (Fleire et al., 2006). In the early spreading phase, dynein motor protein and IQ Motif Containing GTPase Activating Protein 1 (IQGAP1) link the microtubule-organizing centre (MTOC) to the cytoskeleton, prompting cytoskeleton movement towards the contact area after contraction (Schnyder et al., 2011; Wang et al., 2018).

After B cell spreading phase, the B cell membrane contacting the APC-antigen starts to form a central cluster in a process conducted by actin retrograde flow combined with myosin-mediated actin network contraction. F-actin decreases in the cSMAC surrounding merging BCR microclusters but maintains its levels at the periphery of the contact area (Mattila et al., 2013, 2016; Treanor et al., 2011).

Multiple BCR microclusters, or signalosomes, are formed during B cell spreading, amplifying the BCR signalling. During B cell contraction, BCR microclusters and antigen aggregate in the cSMAC, inhibiting BCR signalling and preparing the mechanisms for antigen internalization (Song et al., 2013; Song et al., 2014).

The complex intermolecular play between the rapidly forming BCR proximal signalling complexes (BCR signalosomes) and the actin cytoskeleton, as well as the other immediate cellular responses occurring at the IS, such as antigen extraction and internalization, remain poorly understood. A better understanding of the IS composition would help to unveil the molecular mechanisms leading to fully mounted immune responses.

1.4. The power of protein mass spectrometry (MS), Proteomics

In the heart of all biological process, proteins are coordinating every step. The group of proteins responsible for controlling the processes within a biological system are termed proteome (Hartwell et al., 1999). In order to study protein characteristics, structure and interactions, many biophysical methods have been used.

MS-based proteomics has surfaced and developed over the years, providing a solid foundation for further investigation into the composition and function of these complex systems. Nowadays, we can identify and quantify proteins attached to beads or in a single gel band slice.

The main reasons behind the success of this approach are tied to high-throughput technology with high sensitivity, specificity and a reasonable dynamic range (Gupta et al., 2007).

1.4.1. MS-based proteomics

Liquid chromatography – mass spectrometry (LC-MS)/MS-based proteomics analysis is designed for different objectives: identifying proteins, looking for post-translation modifications, or studying proteins and their interactions in signalling pathways. In pursuance of the best settings for a specific goal, MS-proteomics can be divided into two approaches: top-down proteomics and bottom-up proteomics (Pitt, 2009).

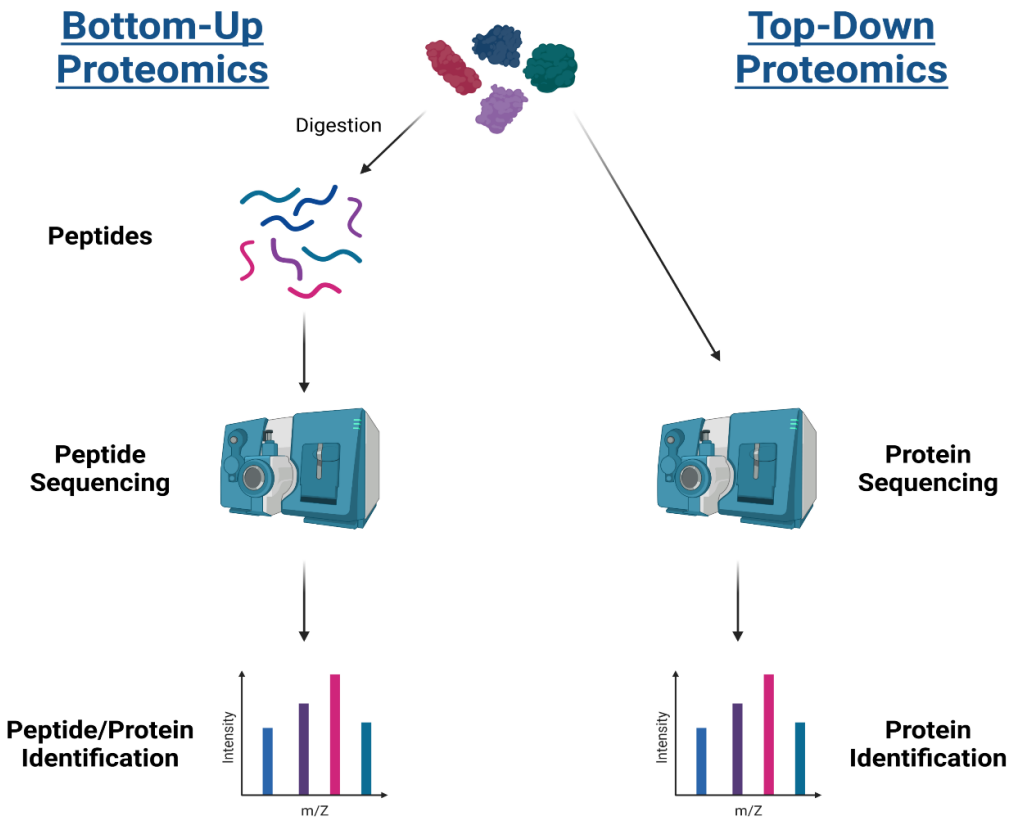

Figure 6. MS-based approaches: bottom-up and top-down proteomics. The bottom-up approach is the MS-based proteomics used. The complex protein mixture is digested, and peptides are sequenced accordingly. The top-down approach allows the user to identify the intact protein fragments and infer about PTMs and even protein structure. The main disadvantage is time consumption.

Bottom-up proteomics, or shotgun proteomics, represents an approach in which a complex protein sample is simplified via gel electrophoresis (Shevchenko et al., 1996) or magnetic beads (Whiteaker et al., 2007). Thereupon, the sample undergoes enzymatic digestion and/or chemical digestion (Gundry et al., 2009; Switzar et al., 2013). The most common methods for digestion are enzymatic ones, more exactly trypsin, that cleaves peptide bonds at the carboxylic terminal of lysine and arginine residues. Generated peptides have a fitting size for MS analysis. To reduce peptide complexity, peptides are loaded onto LC systems, separating peptides based on hydrophobicity. Usually, these LC systems are directly connected to MS systems, where these peptides are scanned and separated by their mass over charge (m/z) ratios. In a complex protein sample, tandem MS analysis (MS/MS) offer higher odds for protein identification. In this step, previously fragmented ions are fragmented again by low energy collision-induced dissociation, allowing separation and identification between ions with similar m/z ratios (Figure 5). (Eng et al., 1994; McDonald et al., 2002; Wolters et al., 2001).

Top-down proteomics allows identifying and sequencing the intact protein fragments with high-throughput quality (Roth et al., 2008). These intact proteins are introduced in the mass spectrometer and are ionized by soft ionization methods, allowing the conservation of labile structural protein characteristics. In this approach, tandem MS analysis is also possible. The main advantages of this method are the availability of sequencing a complete protein, the ability to locate and characterize post-translational modifications (PTM) and the determination of proteins isoforms (structure) (Figure 5). (Catherman et al., 2014; Donnelly et al., 2019; Vinh, 2019).

1.4.2. Proteomics as a gate for BCR activation studies

BCR signalling controls and coordinates a variety of cellular pathways in time and space. To date, several mechanisms and players involved in BCR signalling and regulation, as well as actin reorganization at the IS, have been identified. Notwithstanding, there are still several big open questions, especially regarding cytoskeletal reorganization occurring during BCR activation and the mechanisms leading to antigen internalization and processing.

BCR signalling exerts such a massive influence in shaping the cell dynamics and processes that only a handful of techniques provide a solid approach to capture this complexity. Quantitative mass spectrometry-based proteomics has emerged as one of these techniques. Matsumoto and colleagues provided the first view of tyrosine-phosphorylated proteins in BCR and TCR signalling using immunoaffinity chromatography based on tyrosine proteins enrichment when activated

with anti-IgM (Matsumoto et al., 2009). Satpathy and associates monitored BCR dynamics looking into phosphoproteome and ubiquiproteome. Here, they used a stable isotope labelling by amino acids in cell culture approach, or SILAC, to label A20 cells and biotinylated anti-IgG $F(ab')_2$ for activation at different timepoints (Satpathy et al., 2015). Li and associates took advantage of selective proteomic proximity labelling using tyramide (SPPLAT), a proximity labelling technique, and anti-IgM-HRP antibodies to study BCR dynamics in the chicken B cell line DT40 (Li et al., 2014). Recently, our own lab used a different proximity labelling technique, APEX2, known to be more sensible and specific, to study BCR signalosomes. This technique provides the sensitivity needed for studying the proteosome and protein environments in the various intracellular compartments (Awoniyi et al., bioRxiv).

Despite the efforts to characterize these highly dynamic protein responses, previous studies have largely focused on the changes provoked in B cells after activation with soluble antigen, instead of the more *in vivo* relevant surface-bound antigen.

During my thesis, I established a novel protocol to extract proteins from the IS using mouse or human primary B cells. This protocol, based on Prof. Martin Humphries' (Jones et al., 2015) and Prof. Alexandre Carisey´s work (Meyer et al, *submitted*), relies on the isolation of bead-bound proteins for downstream proteomic analysis to uncover the proteins recruited to the IS during B cell activation *in vivo*. We generated a list of proteins only present or enriched in the BCR activated samples, forming the IS, compared to the control adhesive structures obtained via engagement of transferrin receptors. Our work, although preliminary, aims to unveil potential new candidate proteins regulating the triggering of the immune response and thereby ultimately also the cell fate and mounting of the successful antibody response.

2. Methods and materials

2.1. Mice

Wild-type C57BL/6NCrl mice (Charles River Laboratories, Germany) were purchased from the University of Turku Central Animal Laboratory (UTU-CAL, Turku, Finland) and bred in the UTU-CAL facility. The experiments were done with mice between 8 to 12 weeks old.

Mice were on a C57BL/6 background and maintained under specific pathogen free controlled conditions. All animal experiments were approved by the Ethical Committee for Animal Experimentation in Finland and in adherence with the rules and regulations of the Finnish Act on Animal Experimentation (62/2006; animal license numbers: 7574/04.10.07/2014, KEK/2014-1407-Mattila, 10727/2018).

2.2. Human peripheral blood

The buffy coat fractions, collected from healthy blood donors with a negative human immunodeficiency virus (HIV), hepatitis B surface antigen (HBsAg), and hepatitis C virus (HCV) status were obtained from Finnish Red Cross blood services. The use of anonymized PBMCs from blood donors was conducted in accordance with the rules of the Finnish Supervisory Authority for Welfare and Health (Valvira).

2.3. Mouse primary B cell isolation

A single-cell suspension of splenocytes was obtained by mechanical disintegration of the spleen through a 70 µm cell strainer (#22363548, Thermo Fisher Scientific). Splenocytes were resuspended in B cell isolation buffer (Phosphate-buffered saline without Ca^{+2} and Mg^{+2} [PBS], 2% fetal calf serum [FCS], 1 mM EDTA) and isolated using a negative isolation kit (EasySep™ Mouse B Cell Isolation Kit, #19854, StemCell Technologies) according to the manufacturer's instructions. Isolated B cells were let to recover in complete RPMI [cRPMI; RPMI 1640 with 2.05 mM L-glutamine supplemented with 10% FCS, 50 µM β-mercaptoethanol, 4 mM L-glutamine, 10 mM HEPES and 100 U/ml penicillin/streptomycin] in an incubator at +37°C and 5% CO_2 for at least 1 h before every experiment.

2.4. Human primary B cell isolation

Buffy coats were diluted 1:3 with sterile PBS. The diluted buffy coat was then diluted again with a ratio of 1:3 with Lymphoprep™ Density gradient medium for the isolation of mononuclear cells (density 1.077 g/ml, #07851, StemCell Technologies). A density gradient centrifugation was performed at room temperature (RT), at 800 g for 30 minutes with acceleration and brakes off. The Peripheral blood mononuclear cells (PBMCs) were carefully removed from the gradient and washed three times at RT with sterile PBS (x2 times at 300 g for 10 min, x1 time at 200 g for 10 min). Washed PBMCs were resuspended in cRPMI and counted (TC20 Automated Cell Counter, #1450102, Bio-Rad). Trypan Blue Stain (0.4%) (#T10282, Invitrogen) was used to determine the viability.

For B cell isolation, washed PBMCs were centrifuged at 250 g for 5 minutes at RT and resuspended in B cell isolation buffer. PBMCs were isolated using a negative isolation kit (EasySep™ Human B Cell Isolation Kit, #17954, StemCell Technologies) according to the manufacturer's instructions. Isolated B cells were let to recover in cRPMI in an incubator at +37°C and 5% CO_2 for 1 h before every experiment.

2.5. Synapse isolation

2.5.1. Preparation of beads

20 x 10^6 Dynabeads™ M-450 Tosyl-activated (#14013, Thermo Fisher Scientific) were washed 2 times with Buffer 1 (0.1M sodium phosphate buffer, pH 7.4-8) and resuspended in 1 ml of Buffer 1 containing one of the following ligands: 10 µg of AffiniPure F(ab')$_2$ Fragment Goat Anti-Human IgM, Fc$_{5\mu}$ fragment specific (#109006129, Jackson ImmunoResearch), 10 µg of Purified rat anti-mouse CD71, clone C2 (#553264, BD Bioscience), 10 µg of Fibrinogen from human plasma AlexaFluor™ 546 (AF546) conjugate (#F13192, Thermo Fisher Scientific), 10 µg of Transferrin from human serum AlexaFluor 488™ (AF488) conjugate (#T13342, Thermo Fisher Scientific) or 10 µg of Poly-L-lysine hydrobromide (CAS 25988-63-0, Sigma Aldrich). Beads were incubated for 1-2 hours in a shaker (Thermo-Shaker TS-100, BS-010120-AAI, Biosan) at RT and 950 rpm. After incubation, Buffer 1 with 1% BSA was added to the beads (final concentration of BSA 0.167%) and incubated for 16-24 hours in the shaker at 37ºC and 950 rpm. On the second day, beads were washed 3 times with 20 mM HEPES (#15630106, Thermo Fisher Scientific) and incubated for 2 hours at 1000 rpm and RT in 25 mM bis(sulfosuccinimidyl)suberate

(BS3) (#21580, Thermo Fisher Scientific) diluted in 20 mM HEPES. After incubation, beads were washed 3 times with Buffer 3 (0.2 M Tris 0.1% BSA (w/v), pH 8.5) and incubated for 16–24 hours at 1000 rpm and RT to deactivate the remaining free tosyl groups on the beads. On day 3, beads were washed 3 times with Buffer 2 (PBS with 0.1% bovine serum albumin (BSA) and 2 mM Ethylenediaminetetraacetic acid (EDTA), pH 7.4) and then stored in the same buffer. Coated beads were stored for up to 1 month at 4ºC.

2.5.2. Conjugate formation

Primary B cells from C57BL/6 mice spleens or buffy coat fractions were isolated as described in "2.3 Mouse Primary B Cell Isolation" and "2.4. Human Primary B Cell Isolation", respectively. 20 x 10^6 cells were resuspended in Imaging Medium (RPMI 1640 Medium, no glutamine, no phenol red (#32404014, Thermo Fisher Scientific) supplemented with 1% FCS and 20 mM HEPES) and incubated with 20 x 10^6 coated beads for 15 minutes at 1000 rpm and 37ºC. After conjugation, Di-*tert*-butyl peroxide (DTBP) crosslinker (#20665, Thermo Fisher Scientific) was added for 5 minutes (1000 rpm, 37°C) to a final concentration of 0–10 mM. Finally, DTBP was quenched by adding Tris-HCL 1M pH 8.5 to a final concentration of 150 mM for 5 minutes at RT.

2.5.3. Synapse isolation

Quenched cell – bead conjugates were placed on ice and washed several times to remove unbound cells with cold Cytoskeletal Buffer ([CSK buffer]; 300 mM sucrose, 100 mM sodium chloride, 10 mM PIPES (pH 6.8), 3 mM magnesium chloride). Conjugates were resuspended in CSK buffer with 0.5% Triton X-100 and Pierce™ Protease Inhibitor Mini Tablets, EDTA-free (#A32955, Thermo Fisher Scientific) and sonicated in a BioRuptor, sonicator – MEDIUM/HIGH program, 2–10 cycles 30" on/30" off (Bioruptor sonicator, Diagenode). Afterwards, conjugates were washed 5 times with CSK buffer with 0.5% Triton X-100 to remove cell debris. Bead-bound proteins were then eluted in 2x Laemmli buffer (diluted from 4x Laemmli Sample Buffer, #161-0747, Bio-Rad) with beta-mercaptoethanol (#21985023, Thermo Fisher Scientific) and, incubated first, for 30 minutes at 1000 rpm and 70ºC and, second, for 10 minutes at 1000 rpm and 95ºC. Beads were discarded, and eluted proteins were stored at -20ºC for up to 1 week.

2.6. In-gel digestion

Eluted samples were run on Any kD™ Mini-PROTEAN® TGX™ Precast Protein Gels (#4569034, Bio-Rad), and the gel was stained with Pierce™ Zinc Reversible Stain Kit (#24582, Thermo Fisher Scientific) for protein quantification. For destaining of the gel, Tris-glycine pH 8 (25 mM Tris, 192 mM glycine) was used. For the digestion, the protocol was adapted from Shevchenko et al. (Shevchenko et al. 2007). Each gel lane was cut into 1 or 3 pieces, depending on the experiment, and washed 3 times with MQ water for 10 minutes. Gel pieces were shrunk by covering the gel with 150 µl of 100% Pierce™ Acetonitrile (ACN), LC-MS Grade (#51101, Thermo Fisher Scientific) for 5-10 minutes. Gel pieces were rehydrated for 30 minutes at 56ºC in 150 µl of 20 mM Thermo Scientific™ Pierce™ Dithiothreitol (DTT) (#20291, Thermo Fisher Scientific) and dehydrated again with 150 µl of 100% ACN. Then, gel pieces were rehydrated in 150 µl 55 mM iodoacetamide (IAA) (CAS:144-48-9, Sigma-Aldrich) for 20 min in the dark RT and washed with 100 µl 100 mM ammonium bicarbonate (NH_4HCO_3) (09830-500G, Sigma-Aldrich) and dehydrated as above. Afterwards, 75 µl of 0,02 µg/µl Sequencing Grade Modified Trypsin (v511A, Promega) was added to the gel pieces and let to absorb for 20 minutes on ice. When all trypsin solution was absorbed, 150 µl of 40 mM NH_4HCO_3 / 10% ACN was added to cover the gel pieces completely and incubated for 18 hours at 37ºC. After incubation, 225 µl of 100% ACN was added and incubated for 15 min at 37ºC. Finally, the supernatant was collected into a clean Eppendorf tube, and the extraction was repeated with 150 µl solution containing 50 % ACN / 5% Pierce™ Formic Acid (HCOOH), LC-MS Grade, #85178, Thermo Fisher Scientific).

2.7. Western blot (WB)

For the analysis of BCR signalling, eluted proteins (see "2.5.3 Synapse Isolation") were run on 10% polyacrylamide gels and transferred to polyvinylidene fluoride (PVDF) membranes (Trans-Blot Turbo Transfer System, BioRad). Membranes were blocked with 5% milk in Tris-buffered saline (TBS, pH ~7.4) for 1 h and incubated with primary antibodies in 5% BSA in TBST (TBS, 0.05% Tween-20) O/N at 4°C. Secondary antibody incubations (1:10.000) were done for 1h at RT in 5% milk in TBST for horseradish peroxidase (HRP)-conjugated antibodies. Washing steps were done in 10 ml of TBST for 5 × 5 min. Membranes were scanned with ChemiDoc MP Imaging System (Bio-Rad) after the addition of Immobilon Western Chemiluminescent HRP Substrate

(WBKLS0500, Millipore) and incubation of 5 minutes. Images were background subtracted, and the raw integrated densities for each band were measured in ImageJ.

2.8. Flow cytometry

Data were acquired using a BD LSR Fortessa analyser equipped with four lasers (405, 488, 561 and 640 nm), and data were analysed using FlowJo v10 (Tree Star).

Beads: For bead analysis, beads were coated as described in "2.5.1. Preparation of beads". Some of the coating ligands were already fluorescently labelled (i.e., transferrin Alexa Fluor™ 488 and fibrinogen Alexa Fluor™ 546), and others were detected with fluorescently labelled secondary antibodies (Donkey anti-Goat IgG (H+L) AF488 (#A11055, Thermo Fisher Scientific) to detect goat anti-mouse IgM, and Donkey Anti-Rat IgG (H+L) AF488 (712-545-153, Jackson ImmunoResearch) to detect MHCII and CD71).

Conjugates: For conjugates analysis, conjugates formed as described in "2.5.2 Conjugate formation" were fixed in 4% paraformaldehyde (PFA) (16005-1KG-R, Sigma-Aldrich). After wash, samples were stained with Purified Rat Anti-Mouse CD16/CD32 (Mouse BD Fc Block™) (#553142, BD Biosciences), Donkey anti-Goat IgG (H+L) Cross-Adsorbed Secondary Antibody AF488 (#A11055, Thermo Fisher Scientific) and 4',6-Diamidino-2-Phenylindole, Dihydrochloride (DAPI) (#D1306, Thermo Fisher Scientific) for 30 minutes at RT.

Human cell populations: For immunophenotyping of the isolated human B cells, isolated cells were stained with Allophycocyanin (APC) anti-human CD19 Antibody (#15583 BioLegend), Human TruStain Fc-receptor blocking solution (#6462, BioLegend), AF488 anti-human IgM Antibody (#314533, BioLegend) and Pacific Blue anti-human IgD Antibody (#348223, Biolegend) and incubated on ice for 15 minutes.

2.9. Brightfield and fluorescence microscopy

Samples (cells, conjugates and beads) were plated in a dilution of 1:20 in PBS in a 96-flat well plate and observed under inverted microscope EVOS fl, with an illumination system based on LED cubes. The images were captured using a 40x AMG PlanFluor objective and 4 different filter sets: DAPI, GFP, RFP, and transmitted light.

2.10. Spinning disk confocal microscopy

Images were acquired using a 3i CSU-W1 spinning disk equipped with 405, 488, 561 and 640 nm laser lines and 510–540, 580–654 and 672–712 nm filters and 63× Zeiss Plan-Apochromat objective. SlideBook6 (Intelligent Imaging Innovations Incorporation) software was used for image acquisition.

2.11. Mass spectrometry analysis

Data was collected by LC – electrospray ionization (ESI) – MS/MS using a nanoflow HPLC system (Easy-nLC1200, Thermo Fisher Scientific) coupled to the Orbitrap Fusion Lumos mass spectrometer (Thermo Fisher Scientific) equipped with a nano-electrospray ionization source. Peptides were first loaded on a trapping column and subsequently separated inline on a 15 cm C18 column (75 µm x 15 cm, ReproSil-Pur 3 µm 120 Å C18-AQ, Dr. Maisch HPLC GmbH, Ammerbuch-Entringen, Germany). The mobile phases consisted of water with 0.1% HCOOH (solvent A) and ACN/water (80:20 (v/v)) with 0.1% HCOOH (solvent B). A 60 min chromatography method was used: from 5% to 21% of solvent B in 28 min, to 36% of solvent B in 22 min, from 36% to 100% of solvent B in 5 min, followed by a wash at 100% of solvent B for 5 min.MS data were acquired automatically using Thermo Xcalibur 4.1 software (Thermo Fisher Scientific). A data-dependent acquisition method (DDA) consisting of an Orbitrap MS survey scan of mass range 350–1750 m/z followed by HCD fragmentation was used.

2.12. Protein identification and differential enrichment analysis

Raw files were processed with MaxQuant software version 1.6.17.0 (Cox et al., 2008) with first search peptide tolerance set to 20ppm. Trypsin was set as the digestion enzyme, carbamidomethyl specified as fixed modification, and oxidation, acetylation (Protein N-term), DTBP + alkylation (K) and DTBP + alkylation (Protein N-term) were specified as variable modifications. MS/MS spectra were searched against mouse Swiss-Prot database that was released 01/2021. Peptide and protein false discovery rate were set to 0.01. MaxLFQ and match between runs were enabled.

Proteins were identified Following MaxQuant run and after filtering potential contaminants, proteins only identified by site, reverse hits, and proteins with less than 2 unique peptides. Fold change was calculated using the formular below:

Log_2(Intensity of anti-IgM samples) – Log_2(Intensity of anti-CD71 samples)

Comparison of identified proteins in different samples was prepared in a Venn Diagram using Venny 2.1.0 software (Oliveros, 2007-2015). Enrichment analysis was carried out in Perseus software (Tyanova et al., 2016). For gene ontology analysis, database for annotation, visualization and integrated discovery (DAVID) v6.8 was used to generate functional protein clusters based on the relationship of genes within the list provided by MaxQuant. (Huang et al., 2009).

2.13. Illustrations and statistics

Graphs were created in GraphPad Prism 8, and illustrations were created with BioRender. Figure formatting was done on Inkscape 1.0.

Statistical significances were calculated using unpaired Student's t-test assuming a normal distribution of the data. Statistical values are denoted as: ****P<0.0001.

3. Results

3.1. Development of the mouse immune synapse isolation

In this thesis, the protocol developed to isolate proteins recruited to the B cell IS after cell activation was based on the work describing bead-bound protein isolation for downstream proteomic analysis using adherent cells (Jones et al., 2015) and NK cells (Meyer et al., *submitted*). Therefore, the existing protocols had to be modified for B lymphocytes. This involved several optimisation steps in order to obtain a sufficient protein yield for WB and MS analyses, and to reduce unspecific protein interactions with the beads.

A generic overview of the protocol (Figure 7) and all the conditions tested (Table 1) is shown below. In order to mimic an APC and induce IS formation, magnetic beads were coated with anti-BCR antibodies ($F(ab')_2$ anti-IgM) acting as a surrogate antigen. As a negative control, different ligands that could induce cell adhesion to the beads without BCR signalling and IS formation were tested and selected. Primary mouse B cells were isolated from mouse spleens. Cells and beads were enabled to form conjugates in Eppendorf or polypropylene tubes. Ensuing the IS formation, the proteins were crosslinked with DTBP. This crosslinker is known as a homobifunctional, cleavable and membrane-permeable crosslinker containing amine-reactive groups able to form stable amidine bonds. In order to stop the crosslinker functional activity, quenching buffer was added. Sonication and subsequent washing enabled the displacement of the cell – bead conjugation and the removal of cell debris while maintaining the integrity of crosslinked IS proteins bound to the beads. The proteins on the beads were eluted in Laemmli buffer with β-mercaptoethanol allowing the extraction of the isolated proteins from the beads. Then, the proteins were separated by SDS-PAGE and prepared for mass spectrometry analysis. As mentioned before, for us to reach this endpoint protocol, specific conditions had to be determined to establish an optimal setting for B cell IS isolation. Towards that aim, the success of the isolation was evaluated through checkpoints across the protocol. The checkpoints included the surrogate antigen used for coating the beads, cell – bead ratio used for conjugation, the concentration of cells, the concentration and time of incubation of the crosslinker, sonication program, among others. It allowed to monitor points of variability between conditions and select the most appropriate ones for B cells.

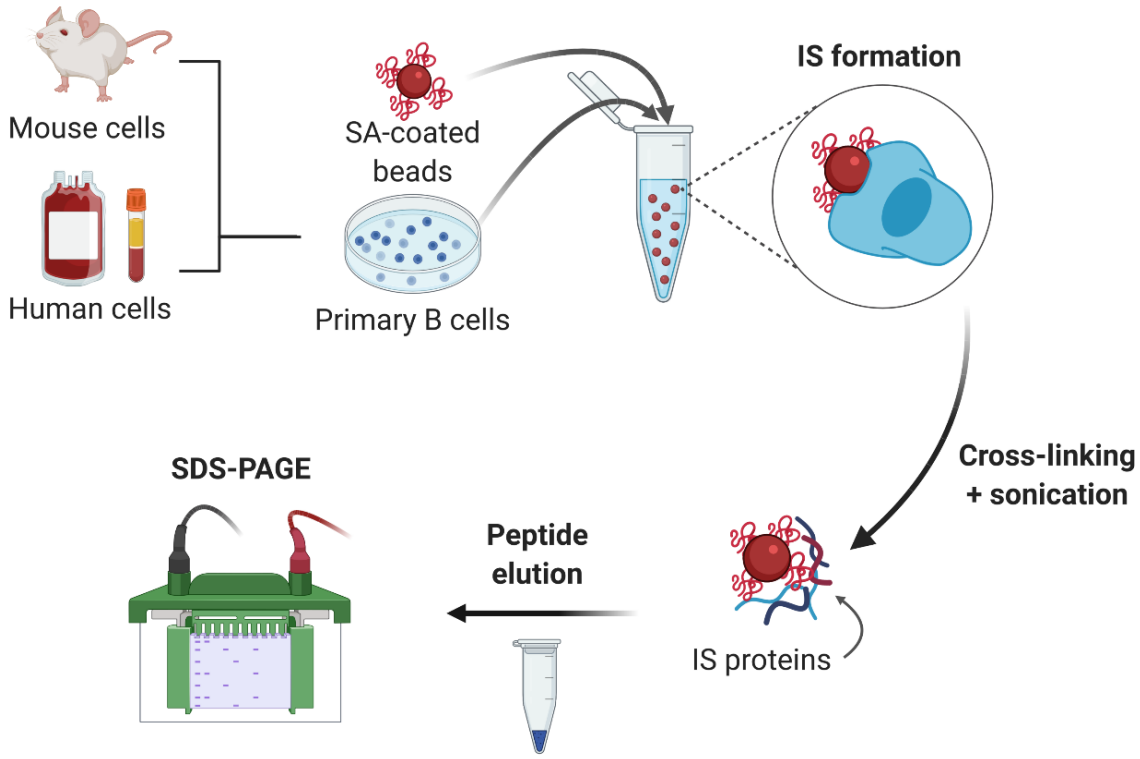

Figure 7. Overview of the IS isolation protocol. Primary B cells are isolated from mouse spleen or human blood and then conjugated with surrogate antigen (SA)-coated magnetic beads. Conjugation leads to B cell IS formation. Ensuing the crosslinking of IS proteins bound on the beads. Sonication coupled with washing removed the cell debris and other contaminants. IS proteins bound on the beads are then eluted in Laemmli Buffer and separated by SDS-PAGE.

3.1.1. Coating of the beads and conjugate formation

Six different ligands were tested for coating. The commonly used, $F(ab')_2$ anti-mouse IgM was used as a surrogate antigen to trigger BCR signalling and IS formation. However, different ligands had to be tested as a negative control. For that purpose, anti-mouse transferrin receptor, or CD71 (transmembrane receptor essential for endocytosis of transferrin into the cells, thus being constitutively expressed in every cell), anti-mouse MHC-II (constitutively being expressed in professional APCs such as B cells), fibrinogen, poly-L-Lysine and transferrin were selected. A combination of anti-CD71 and anti-MHCII was also tested.

The results showed that most of the ligands could be coated onto the magnetic beads. Bead conjugation was considered successful if 1) the coated beads were in a single form and 2) the ligand could be detected on the surface of the beads using flow cytometry.

Table 1 – Control points in mouse IS protocol

Checkpoint	Conditions tested	Final conditions
Coating Ligands (3.1.1)	$F(ab')_2$ anti-mouse IgM, fibronectin-AF564, poly-L-lysine, transferrin-AF488, anti-mouse CD71, anti-mouse MHC-II, anti-mouse CD71+ Rat anti-mouse MHC-II	$F(ab')_2$ anti-mouse IgM, anti-mouse CD71
Ratio cell - bead (3.1.2)	1:2 1:1.5 1:1 2:1	1:1
Cell – bead concentration (3.1.3)	1-20 x 10^6cells/mL + 1-20 x 10^6beads/mL	10 x 10^6cells/mL + 10 x 10^6beads/mL
Crosslinker Incubation Time (3.1.4)	5-30 min	5 min
Crosslinker Concentration (3.1.5)	0.1 mM – 10 mM	2.5 mM
Sonication Program (3.1.6)	Medium – 2, 4, 6, 8 and 10 cycles ON/OFF (30 s) High - 2, 4, 6, 8 and 10 cycles ON/OFF (30 s)	High – 5 cycles ON/OFF (30 s)

As shown by flow cytometry, $F(ab')_2$ anti-IgM displayed a clear fluorescence signal, consistent with an effective coating, and most of the beads were detected as single beads (Figure 8 A-B). This was the desired outcome, considering that a suspension of single beads will theoretically allow more single cell – single bead conjugates. When comparing the control ligands, considerable differences were found. Anti-CD71 (Figure 8 C-D) and anti-MHCII (Figure 8 E-F) antibodies looked promising, as they displayed a high population of single beads. Even though, anti-MHCII antibodies did not provide fluorescence readout, anti-MHCII coated beads were still tested in conjugate formation. Beads coated with CD71+MHCII were also considered but, the results were similar to the anti-MHCII single antibodies usage (Figure 8 G-H).

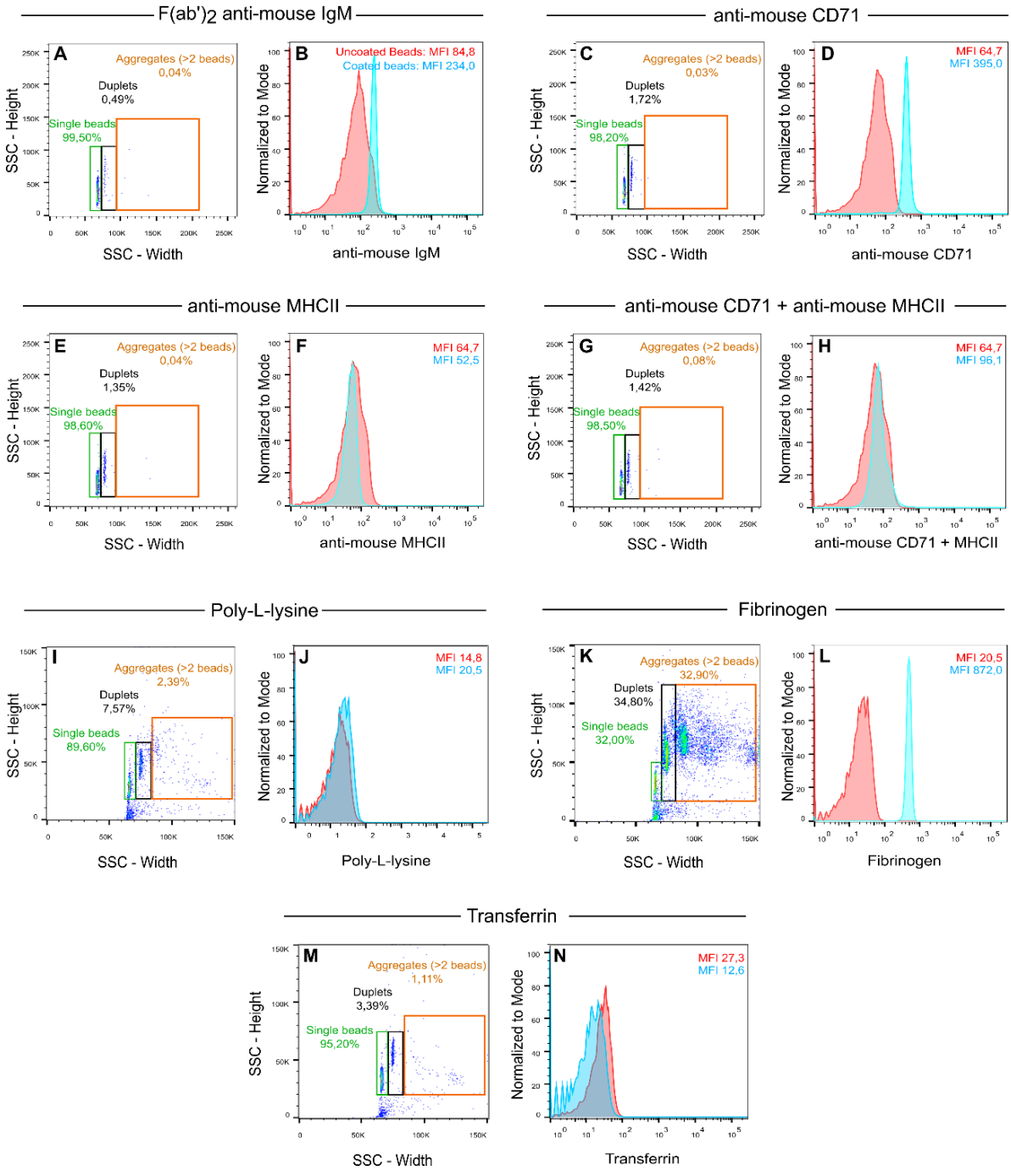

Figure 8. Magnetic beads coated by designated ligands. (A, C, E, G, I, K, M) Coating efficiency for the different ligands, was determined using flow cytometry. SSC-W vs SSC-H (dot plot) was used to differentiate between single beads, duplets and aggregates. (B, D, F, H, J, L, N) Histograms were used to display the fluorescence intensity of the single beads (green gate on the plot). Red histogram: uncoated beads. Blue histogram: coated beads.

Beads coated with Poly-L-lysine showed no signs of bead aggregation, although coating efficiency could not be proved using flow cytometry due to a lack of fluorescence readout (Figure 8 I-J). Fibrinogen, on the other hand, showed the best degree of coating, but also a tendency to

create bead aggregates, as only 32% of the beads were detected as single beads (Figure 8 K-L). Despite being fluorescently labelled, the transferrin signal was not detected on the beads, suggesting that the coating was inefficient (Figure 8 M-N). Therefore, anti-IgM, anti-CD71, anti-MHCII and anti-CD71+anti-MHCII were selected for further testing.

Next, conjugate formation was assessed. Cells and beads were incubated together for 15 minutes at 37ºC and then analysed under the inverted brightfield microscopy. In addition, unbound cells were washed and counted to determine the percentage of conjugates. The difference in the numbers of conjugates was clear when comparing different control ligands with anti-IgM coated beads. F(ab')2 IgM coated beads achieved the best conjugation efficiency (Figure 9A and E), followed by anti-CD71 coated beads (Figure 9B and E). Anti-MHCII and the combination of anti-CD71 + anti-MHCII achieved a very modest percentage of conjugation (Figure 9C, D and E). Therefore, anti-CD71 coated beads were selected as the negative control ligand, or non-activatory ligand.

3.1.2. Ratio cell – bead

Once the non-activatory ligand was selected, different parameters were tested to optimise the conjugation protocol. First, the quality and number of conjugates formed was assessed by imaging them in a inverted brightfield microscopy. Based on the existing protocols, cell – bead ratios of 2:1, 1:1.5, 1:1, and 1:2 were tested. The results indicated that using a higher number of cells (2:1 ratio) did not increase the likelihood of conjugate formation, and on the other hand, an increased number of beads (1:2 ratio) led to bead aggregation. Given the goal to obtain single cell-bead conjugates, 1:1 and 1:1,5 were the best options, as they allowed the formation of single conjugates without bead aggregation (data not shown). Therefore, cell – bead ratio of 1:1 was the ratio decided to carry out other procedures.

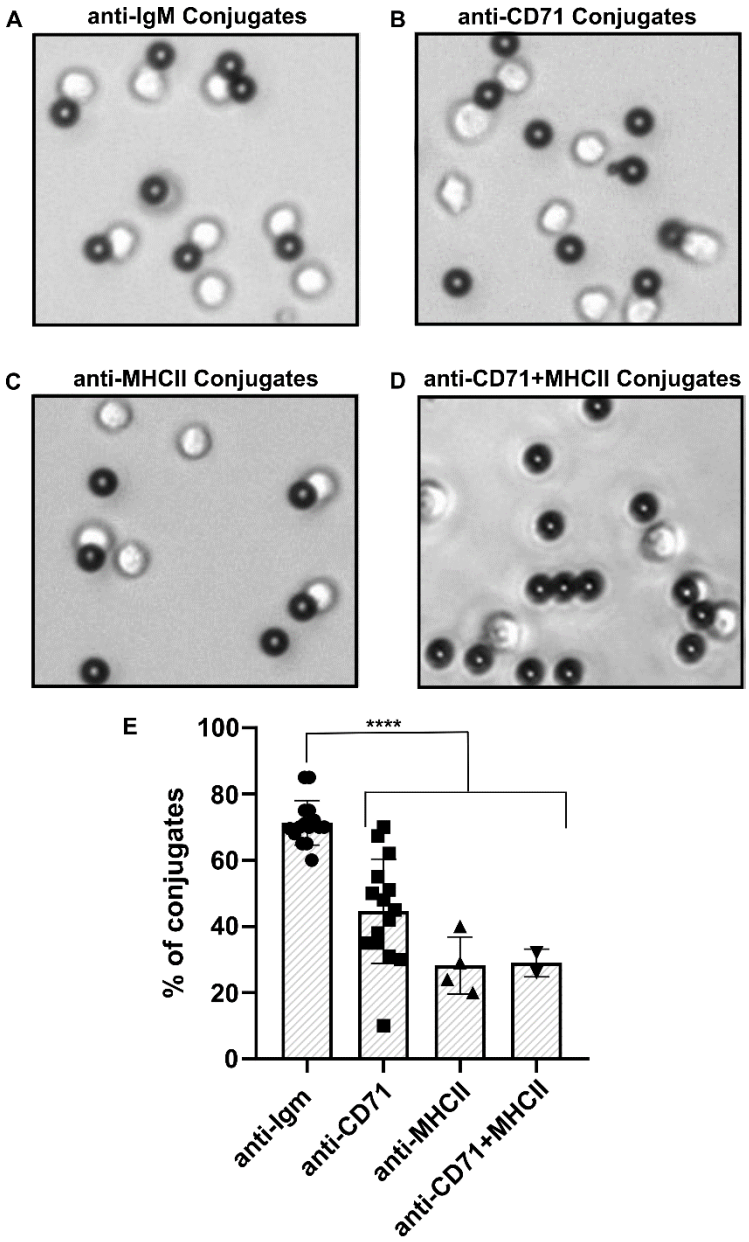

Figure 9. Conjugate formation with beads coated with different ligands. (A) Anti-IgM, (B) anti-CD71, (D) anti-MHCII, or (D) anti-CD71+anti-MHCII coated beads were incubated with cells to form conjugates and analysed using a inverted brightfield microscopy (E) After conjugation, unbound cells were washed and collected into a new tube for counting. The graph shows the average percentage of conjugates [100 – (unbound cells/total cells)*100] per experiment using coated beads with different ligands. Anti-IgM: 71,4 ± 1.7 % (*n*=15). Anti-CD71 44.6 ± 4.0 % (*n*=15). Anti-MHCII: 28.3 ± 4.4 % (*n*=4). Anti-CD71+anti-MHCII: 29.0 ± 3.0 % (*n*=2). Dots represent the number of individual experiments (*n*). **** P < 0.0001 (unpaired Student's t-test).

3.1.3. Cell – bead concentration

Next, cell – bead concentration was improved for a better conjugation and effective sonication of conjugates. Cell – bead conjugation was evaluated at concentrations of 1 – 20 million cells and 1 – 20 million beads per millilitre in Eppendorf tubes (1.5 millilitres) and

polypropylene tubes (15 millilitres). Ratio of cell – bead was systematically the same (1:1). Final concentration was settled on 10 million cells per millilitre since it provided the best conjugate formation without aggregation of cell – bead or bead – bead.

Through inverted brightfield microscopy, conjugates sonicated in 15 mL polypropylene tubes revealed significant debris, and contaminations contrary to the samples in eppendorfs (data not shown). Sonication in 15 mL tubes involved different sonication mechanisms not as sterile as the ones involved in sonication in eppendorf tubes. Given the sonicator features, eppendorf were chosen as the preferred tubes.

A lower concentration (<5 million cells per millilitre) implied a processing of the samples in several eppendorfs which could vary conditions between samples. A higher concentration (>15 million cells per millilitre) interfered with the sonication. Here, inverted brightfield microscopy was employed again to assess the conjugates and cells sonication. The results showed that even after 10 cycles of sonication, the samples contained a high number of conjugates and intact cells, consonant with a poor sonication (data not shown).

Eventually, a cell concentration of 10 million cells per millilitre in Eppendorf tubes was chosen since it gave the best settings for both conjugation and sonication.

Next, cell – bead conjugation time was tested. Two time points, 15 minutes and 30 minutes, were selected after a literature revision suggested that later timepoints might miss some of the early and more dynamic processes vital for early B cell signalling in the IS. using inverted brightfield microscopy and by counting unbound cells after conjugation, no significant differences were found in the percentage of conjugates (data not shown). Hence, since a longer incubation time did not increase the number of conjugates, a conjugation time of 15 minutes was adopted.

3.1.4. Incubation time with the DTBP crosslinker

Afterwards, duration of the crosslinker activity was assayed. The effect of 5-, 15- and 30-minutes incubation with DTBP on conjugate formation using anti-IgM coated beads was tested. The samples were analysed by flow cytometry, and the cell, bead and conjugate populations were gated based on FSC (size) and SSC (granularity). Results pointed for a semblance between the three incubation times regarding the percentage of conjugates (Figure 10A, C, E). In addition to the FSC-SSC analysis, samples were stained with AF488 anti-goat IgG to label the coated beads and DAPI to label the cell nucleus. The DAPI staining unambiguously showed that the gated single cell populations and conjugate populations were indeed cells ($DAPI^+$). However, with anti-goat

IgG staining was not possible to clearly gate the stained population (beads) from the background (cells) due to the low signal (Figure 10B, D, E). Despite that, there is a clear shift in the AF488 channel when comparing the conjugate and the single-cell population, suggesting that the conjugate population is indeed formed by beads ($AF488^{+}$) and cells ($DAPI^{+}$). Considering that time of incubation with the crosslinker did not pose any hindrance, an incubation time of 5 minutes was selected.

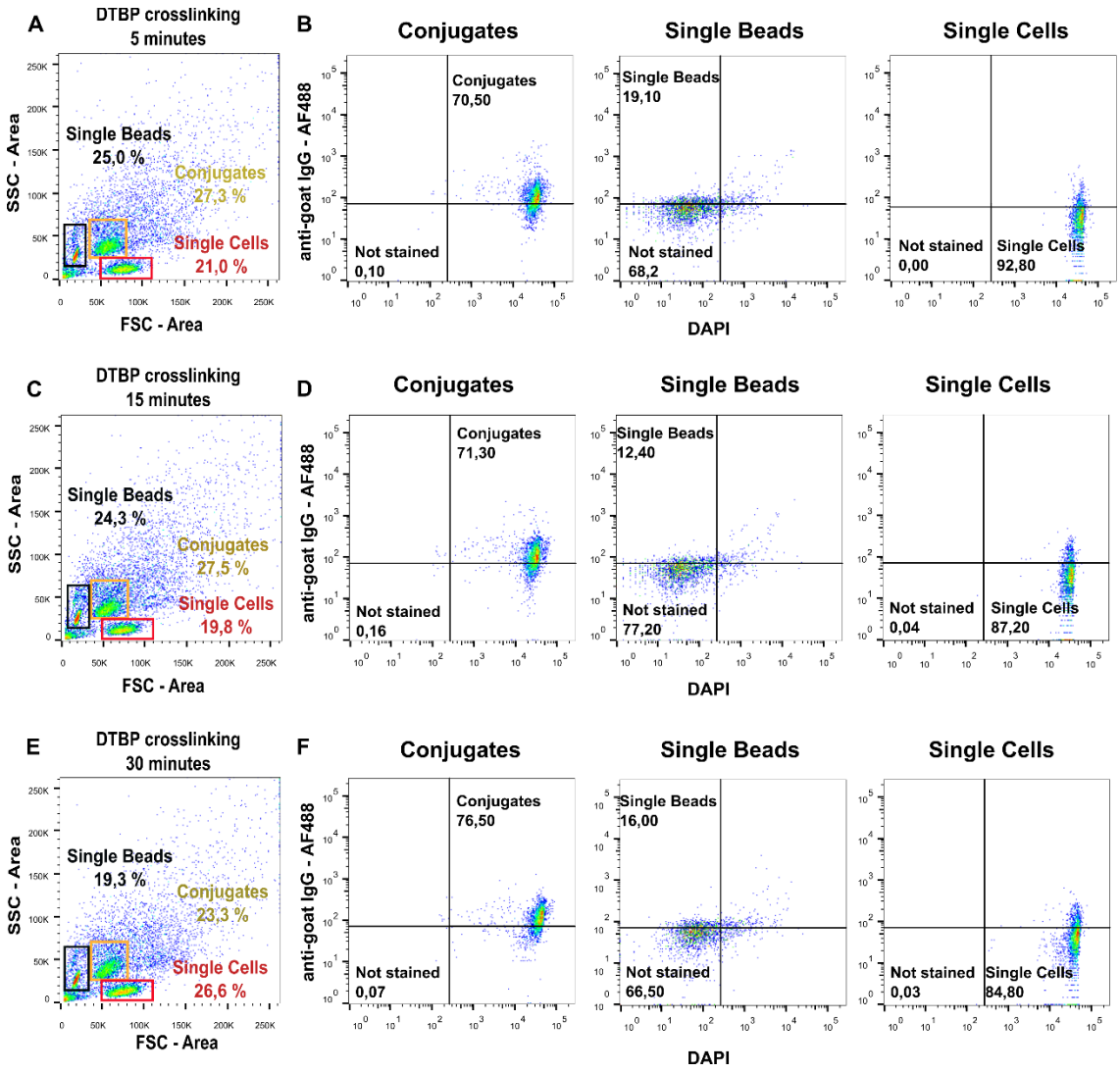

Figure 10. Conjugate formation with different times of crosslinker incubation. Conjugate formation after 5-,15- and 30-minute incubation with crosslinker was determined using flow cytometry. (A, C, E) FSC-A vs SSC-A (dot plot) was used to differentiate between single beads (black gate), single cells (red gate) and conjugates (yellow gate). (B, D, F) DAPI (cell marker) vs IgG-AF488 (bead marker) was used to verify the composition of the different populations.

3.1.5. DTBP concentration

In regard to crosslinker concentration, three small-scale proteomic experiments were set to test 3 different DTBP concentrations – 0.5 mM, 2,5 mM and 5 mM. The lowest concentration did not provide a substantial protein dataset for further analysis. Proteomic data consisted in a total list of less than 500 protein hits, which consisted mainly in keratins, histones and conservative proteins present in both anti-IgM samples and the non-activatory control samples. While testing the other crosslinker concentrations, it was noticeable that a higher concentration could promote more crosslinking. From a 2.5 mM crosslinker concentration, an average of 500 total proteins were identified comparing to 700 total proteins identified in pull-downs from 5.0 mM crosslinker concentration (*data not shown*). For reference, both concentrations, 2.5 mM and 5.0 mM were used in further experiments and compared.

3.1.6. Sonication program

The aim of sonication was to remove the cells from the beads leaving only the crosslinked proteins for elution. Hence, different sonication programs (time and intensity) were tested to determine the best settings to break the cells without damaging the proteins crosslinked. For this, primary B cells were conjugated with anti-IgM coated beads (1:1) following the settings determined in the previous sections. Then, the "medium" and "high" programs in Bioruptor bath sonicator using 2-10 sonication cycles were carried out. In both programs, 2 cycles of intermittent sonication were not enough to separate the cell – bead conjugates (Figure 11A-B). From the medium intensity settings, it was noticeable a considerable number of conjugates remaining even after 6-8 cycles of sonication (Figure 11A). At 10 cycles, cells and beads were mostly separated (Figure 11A). From the high intensity program, most cells and beads were separated at between 4 and 6 cycles of sonication (Figure 11B). At 10 cycles there was already cell debris accumulation (Figure 11B). Although some cells remained intact after 10 cycles with both of the programs, the following washing step removed cell debris and intact cells, as far as they were detached from the beads. Therefore, the high intensity program with 5 cycles of sonication was preferred.

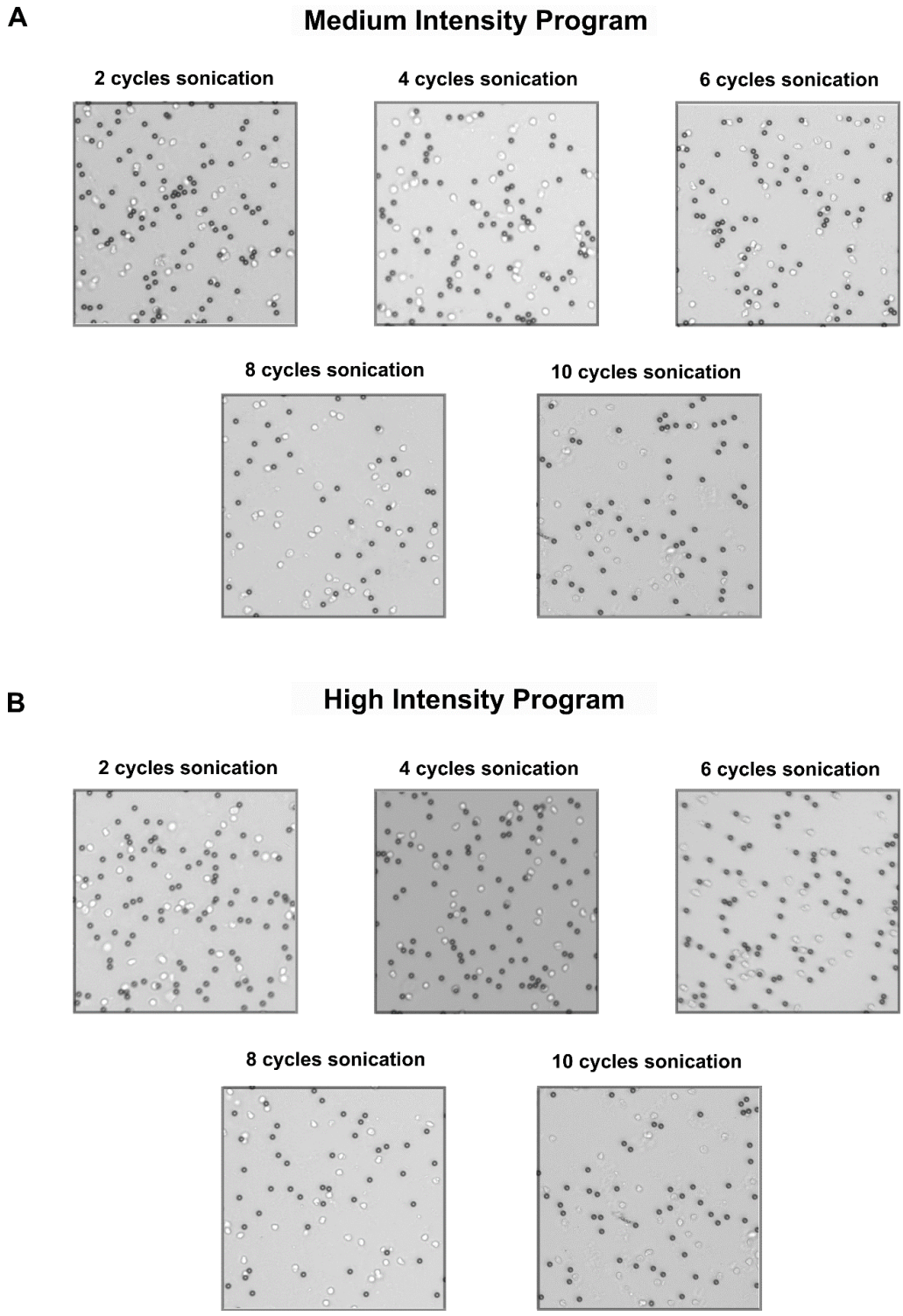

Figure 11. Comparison between sonication programmes. Two independent samples went through sonication: one was sonicated using a (A) medium intensity program, and the other using a (B) high intensity program. Every 2 cycles of sonication, an aliquot of the sample was transferred to a 96-well plate (1:20 in PBS) and imaged by inverted brightfield microscopy.

3.2. Validation of the protocol

3.2.1. B cell activation and IS formation

An experimental validation of the protocol was conducted in order to validate the protocol and results obtained from the control points. First, as expected based on the optimization steps, samples were confirmed through inverted brightfield microscopy to be mostly in single conjugates (Figure 12A). Furthermore, a significant difference in the number of conjugates originated with IgM beads compared to CD71 beads was noticeable as shown before in Figure 9E.

Next, taking advantage of Spinning Disk confocal microscopy, the organisation of the cytoskeleton and cell signalling was analysed in cells conjugated with the different coated beads. After conjugation with IgM beads, an increase in actin intensity could be observed on the cell – bead contact surface (IS) by F-actin staining with fluorescent phalloidin, indicating a successful formation of an IS by cell spreading. When using the anti-CD71 beads, no changes were observed in the cytoskeleton. Signalling proteins, as Syk, Lyn, Btk, PLC-ɣ, are phosphorylated in tyrosine residues. As a readout for the signalling, cells were stained with anti-phosphotyrosine (anti-pY) antibody that recognises tyrosine residues in the phosphorylated state. Cells binding to anti-IgM beads showed an increase in pY signalling at the contact area, colocalising with the actin. Cells interacting with the negative control beads on the other hand did not show increased pY signalling. (Figure 12 B).

To further corroborate these findings, BCR signalling was also investigated using WB. BCR activation culminates in the phosphorylation of key effector proteins, like Syk, which is recognized to be one of the first proteins recruited to the IS. For that, 10 million cells were conjugated with 10 million beads with either anti-IgM coated beads or anti-CD71 coated beads. After conjugation, unbound cells were washed, and IS proteins bound on the beads were eluted. As a control, whole cell lysate (WCL) was prepared from 5 million cells and 10 million cells, respectively. Analysing the pSyk/tSyk signal massive increase in pSyk was verified in the cells interacting with anti-IgM beads compared to the WCLs and anti-CD71 conjugates. Additionally, GAPDH, a cytosolic protein, did not display signal in beads elutes (Figure 12C). Taken together, these results verified that anti-IgM beads, but not the control anti-CD71, are able to trigger BCR signalling and actin polarisation, successfully mimicking the immune synapse.

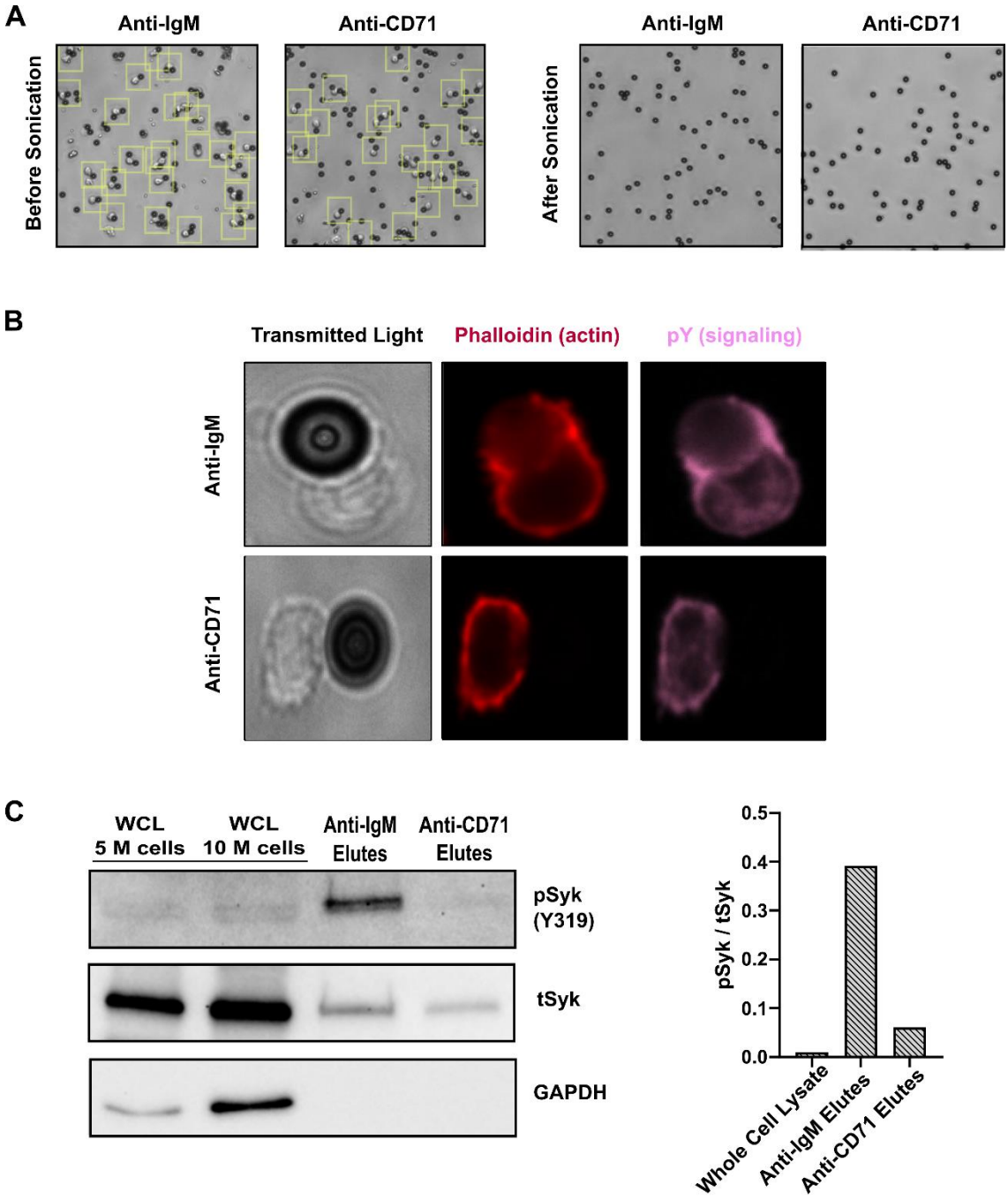

Figure 12. Protocol Validation shows B cell activation in anti-IgM conjugates but not in anti-CD71 conjugates. Conjugation using 10 million cells and 10 million anti-IgM or anti-CD71 beads was done according to the protocol. (A)Inverted brightfield microscopy was used to image conjugates before and after sonication. Yellow gates were used to highlight single conjugates originated from each condition. The results are presentative of a set of 10 experiments. (B) Conjugates were stained with fluorescent phalloidin (Alexa Fluor 555) and anti-pY antibody to assess the degree of BCR activation with each set of coated beads. Images were obtained with Spinning Disk confocal microscopy right after conjugation and IS proteins crosslinking (n = 1). (C) pSyk/tSyk ratio and GAPDH (cytosolic protein) was evaluated by Western Blot. 10 million cells and 10 million coated beads of each condition were conjugated and afterwards, unbound cells were washed, and bead bound IS proteins were eluted. The results from beads lysates were compared with non-activated WCL (n = 1).

3.2.2. Elution of IS proteins

Finally, crosslinked proteins were tested for elution and protein recovery from the beads for proteomics analysis. To do that, 10 million cells and 10 million beads per condition were conjugated, unbound cells were washed afterwards, and the samples sonicated as detailed before. Following sonication, several washes to remove cell debris and other unbound components were performed. Finally, using Laemmli buffer with beta-mercaptoethanol, protein crosslinking was reversed, and proteins were eluted from the beads. From 10 million cells, the protein retrieved from IgM beads was 0,81 µg and from CD71 beads was 0,44 µg. This was a major problem and a shortcoming of this kind of method. Nonetheless, an enrichment on tSyk and tLyn was demonstrated in IgM beads eluted proteins when compared to CD71 eluted proteins, evidencing that IS proteins can be successfully pull-downed using this method (Figure 13).

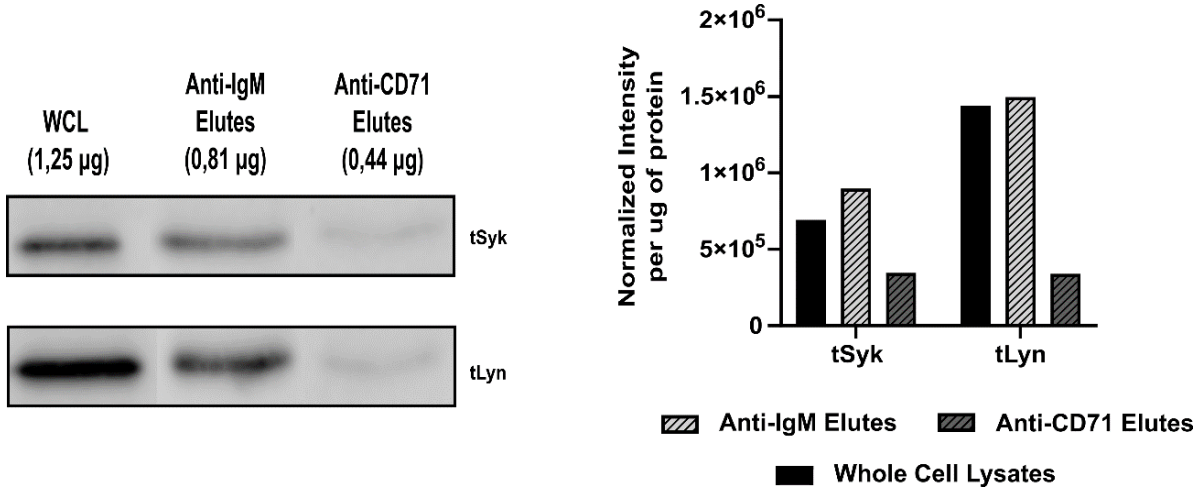

Figure 13. Eluted Proteins from anti-IgM anti-CD71 beads. 10 million cells and 10 million beads per condition were conjugated, unbound cells were removed, and bound cells were washed and sonicated. Crosslinked proteins on beads were then washed several times and eluted in Laemmli Buffer with β-mercaptoethanol. Samples were run (SDS-PAGE) and quantified using zinc staining (µg of proteins is shown in parenthesis). The gel was transferred to a membrane and blotted for tSyk and tLyn (left image). The quantification of Lyn and Syk normalised to the total amount of protein is shown on the right (n = 1).

3.3. Immune synapse proteome analysis

An in-depth analysis of the IS proteome is likely to bring new insights to which proteins are playing a central role in immune synapse regulation. The preliminary data obtained from a total of 8 experiments with MS analysis should be viewed with some consideration as the experimental conditions were still under partial optimization and not all biological replicates were accomplished

with final settings. For this reason, statistical analysis of the protein hits and protein enrichment will be performed in the future with new replicates.

The 8 experiments had fundamental differences between each other in terms of trypsin digestion and DTBP crosslinker concentration. Trypsin digestion was employed in two different manners. In the set A of experiments (6 experiments; "limited digestion"), samples were cut and digested in a single eppendorf tube per condition (Figure 14A); in the set B (2 experiments; "extensive digestion"), samples were cut in 3 parts and every part was digested in a different eppendorf tube (Figure 14B). Regarding the concentration of DTBP crosslinker, in 2 experiments it was employed a concentration of 5 mM and in 6 experiments it was employed a concentration of 2.5 mM.

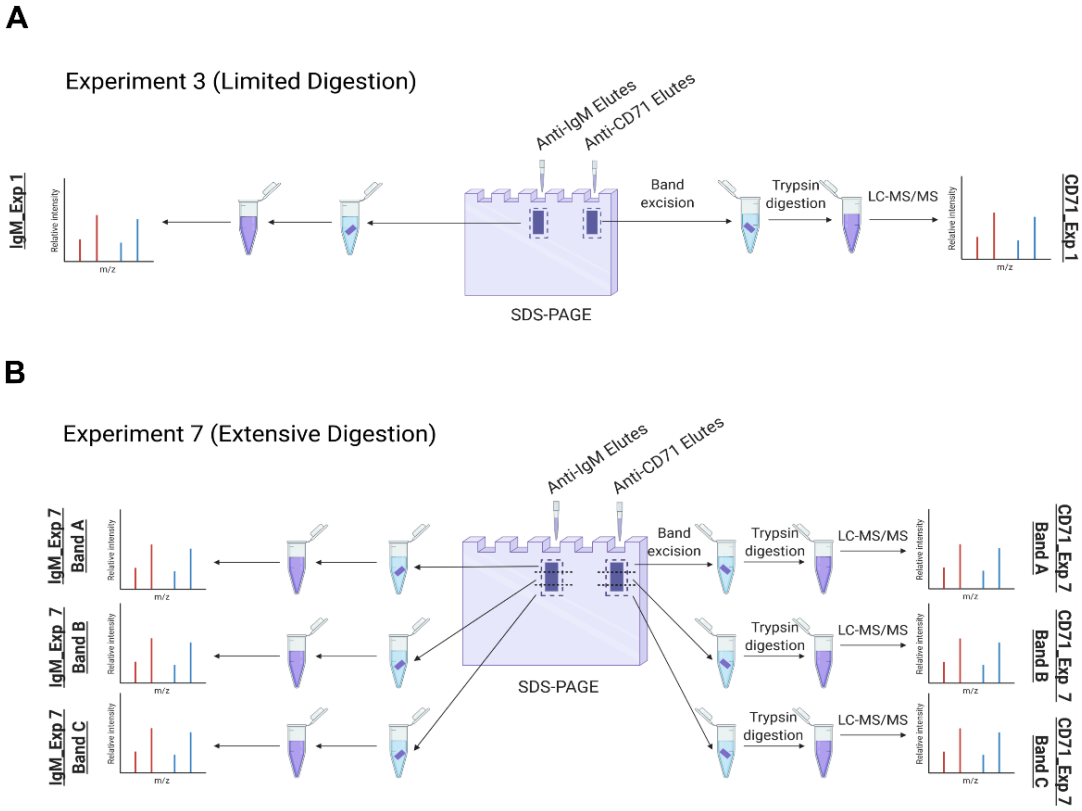

Figure 14. Trypsin digestion schematic from MS experiment 3 (limited digestion) and experiment 7 (extensive digestion). (A) In Experiment 3, anti-IgM elutes and anti-CD71 elutes were run separately for 1 cm. Each gel lane was cut and digested in one single eppendorf. (B) In Experiment 7, anti-IgM elutes and anti-CD71 elutes were also run separately for 1 cm, however each gel lane was cut in three, and digested in three different eppendorfs per condition.

Table 2 – List of experiments and respective conditions*

Experiment	Trypsin Digestion	DTBP crosslinker	Exclusively identified proteins in anti-IgM elutes (% percentage of proteins in anti-IgM elutes compared to total proteins identified)
Experiment 1	Limited	2.5 mM	123 (8,5%)
Experiment 2	Limited	2.5 mM	282 (35,0%)
Experiment 3	Limited	2.5 mM	125 (25.8%)
Experiment 4	Limited	2.5 mM	230 (16,7%)
Experiment 5	Limited	5 mM	331 (28,3%)
Experiment 6	Limited	2.5 mM	355 (13,9%)
Experiment 7	Extensive	2.5 mM	502 (23,6%)
Experiment 8	Extensive	5 mM	443 (6,1%)

*The variation in the key experimental conditions and the numbers of identified proteins in the samples with anti-IgM beads are indicated. *

Looking at the overall results, when an extensive trypsin digestion was performed, there was an increase in the number of total proteins identified. Moreover, a higher concentration (5 mM) of DTBP did not significantly affect the amount of identified proteins exclusively in IgM samples.

From the set of 8 experiments: 1 protein was identified in 6 experiments, 1 protein identified in 5 experiments, 12 proteins identified in 4 experiments, 88 proteins identified in 3 experiments, 389 proteins identified in 2 experiments and 1420 were only identified in 1 experiment (Supplementary Data). From the proteins appearing in 4 or more common lists, CD79a, IgM heavy chain, IgM light chain were highlighted. These proteins were expected to be found in anti-IgM samples as they are part of the subunits of IgM BCR that are activated by the anti-IgM beads. Moreover, a cytoskeleton-associated protein JAK1 was also identified in 4 experimental sets.

One limiting step in the number of proteins identified was likely trypsin digestion, and one of the reasons trypsin digestion was performed by two different approaches. To better understand

the potential disparities between protocols, two successful experiments with both methods: limited digestion (Experiment 3) and extensive digestion (Experiment 7) are further compared below.

In Experiment 3, 484 total proteins with 2 or more unique peptides were identified. 125 (25.8%) protein hits were exclusive to anti-IgM samples and 81 (16.7%) protein hits were exclusive to anti-CD71 samples, while both samples shared 278 (57.4%) protein hits (Figure 15A). Several relevant proteins forming the BCR itself (IgM heavy chain and IgM light chain), involved in signalling (Syk, Lyn, CD79a, CD79b) and the regulation of the actin cytoskeleton (ezrin) were enriched in anti-IgM samples compared to anti-CD71 samples (Figure 15 B). Transferrin receptor was identified only in anti-CD71 samples, concomitant with the expectations. A preliminary gene ontology analysis was run using DAVID software for proteins exclusively identified or enriched in anti-IgM samples. The results showed that identified proteins were heavily associated with BCR signalling pathways, antigen processing and endocytosis (Figure 15C).

In Experiment 7, 2125 proteins with 2 or more unique peptides were identified. 502 protein hits (23.6%) were exclusive to anti-IgM samples and 107 protein hits (5.1%) were exclusive to anti-CD71 samples, while both elutes shared 1516 protein hits (71.3%) (Figure 16A). There were some similarities to proteins found in Experiment 3 although a massive enrichment in proteins related to RNA processing and cell cycle regulation was seen (Transcriptional repressor CTCF, E3 ubiquitin-protein ligase RNF213). Proteins related to immune synapse were enriched compared to CD71 elutes.

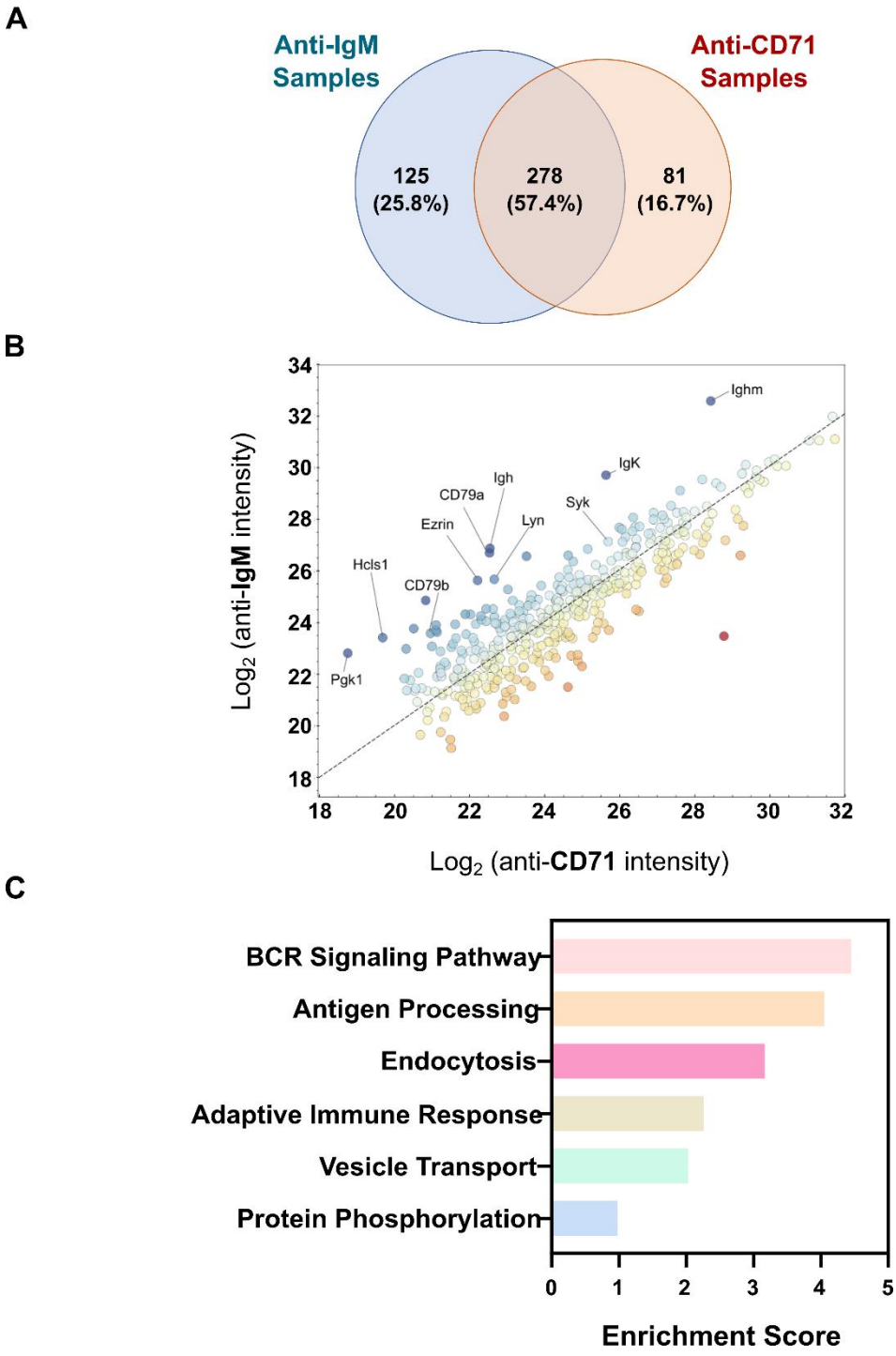

Figure 15. An example of the MS analysis of IS proteome (experiment 3). (***Preliminary Data).*** Proteins identified in MaxQuant run were filtered for potential contaminants, proteins only identified by site, reverse hits, and proteins with less than 2 unique peptides were removed. (A) In Venn Diagram, created in Venny software, proteins were distributed per sample where they were identified. (B) Protein enrichment analysis was produced in Perseus software taking in account the formula: Log2(Intensity of anti-IgM samples) – Log2(Intensity of anti-CD71 samples). Blue shades represented the proteins identified in anti-IgM samples and in yellow shades the proteins identified in anti-CD71 samples. (C) GO enrichment analysis was created using DAVID software. Proteins identified exclusively or enriched in anti-IgM samples were clustered in GO clusters attending their biological function.

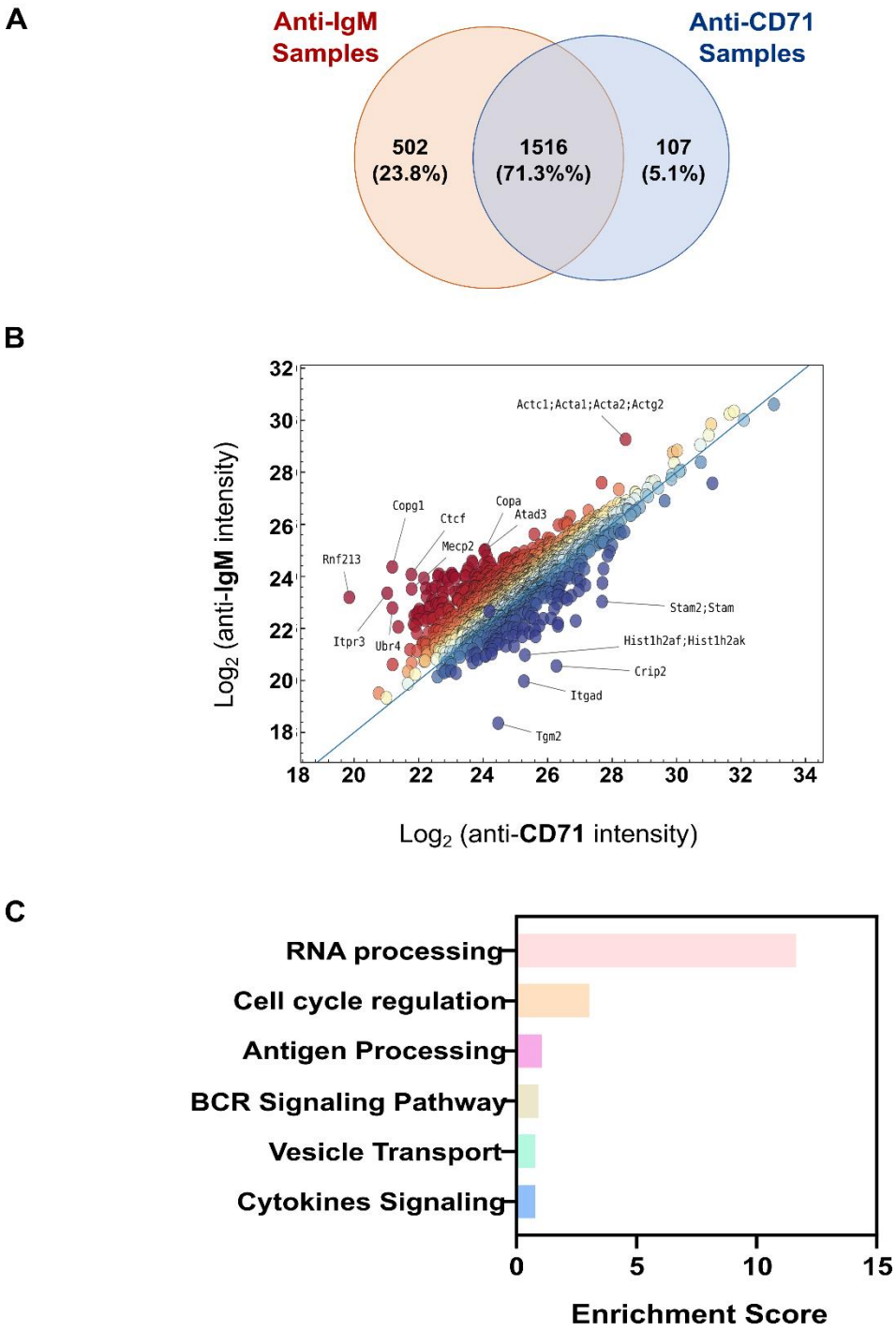

Figure 16 An example of the MS analysis of IS proteome (experiment 7). (***Preliminary Data)***. Proteins identified in MaxQuant run were filtered for potential contaminants, proteins only identified by site, reverse hits, and proteins with less than 2 unique peptides were removed. (A) In Venn Diagram, created in Venny software, proteins were distributed per sample where they were identified. (B) Protein enrichment analysis was produced in Perseus software taking in account the formula: Log2(Intensity of anti-IgM samples) – Log2(Intensity of anti-CD71 samples). Yellow shades represented the proteins identified in anti-IgM samples and in blue shades the proteins identified in anti-CD71 samples. (C) GO enrichment analysis was created using DAVID software. Proteins identified exclusively or enriched in anti-IgM samples were clustered in GO clusters attending their biological function.

3.4. Development of IS isolation in human

In order to optimise the synapse isolation protocol using human B cells, a B cell isolation protocol starting from buffy coats was first set up. Peripheral blood mononuclear cells (PBMCs) were isolated by density centrifugation from a buffy coat ordered from the Finnish Blood Bank. The isolated PBMC layer contained a heterogeneous lymphocyte population (T cells, B cells, and NK cells) along with dendritic cells and monocytes. In addition, a big percentage of erythrocytes was found in the PBMC fraction after washing (Figure 17A and 17E). In a buffy coat, the average portion of B cells was around 5–15% of the PBMCs (Figure 17A–D), and therefore B cell isolation was a crucial step in the protocol. After B cell isolation using a negative selection isolation kit, an enriched population (95%) of B cells based on CD19 staining was obtained Figure 17E–H).

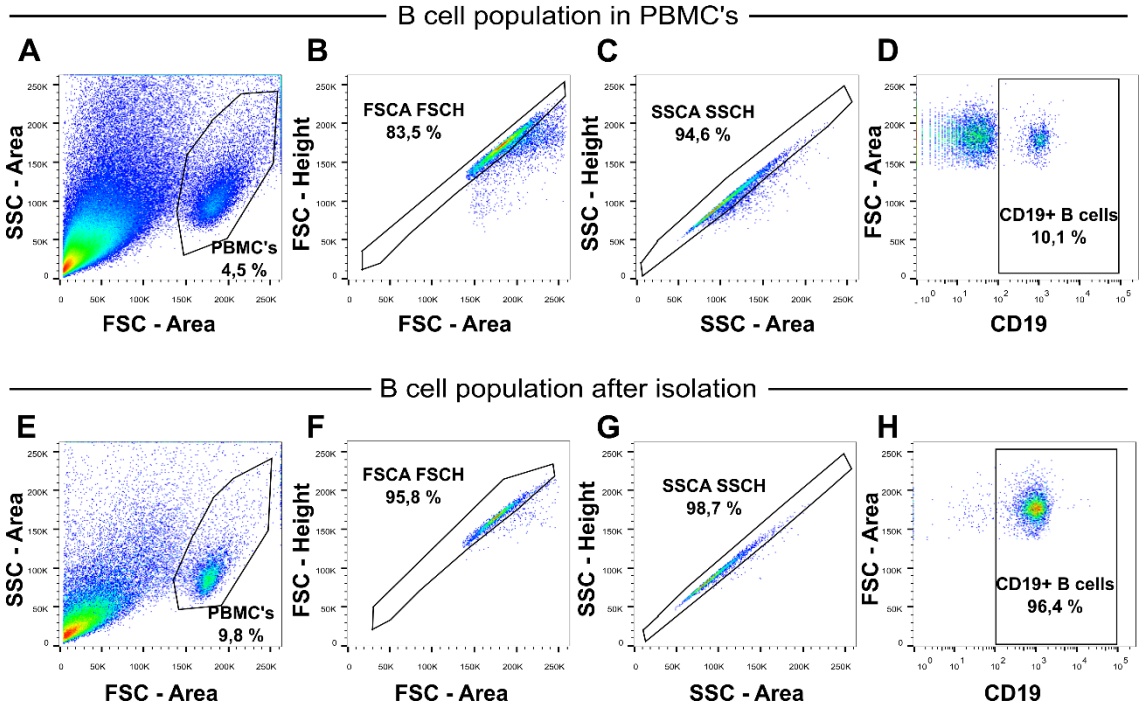

Figure 17. Gating strategy for FACS isolation of human B cells from PBMCs. Isolation efficiency for the human B cells was determined using flow cytometry. (A, E) FSC-Area vs SSC-area was used first to gate the PBMCs and discard erythrocytes and debris. (B, F) Using the PBMC gate, doublets were removed using FSC-Area vs FSC-Height. (C, G) Using the FSCA-FSCH gate, single cells were selected using SSC-Area vs SSC-Height. (D, H) Single cells were gated based on the CD19 staining and CD19+ cells were identified as B cells (10,1% before isolation and 96.4% after isolation).

As $(Fab')_2$ anti-human IgM was used to coat the beads, it was important to assess the percentage of IgM^+ cells in the blood. Hence, the immunoglobulin isotypes and the natural variability between donors was explored. PBMCs from 3 different healthy donors were isolated, 2 of which were from previous frozen PBMC's (Figure 18 A-B). Lymphocytes were gated as described in Figure 17. B cell populations (Figure 18 G-I) presented substantial changes between donors. First donor displayed a B cell population with more than 50% were solely IgD^+, and only 23% of the B cells were IgM^+ (Figure 18 G). The second donor presented a 46% B cell population composed of IgM^+ B cells (Figure 18 H). The third donor was characterized by a total population of IgM^+ B cells around 22% (Figure 18 I).

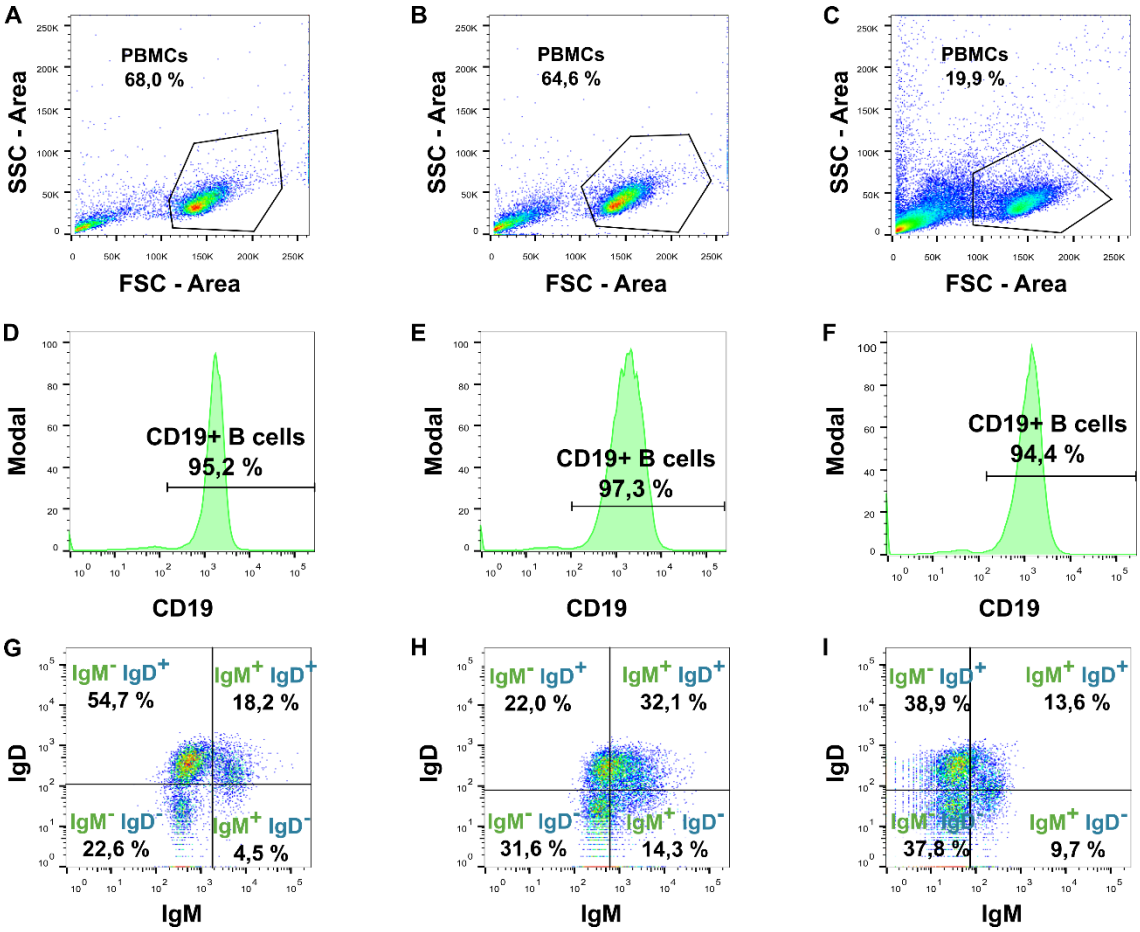

Figure 18. Gating strategy for FACS characterization of B cell population isotypes.. B cell population isotypes from 3 different donors were determined using flow cytometry. AF488 anti-human IgM was used to staining B cell IgM isotypes and Pacific Blue anti-human IgD to stain B cell IgD isotypes. The same gating strategy shown in Figure 17 (PBMCs -> singlets -> singlets -> B cells) was followed. (A, B, C) PBMCs, (D, E, F) B cells, and (G, H, I) B cell subpopulations based on IgM/IgD staining for three independent donors (n = 3).

Next, conjugation and activation of human B cells with coated beads was tested. Cell – bead conjugates were stained with phalloidin (F-actin) and phospho-Btk (pBtk; BCR signalling) and imaged with spinning disk confocal microscopy. The results showed cell activation when conjugates were formed with anti-IgM beads, but not with anti-CD71 beads. In IgM beads, pBTK and CD79a were enriched in the region where the cell was in contact with the bead (Figure 19A-B), contrary to anti-CD71 conjugates, where the localization of BTK and CD79a remained similar throughout the whole cell (Figure 19C-D). Actin protrusions, engulfing the bead, were also visible in anti-IgM which is typical of a spreading phase during IS (Figure 19A-B). Overall, in CD71 beads, actin protrusions were not seen (Figure 19C-E). Additionally, CD71 localization was also evenly distributed in the cell after conjugation (Figure 19E). Thus, there was no CD71 recruitment to the conjugation site, which suggested the conditions did not trigger any significant activation of cellular pathways. Table 3 shows the optimizations made in mouse and the progress made in human B cells until the date.

Table 3 – Control points in human IS protocol

Checkpoint	Tested in human
Coating Ligands	$F(ab')_2$ anti-human IgM, anti-human CD71
Ratio cell - bead	1:1
Cell – bead concentration	10 x 10^6cells/mL + 10 x 10^6beads/mL
Crosslinker Incubation Time	
Crosslinker Concentration	
Sonication Program	

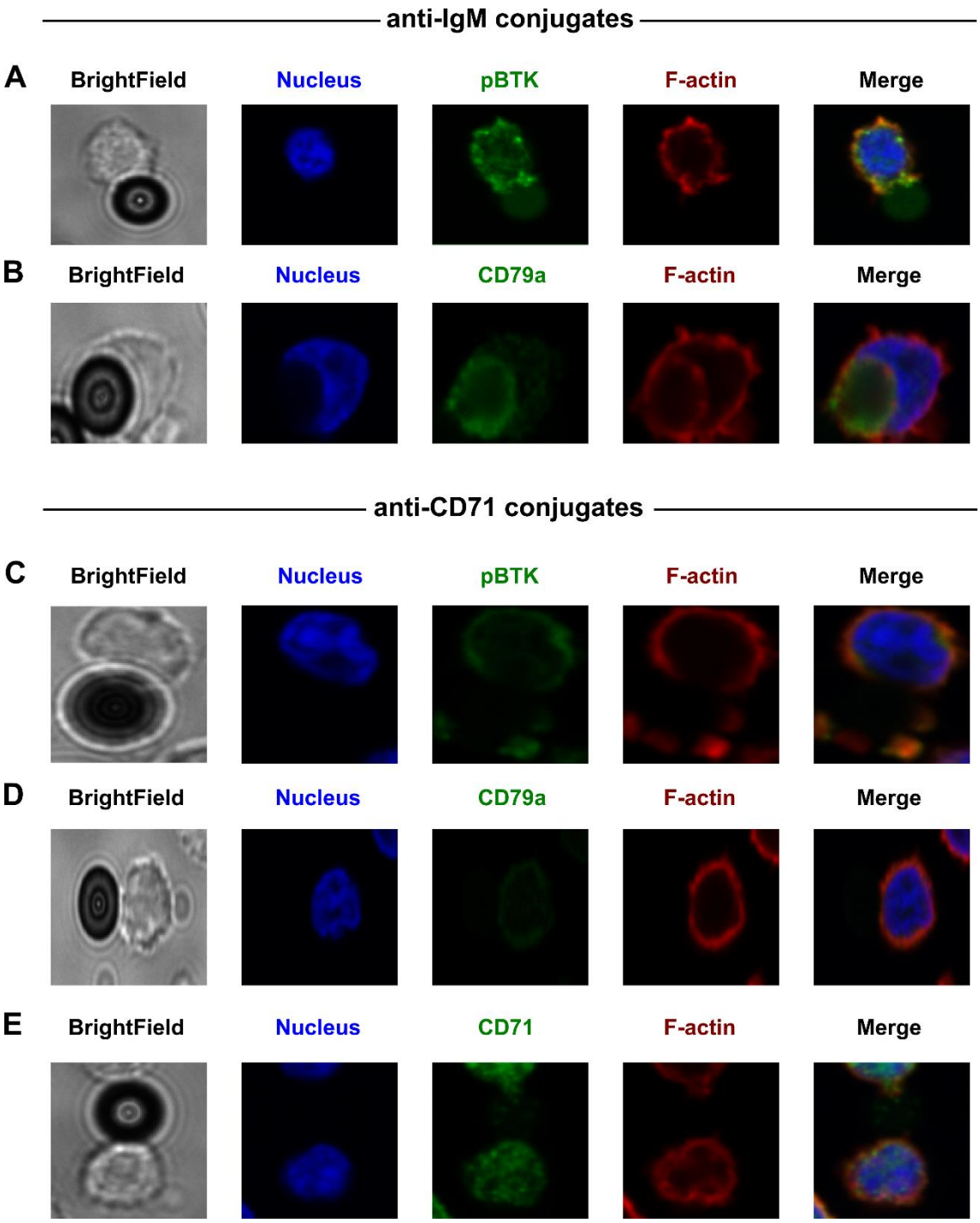

Figure 19. Spinning disk microscopy images from conjugation of human cells with anti-IgM beads and anti-CD71 beads. Human B cells were conjugated with (A, B) anti-IgM or (C, D, E) anti-CD71 coated beads as detailed before and stained with DAPI (nucleus, blue), phalloidin (F-actin, red) and anti-pBTK, anti-CD79a and anti-CD71 (AF488, green). Images were acquired using a 3i CSU-W1 spinning disk confocal microscope and processed in SlideBook6.

4. Discussion

The nature of BCR signalling and the transformations which B cells go through during activation are a topic of intensive studies. BCR signalling is a complex multi-step cascade involving a high number of players regulating not only signalling but also the actin cytoskeleton, vesicle trafficking, as well as antigen recognition and processing. MS has been used in the past to address some of the uncertainties behind protein recruitment to the BCR after activation (Awoniyi et al., BioRxiv; Li et al., 2019; Liu et al., 2020; Satpathy et al., 2015). However, these studies employed cell lines and only investigated the changes provoked by soluble antigen. While soluble antigen has been long known to trigger BCR signalling, antigen in surface-bound form has been highlighted in the recent years to lower the threshold of B cell activation and is now recognized as the main trigger of BCR activation *in vivo* (Batista et al., 2001; Carrasco et al., 2007). Importantly, the protocol developed in this thesis delivers new insights to BCR signalling and coordination, by unravelling proteins forming and locating at the immunological synapse in primary B cells. During this work, the development of the protocol to isolate IS proteins from mouse primary B cells was finalized and several steps also for the isolation of the human B cell IS were optimized.

4.1. Optimisation of the protocol using mouse cells

In order to develop a functional protocol, we ascertained 8 main control points: ligands for coating the magnetic beads, time and cell – bead ratio of conjugation, conjugate concentration, time and reagent concentration for DTBP crosslinking, and sonication programs.

Coating: In order to achieve B cell activation and IS formation, magnetic beads were coated with anti-IgM antibodies (goat anti-mouse IgM $F(ab')_2$ fragments) working as surrogate antigens (Arbogast et al., 2019; Donahue et al., 2003; Vitetta et al., 1980; Wortis et al., 1995). Different substrates that could promote B cell adhesion without prompting activation were tested. Fibrinogen (Grinnell et al., 1986; Narumlya et al., 1994), poly-L-lysine (Cohen et al., 1977; Mazia et al., 1975), transferrin (Neckers et al., 1985), anti-CD71 antibodies (Nagy-Baló et al., 2020) and anti-MHCII antibodies (Roche et al., 2015). Transferrin receptor protein 1 (TfR), or CD71, is a ubiquitous transmembrane receptor essential for transferrin uptake into the cells, and it has been used in the past as a control in B cell activation studies (Ketchum et al., 2018). A comparison between each ligand was carried out in terms of the success in coating of the beads without bead

aggregation and generating conjugates with the mouse primary B cells. Anti-CD71 coated beads were ultimately considered the best for non-activatory conjugates, as a clear and homogenous shift in the intensity levels was observed by FACS, similarly to the anti-IgM coated beads (Figure 8), and they produced the highest number of conjugates out of all control conditions tried (Figure 9).

Cell – bead ratio: For isolation of cytotoxic synapse components of NK cells, Meyer and associates used a cell-bead ratio of 1:2 (Jones et al. 2015). In mouse primary B cells, a 1:2 ratio yielded a high number of conjugates, but also major aggregates. After testing, a cell – bead ratio of 1:1 was selected as the best efficiency of single conjugates.

Cell concentration: Cell concentration was important to optimize for conjugation and sonication. A higher cell concentration was found to produce higher unspecific cell or bead aggregation. A cell concentration 10-20 million cells per mL, depending on the nature of the experiment, should have been appropriate to avoid this concern (Meyer et al, *submitted*). Although an increase of cell concentration was related to a drop in the conjugate formation efficiency (data not shown), the major impact was seen in sonication. A higher concentration was associated with a suboptimal sonication, allowing intact conjugates to remain in the samples even after washing. When eluting the proteins on the beads, proteins in the intact cells of the conjugates would also be eluted and lead to masking of the proteins specific for IS. Moreover, since eppendorf tubes were being used, the accessible volume for conjugation and sonication was limited (< 1.5 millilitres). Thus, we kept a cell concentration of 10 million cells per mL throughout the protocol.

Conjugation time: When talking about conjugation time, or IS formation time, the literature refers to a span of 5 minutes to 30 minutes from B cell spreading to a B cell contraction and, consequently, to the full maturation of the IS (Bello-Gamboa et al., 2019; Ibañez-Vega et al., 2019; Kuokkanen et al., 2015; Spillane et al., 2018). Due to the dynamic and spatiotemporally regulated segregation of the molecules involved in IS; different conjugation times can disclose distinct results. Since the objective was to uncover new molecules regulating the cytoskeletal organization, antigen extraction, vesicle trafficking and other signalling pathways conjugation time of 15 minutes was chosen, which could be considered as the moment when the synapse starts to mature after spreading and antigen extraction processes are activated. This time could be adjusted in future studies to investigate, for instance, early BCR signalling.

Time and concentration for DTBP incubation: In order to get the proteins recruited to the IS isolated, DTBP, a reversible membrane-permeable crosslinker, was employed. DTBP has been considered a powerful tool to stabilize protein-protein interactions in different biological settings. Regarding the time of crosslinking, the results showed a similar conjugate formation in the three conditions tested (Figure 10), so the shortest time of incubation (5 minutes) was selected for further testing to minimize excessive cross-linking that could lead to isolation of IS-unspecific proteins. Other than that, not much is known about the possible side-effects of the crosslinker on B cells. Our collaborator has successfully applied it to NK cells with a concentration of 5 mM (Meyer et al, *submitted)*, however, Jones et al showed that 3 mM concentration was enough for focal adhesion isolation (Jones et al. 2015) and another report showed that 0.5 mM should be enough for crosslinking the proteins in vicinity (Hammarén, 2012). Concentration of 0.5 mM (*data not shown*) was discarded as identified proteins were mainly consisted of background proteins such as keratins and histones, which indicated a crosslinking defect. MS experiments were proceeded with 2.5 mM and 5 mM to ascertain practical differences in protein retrieval and identification.

Sonication programme: Sonication proved to be sensitive for different conditions and extensive testing was required. The sonication was optimized to separate the cells from the beads but not to degrade the proteins crosslinked on the beads. In theory a medium intensity (200 W) sonication would be enough for shearing the plasma membrane (Islam et al., 2017; Pchelintsev et al., 2016), and a high intensity (320 W) sonication could lead to protein degradation. A higher cell concentration was also found to affect the sonication extent. Hence, both medium and high intensity sonication for 2-10 cycles (ON/OFF 30 seconds) were tested. The medium program achieved good results after >10 cycles. However, considering that the sonication was done in a cold bath and not in proper ice, and the sonication process itself generates heat, the protein integrity could be also damaged if the sonication went on for extended cycles. Hence, a high intensity program using 4-6 cycles was chosen and it yielded a high efficiency in removing the cells from the beads.

4.2. Validation of mouse IS isolation protocol

Conjugation efficiency with the non-activatory controls was found far from ideal: anti-IgM coated beads generated almost twice as much conjugates as anti-CD71 beads (Figure 9). Still, from the alternatives provided, the anti-CD71 beads presented the best outcome. Moreover, sonication settings were finetuned for efficient sonication without much protein loss, a glaring challenge of the protocol since only limited amount of protein was retrieved for the MS analysis. The small amount of retrieved protein also made the protein quantification problematic as well as challenged for MS analysis.

The pSyk/tSyk ratio was a clear indicator of successful cell activation upon conjugation with anti-IgM beads in comparison to anti-CD71 beads. The absence of GAPDH signal in the isolated IS samples indicated efficient exclusion of unspecific cytoplasmic proteins. Additionally, an enrichment of other signalling proteins was also confirmed on anti-IgM beads compared to anti-CD71 beads. This all indicated a successful optimization of the IS isolation protocol and allowed me to proceed to MS analysis.

4.3. Mouse immune synapse proteome analysis

The MS analyses of the IS proteome were executed throughout the development of the protocol. Initial 6 MS experiments were executed on a trial-and-error premise to assess which condition would be the most suited for our study. From a total of 8 MS experiments, three major changes must be discussed.

In experiment 1, the non-activatory control beads were coated with anti-MHCII antibodies instead of the anti-CD71 antibodies used in the following experiments. The results produced from the experiment were unsatisfactory and the number of proteins identified exclusively in anti-IgM samples was the least of all experiments.

Trypsin Digestion was a substantial point of optimization in MS sample preparation. In-gel digestion and on-bead digestion were compared. However, from on-bead digestion, the retrieved protein amount was found not sufficient for MS analysis. Thus, the in-gel digestion was preferred for further MS experiments. Trypsin is responsible for peptide bond hydrolysis, and a better enzyme penetration to the gel produces an increase in the number of peptides identified. Hence, to enhance trypsin activity, gel lanes were next cut in 3 bands that were then individually processed into smaller pieces for digestion. Indeed, experiments 7 and 8 had an average around

2000 unique peptides identified, while with limited digestion, these numbers fell down to 800 unique peptides identified. Nonetheless, the number of peptides exclusive to anti-IgM samples in experiment 7 (2.5 mM crosslinker concentration and extensive trypsin digestion) was close to percentage of the other experiments with limited digestion. Moreover, in the experiment 8 (5.0 mM crosslinker concentration and extensive trypsin digestion), the results showed a steep decrease in peptides identified exclusively in anti-IgM samples compared to the total number of peptides identified, suggesting excessive cross-linking decreasing the selectivity of the isolation.

The last optimization step was the concentration of DTBP. The two concentrations, 2.5 mM and 5 mM represented a massive difference in total proteins identified but not so much in proteins identified exclusively in IgM elutes. The higher DTBP concentration in the experiment 8 led to more proteins retrieved. However, better results were achieved when more efficient trypsin digestion was combined with a lower concentration of the crosslinker, in experiment 7. There, the total number of proteins identified was also very high but with better IS-specificity indicated by more proteins selectively in anti-IgM samples. Hence, 2.5 mM was determined as the optimal DTBP concentration.

Overall, the results pointed towards a successful protocol, even though the necessary biological replicates are needed for statistical analysis. In the pathway analysis of the data, proteins identified in at least 3 experiments were clustered in immune system processes, such as BCR signalling pathways and B cell differentiation (transcription factor EB, toll-like receptor 9, CD79b, complement receptor 2, CD79a) and protein phosphorylation (cyclin T1, G-protein-coupled receptor kinase, c-src tyrosine kinase, serine/threonine kinase 10, Janus kinase 1).

CD79a and CD79b, that form the integral signalling part of the BCR, were identified in anti-IgM samples only, proving trust to our analysis and to the specificity of the isolated IS. Alluding to this preliminary analysis, 4 proteins of interest were identified that could provide insightful information for BCR dynamics. Complement receptor type 2, CR2 or CD21, that clusters with CD19 and CD81 to form a coactivator complex coupled with BCR in mice that modulates Ca^{2+} response, cytokine production and enhance in B cell activation (Kovács et al., 2021; Killick et al., 2017). Cytoskeleton-associated protein 4, CKAP4, is a relatively unknown protein that acts as a cytoskeleton binding protein and a stabilizer of the endoplasmic reticulum. Its function has just started to get unveiled with implications in cancer, cell proliferation and migration (Li et al., 2021). Jak1, a tyrosine-protein kinase, is known to have a role in T cell immune synapse formation and maintenance of the adhesive contacts between APCs and T cells yet (Cascio et al., 2015; Howell

et al., 2019). Jak1 function in B cell is not described. Finally, intersectin-2 is a protein involved in B cell – T cell conjugation and an effector in TCR endocytosis. In B cells, an intersectin-2 deficiency has been shown to lead to an impairment in BCR engagement and cytoskeleton remodelling (Burbage et al., 2018; Malinova et al., 2020; McGavin et al., 2001).

Gene ontology analysis performed for two promising experiments with different trypsin digestion (experiment 3, limited digestion, and experiment 7, extensive digestion) also pointed for proteins involved in BCR signalling and protein phosphorylation. What is more, an enrichment of protein clusters in antigen processing, endocytosis and vesicle trafficking was shown in these experiments. The difference in the number of proteins identified in experiment 7 compared to experiment 3 is remarkable; 2125 vs 484. Nonetheless the difference in proteins identified was concentrated in RNA processing and cell cycle regulation. More biological replicates are needed to clarify our preliminary results.

4.4. Development of IS isolation protocol for human B cells

Isolation of human B cells from buffy coats, a protocol not attempted before in our lab, went according to plans as viable B cells were isolated with 95% purify. However, an important point to consider when using human primary B cells from donors was the variability in the BCR subtype expressed by the B cells, which is influenced by, for instance, the infection history and age of the donor. In 3 donors tested, the B lymphocyte isotypes differed greatly (Figure 18G-I). Since the anti-IgM coated beads were used to activate the cells, only IgM+ cells responded to the stimulus and formed the IS ultimately resulting in big differences in the protein yields caused by the percentage of IgM^+ B cells. B cell signalling is characterized by phosphorylation of key protein effectors, such as Btk, readily activating downstream cascades. The results showed a shift in the localization of CD79a and phosphorylated BTK to the contact site of the anti-IgM bead and the B cell, but not to the contact site of the anti-CD71 beads. Hence, human B cells were activated exclusively when conjugated with anti-IgM beads and not when conjugated with anti-CD71 beads, demonstrating that the protocol will also be applicable to human cells after more optimization to guarantee a sufficient protein yield for MS analysis.

5. Conclusions

In this study, we developed a novel pull-down technique to isolate the proteins recruited to the B cell immune synapse for proteomic analysis. We took advantage of the expertise of our group and our collaborators to establish a method to mimic an *in vivo* interaction between B cells and APCs in order to explore the mechanisms underlying B cell activation.

We first optimized the approach for mouse primary B cells, evaluating different parameters in every step of the protocol. MS experiments were performed over the course of optimization. While we could conjecture about the protein information gathered over each experiment, they were performed with different settings. Thus, statistical analysis and an in-depth consideration will have to wait until we have the necessary biological replicates with the optimized protocol.

The protocol optimization for the human B cells was carried out until the final control points. Owing to different BCR isotype frequencies and other possible slightly different cellular features, the optimal settings can differ between mouse and human B cells. Ultimately, human MS experiments should provide a valuable dataset for analysis and comparison to the mouse model and other IS pulldown datasets.

For the future, aside from performing the MS biological replicates for the mouse B cells and finalization of the protocol and the experiments for human B cells, analysis of the IS proteome is likely to lead to identification of new players potentially involved in BCR signalling pathways, as well as in the critical cell biological features of the IS, like the protein machineries regulating the cytoskeletal organization, antigen extraction or vesicle traffic. The interesting uncharacterized proteins identified in the B cell synapse will be further studied using immunological, cell biological and microscopy methodologies to characterize their specific functions in the B cell IS.

6. References

A, Caballero, Katkere B, Wen XY, Drake L, Nashar TO, and Drake JR. 2006. "Functional and Structural Requirements for the Internalization of Distinct BCR-Ligand Complexes." *European Journal of Immunology* 36(12):3131–45.

A, Lanzavecchia. 1987. "Antigen Uptake and Accumulation in Antigen-Specific B Cells." *Immunological Reviews* 99(1):39–51.

Alberts, Bruce, Alexander Johnson, Julian Lewis, Martin Raff, Keith Roberts, and Peter Walter. 2002b. "The Adaptive Immune System."

Amarante-Mendes, Gustavo P., Sandy Adjemian, Laura Migliari Branco, Larissa C. Zanetti, Ricardo Weinlich, and Karina R. Bortoluci. 2018. "Pattern Recognition Receptors and the Host Cell Death Molecular Machinery." *Frontiers in Immunology* 9(OCT):2379.

Anon. n.d. "-Venny-. Venn Diagrams for Comparing Lists. By Juan Carlos Oliveros." Retrieved July 19, 2021 (https://bioinfogp.cnb.csic.es/tools/venny_old/venny.php).

Arbogast, Florent, Johan Arnold, Philippe Hammann, Lauriane Kuhn, Johana Chicher, Diane Murera, Justine Weishaar, Sylviane Muller, Jean Daniel Fauny, and Frédéric Gros. 2019. "ATG5 Is Required for B Cell Polarization and Presentation of Particulate Antigens." *Autophagy* 15(2):280–94.

Avalos, Ana Maria, and Hidde Ploegh. 2014. "Early BCR Events and Antigen Capture, Processing, and Loading on MHC Class II on B Cells." *Frontiers in Immunology* 5(MAR):92.

Awoniyi, Luqman O., Vid Šuštar, Sara Hernández-Pérez, Marika Vainio, Alexey V. Sarapulov, Petar Petrov, and Pieta K. Mattila. "APEX2 Proximity Biotinylation Reveals Protein Dynamics Triggered by B Cell Receptor Activation." *BioRxiv* 2020.09.29.318766.

Baba, Yoshihiro, and Tomohiro Kurosaki. 2015. "Role of Calcium Signaling in B Cell Activation and Biology." *Current Topics in Microbiology and Immunology* 393:143–74.

Batista, F. D., D. Iber, and M. S. Neuberger. 2001. "B Cells Acquire Antigen from Target Cells after Synapse Formation." *Nature* 411(6836):489–94.

Batista, Facundo D., and Naomi E. Harwood. 2009. "The Who, How and Where of Antigen Presentation to B Cells." *Nature Reviews Immunology* 9(1):15–27.

Batista, Facundo D., and Michael S. Neuberger. 2000. "B Cells Extract and Present Immobilized Antigen: Implications for Affinity Discrimination." *EMBO Journal* 19(4):513–20.

Bello-Gamboa, A., J. M. Izquierdo, M. Velasco, S. Moreno, A. Garrido, L. Meyers, J. C. Palomino, V. Calvo, and M. Manuel Izquierdo. 2019. "Imaging the Human Immunological Synapse." *J. Vis.*

Exp(154):60312.

Blanchoin, Laurent, Rajaa Boujemaa-Paterski, Cécile Sykes, and Julie Plastino. 2014. "Actin Dynamics, Architecture, and Mechanics in Cell Motility." *Physiological Reviews* 94(1):235–63.

Bork, P., C. Sander, and A. Valencia. 1992. "An ATPase Domain Common to Prokaryotic Cell Cycle Proteins, Sugar Kinases, Actin, and Hsp70 Heat Shock Proteins." *Proceedings of the National Academy of Sciences of the United States of America* 89(16):7290–94.

Burbage, Marianne, Francesca Gasparrini, Shweta Aggarwal, Mauro Gaya, Johan Arnold, Usha Nair, Michael Way, Andreas Bruckbauer, and Facundo D. Batista. 2018. "Tuning of in Vivo Cognate B-T Cell Interactions by Intersectin 2 Is Required for Effective Anti-Viral B Cell Immunity." *ELife* 7.

Burrell, Christopher J., Colin R. Howard, and Frederick A. Murphy. 2017. "Innate Immunity." *Fenner and White's Medical Virology* 57–64.

Carrasco, Yolanda R. 2020. "Molecular Cues Involved in the Regulation of B Cell Dynamics: Assistants of Antigen Hunting." *Journal of Leukocyte Biology* 107(6):1107–13.

Carrasco, Yolanda R., and Facundo D. Batista. 2007. "B Cells Acquire Particulate Antigen in a Macrophage-Rich Area at the Boundary between the Follicle and the Subcapsular Sinus of the Lymph Node." *Immunity* 27(1):160–71.

Carrasco, Yolanda R., Sebastian J. Fleire, Thomas Cameron, Michael L. Dustin, and Facundo D. Batista. 2004. "LFA-1/ICAM-1 Interaction Lowers the Threshold of B Cell Activation by Facilitating B Cell Adhesion and Synapse Formation." *Immunity* 20(5):589–99.

Castro, Maria Angela Gomes de, Hanna Wildhagen, Shama Sograte-Idrissi, Christoffer Hitzing, Mascha Binder, Martin Trepel, Niklas Engels, and Felipe Opazo. 2019. "Differential Organization of Tonic and Chronic B Cell Antigen Receptors in the Plasma Membrane." *Nature Communications 2019 10:1* 10(1):1–11.

Catherman, Adam D., Owen S. Skinner, and Neil L. Kelleher. 2014. "Top Down Proteomics: Facts and Perspectives." *Biochemical and Biophysical Research Communications* 445(4):683–93.

Chaplin, David D. 2010. "Overview of the Immune Response." *Journal of Allergy and Clinical Immunology* 125(2 SUPPL. 2):S3.

Chaudhuri, Abhishek, Bhaswati Bhattacharya, Kripa Gowrishankar, Satyajit Mayor, and Madan Rao. 2011. "Spatiotemporal Regulation of Chemical Reactions by Active Cytoskeletal

Remodeling." *Proceedings of the National Academy of Sciences of the United States of America* 108(36):14825–30.

Cohen, C. M., D. I. Kalish, B. S. Jacobson, and D. Branton. 1977. "Membrane Isolation on Polylysine-Coated Beads. Plasma Membrane from HeLa Cells." *Journal of Cell Biology* 75(1):119–34.

Cox, Jürgen, and Matthias Mann. 2008. "MaxQuant Enables High Peptide Identification Rates, Individualized p.p.b.-Range Mass Accuracies and Proteome-Wide Protein Quantification." *Nature Biotechnology 2008 26:12* 26(12):1367–72.

DeFranco, Anthony L. 1997. "The Complexity of Signaling Pathways Activated by the BCR." *Current Opinion in Immunology* 9(3):296–308.

Dominguez, Roberto, and Kenneth C. Holmes. 2011. "Actin Structure and Function." *Annual Review of Biophysics* 40(1):169–86.

Donahue, Amber C., and David A. Fruman. 2003. "Proliferation and Survival of Activated B Cells Requires Sustained Antigen Receptor Engagement and Phosphoinositide 3-Kinase Activation." *The Journal of Immunology* 170(12):5851–60.

Donnelly, Daniel P., Catherine M. Rawlins, Caroline J. DeHart, Luca Fornelli, Luis F. Schachner, Ziqing Lin, Jennifer L. Lippens, Krishna C. Aluri, Richa Sarin, Bifan Chen, Carter Lantz, Wonhyeuk Jung, Kendall R. Johnson, Antonius Koller, Jeremy J. Wolff, Iain D. G. Campuzano, Jared R. Auclair, Alexander R. Ivanov, Julian P. Whitelegge, Ljiljana Paša-Tolić, Julia Chamot-Rooke, Paul O. Danis, Lloyd M. Smith, Yury O. Tsybin, Joseph A. Loo, Ying Ge, Neil L. Kelleher, and Jeffrey N. Agar. 2019. "Best Practices and Benchmarks for Intact Protein Analysis for Top-down Mass Spectrometry." *Nature Methods* 16(7):587–94.

Drake, James R. 2018. "The Immunobiology of Ubiquitin-Dependent B Cell Receptor Functions." *Molecular Immunology* 101:146–54.

Dykstra, Michelle, Anu Cherukuri, Hae Won Sohn, Shiang Jong Tzeng, and Susan K. Pierce. 2003. "Location Is Everything: Lipid Rafts and Immune Cell Signaling." *Annual Review of Immunology* 21:457–81.

Eng, Jimmy K., Ashley L. McCormack, and John R. Yates. 1994. "An Approach to Correlate Tandem Mass Spectral Data of Peptides with Amino Acid Sequences in a Protein Database." *Journal of the American Society for Mass Spectrometry* 5(11):976–89.

Erickson, Harold P. 2007. "Evolution of the Cytoskeleton." *BioEssays* 29(7):668–77.

F, Melchers, and Corbel C. 1983. "Studies on B-Cell Activation in Vitro." *Annales d'immunologie* 134D(1):63–73.

FD, Batista, and Neuberger MS. 1998. "Affinity Dependence of the B Cell Response to Antigen: A Threshold, a Ceiling, and the Importance of off-Rate." *Immunity* 8(6):751–59.

Feng, Yangyang, Yu Wang, Shaocun Zhang, Kabeer Haneef, and Wanli Liu. 2020. "Structural and Immunogenomic Insights into B-Cell Receptor Activation." *Journal of Genetics and Genomics* 47(1):27–35.

Fleire, S. J., J. P. Goldman, Y. R. Carrasco, M. Weber, D. Bray, and F. D. Batista. 2006. "B Cell Ligand Discrimination through a Spreading and Contraction Response." *Science* 312(5774):738–41.

Fletcher, Daniel A., and R. Dyche Mullins. 2010. "Cell Mechanics and the Cytoskeleton." *Nature* 463(7280):485–92.

Freeman, Spencer A., Victor Lei, May Dang-Lawson, Kensaku Mizuno, Calvin D. Roskelley, and Michael R. Gold. 2011. "Cofilin-Mediated F-Actin Severing Is Regulated by the Rap GTPase and Controls the Cytoskeletal Dynamics That Drive Lymphocyte Spreading and BCR Microcluster Formation." *The Journal of Immunology* 187(11):5887–5900.

Freitas, Antonio A., and Benedita Rocha. 2000. "POPULATION BIOLOGY OF LYMPHOCYTES: The Flight for Survival." *Annu. Rev. Immunol* 18:83–111.

Friess, Mario D., Kristyna Pluhackova, and Rainer A. Böckmann. 2018. "Structural Model of the MIgM B-Cell Receptor Transmembrane Domain From Self-Association Molecular Dynamics Simulations." *Frontiers in Immunology* 9:2947.

G, Cascio, Martín-Cófreces NB, Rodríguez-Frade JM, López-Cotarelo P, Criado G, Pablos JL, Rodríguez-Fernández JL, Sánchez-Madrid F, and Mellado M. 2015. "CXCL12 Regulates through JAK1 and JAK2 Formation of Productive Immunological Synapses." *Journal of Immunology (Baltimore, Md. : 1950)* 194(11):5509–19.

Gasparrini, Francesca, Christoph Feest, Andreas Bruckbauer, Pieta K. Mattila, Jennifer Müller, Lars Nitschke, Dennis Bray, and Facundo D. Batista. 2016. " Nanoscale Organization and Dynamics of the Siglec CD 22 Cooperate with the Cytoskeleton in Restraining BCR Signalling ." *The EMBO Journal* 35(3):258–80.

Gasteiger, Georg, Andrea D'Osualdo, David A. Schubert, Alexander Weber, Emanuela M. Bruscia, and Dominik Hartl. 2017. "Cellular Innate Immunity: An Old Game with New Players." *Journal of Innate Immunity* 9(2):111–25.

Geahlen, Robert L. 2009. "Syk and PTyr'd: Signaling through the B Cell Antigen Receptor." *Biochimica et Biophysica Acta - Molecular Cell Research* 1793(7):1115–27.

Goding, J. W. 1996. "7 - Introduction to Monoclonal Antibodies BT - Monoclonal Antibodies (Third

Edition)." 116–40.

Gonzalez, Segundo, Ana Pilar González-Rodríguez, Beatriz Suárez-Álvarez, Alejandro López-Soto, Leticia Huergo-Zapico, and Carlos Lopez-Larrea. 2011. "Conceptual Aspects of Self and Nonself Discrimination." *Self Nonself* 2(1):19.

Grinnell, Frederick, and Benjamin Geiger. 1986. "Interaction of Fibronectin-Coated Beads with Attached and Spread Fibroblasts. Binding, Phagocytosis, and Cytoskeletal Reorganization." *Experimental Cell Research*162(2):449–61.

Gundry, Rebekah L., Melanie Y. White, Christopher I. Murray, Lesley A. Kane, Qin Fu, Brian A. Stanley, and Jennifer E. Van Eyk. 2009. "Preparation of Proteins and Peptides for Mass Spectrometry Analysis in a Bottom-up Proteomics Workflow." *Current Protocols in Molecular Biology* CHAPTER(SUPPL. 88):Unit10.25.

Gupta, Neetu, Bernd Wollscheid, Julian D. Watts, Barbara Scheer, Ruedi Aebersold, and Anthony L. DeFranco. 2006. "Quantitative Proteomic Analysis of B Cell Lipid Rafts Reveals That Ezrin Regulates Antigen Receptor-Mediated Lipid Raft Dynamics." *Nature Immunology* 7(6):625–33.

Gupta, Nitin, Stephen Tanner, Navdeep Jaitly, Joshua N. Adkins, Mary Lipton, Robert Edwards, Margaret Romine, Andrei Osterman, Vineet Bafna, Richard D. Smith, and Pavel A. Pevzner. 2007. "Whole Proteome Analysis of Post-Translational Modifications: Applications of Mass-Spectrometry for Proteogenomic Annotation." *Genome Research*17(9):1362–77.

Hae, Won Sohn, Pavel Tolar, and Susan K. Pierce. 2008. "Membrane Heterogeneities in the Formation of B Cell Receptor-Lyn Kinase Microclusters and the Immune Synapse." *Journal of Cell Biology* 182(2):367–79.

Hamoudi, R. A., A. Appert, H. Ye, A. Ruskone-Fourmestraux, B. Streubel, A. Chott, M. Raderer, L. Gong, I. Wlodarska, C. De Wolf-Peeters, K. A. MacLennan, L. De Leval, P. G. Isaacson, and M. Q. Du. 2010. "Differential Expression of NF-B Target Genes in MALT Lymphoma with and without Chromosome Translocation: Insights into Molecular Mechanism." *Leukemia* 24(8):1487–97.

Hartwell, Leland H., John J. Hopfield, Stanislas Leibler, and Andrew W. Murray. 1999. "From Molecular to Modular Cell Biology." *Nature* 402(6761 SUPPL. 1):C47–52.

Howell, Michael D., Fiona I. Kuo, and Paul A. Smith. 2019. "Targeting the Janus Kinase Family in Autoimmune Skin Diseases." *Frontiers in Immunology* 10:2342.

Ibañez-Vega, Jorge, Danitza Fuentes, Jonathan Lagos, Jorge Cancino, and María Isabel Yuseff.

2019. "Studying Organelle Dynamics in B Cells during Immune Synapse Formation." *Journal of Visualized Experiments* 2019(148):59621.

Islam, Mohammed Shehadul, Aditya Aryasomayajula, and Ponnambalam Ravi Selvaganapathy. 2017. "A Review on Macroscale and Microscale Cell Lysis Methods." *Micromachines* 8(3).

Jones, Matthew C., Jonathan D. Humphries, Adam Byron, Angélique Millon-Frémillon, Joseph Robertson, Nikki R. Paul, Daniel H. J. Ng, Janet A. Askari, and Martin J. Humphries. 2015. "Isolation of Integrin-Based Adhesion Complexes." *Current Protocols in Cell Biology* 2015:9.8.1-9.8.15.

Jü rgen Roth, Heinz, Heinrich Schmidt-Gayk, Holger Weber, and Christoph Niederau. n.d. "Accuracy and Clinical Implications of Seven 25-Hydroxyvitamin D Methods Compared with Liquid Chromatography-Tandem Mass Spectrometry as a Reference."

Ketchum, Christina M., Xiaoyu Sun, Alexandra Suberi, John T. Fourkas, Wenxia Song, and Arpita Upadhyaya. 2018. "Subcellular Topography Modulates Actin Dynamics and Signaling in B-Cells." *Molecular Biology of the Cell* 29(14):1732.

KG, Kovács, Mácsik-Valent B, Matkó J, Bajtay Z, and Erdei A. 2021. "Revisiting the Coreceptor Function of Complement Receptor Type 2 (CR2, CD21); Coengagement With the B-Cell Receptor Inhibits the Activation, Proliferation, and Antibody Production of Human B Cells." *Frontiers in Immunology* 12.

Killick, Justin, Gregoire Morisse, Dirk Sieger, and Anne L. Astier. 2017. "Complement as a Regulator of Adaptive Immunity." *Seminars in Immunopathology 2017 40:1* 40(1):37–48.

Kneussel, Matthias, and Wolfgang Wagner. 2013. "Myosin Motors at Neuronal Synapses: Drivers of Membrane Transport and Actin Dynamics." *Nature Reviews Neuroscience* 14(4):233–47.

Kuokkanen, Elina, Vid Šuštar, and Pieta K. Mattila. 2015. "Molecular Control of B Cell Activation and Immunological Synapse Formation." *Traffic* 16(4):311–26.

Kurosaki, T., A. Maeda, M. Ishiai, A. Hashimoto, K. Inabe, and M. Takata. 2000. "Regulation of the Phospholipase C-Γ2 Pathway in B Cells." *Immunological Reviews* 176:19–29.

Kurosaki, Tomohiro. 2011. "Regulation of BCR Signaling." *Molecular Immunology* 48(11):1287–91.

LaRosa, David F., and Jordan S. Orange. 2008. "1. Lymphocytes." *Journal of Allergy and Clinical Immunology* 121(2):S364–69.

Lee, Jinmin, Prabuddha Sengupta, Joseph Brzostowski, Jennifer Lippincott-Schwartz, and Susan K. Pierce. 2017. "The Nanoscale Spatial Organization of B-Cell Receptors on Immunoglobulin M- and G-Expressing Human B-Cells." *Molecular Biology of the Cell*

28(4):511–23.

Li, Jingwen, Wei Yin, Yukai Jing, Danqing Kang, Lu Yang, Jiali Cheng, Ze Yu, Zican Peng, Xingbo Li, Yue Wen, Xizi Sun, Boxu Ren, and Chaohong Liu. 2019. "The Coordination between B Cell Receptor Signaling and the Actin Cytoskeleton during B Cell Activation." *Frontiers in Immunology* 10(JAN):1–13.

Li, Shuang-Xi, Juan Li, Li-Wei Dong, and Zhi-Yong Guo. 2021. "Cytoskeleton-Associated Protein 4, a Promising Biomarker for Tumor Diagnosis and Therapy." *Frontiers in Molecular Biosciences* 7:501.

Li, Xue Wen, Johanna S. Rees, Peng Xue, Hong Zhang, Samir W. Hamaia, Bailey Sanderson, Phillip E. Funk, Richard W. Farndale, Kathryn S. Lilley, Sarah Perrett, and Antony P. Jackson. 2014. "New Insights into the DT40 B Cell Receptor Cluster Using a Proteomic Proximity Labeling Assay." *Journal of Biological Chemistry* 289(21):14434–47.

Liu, Jun, Ying Wang, Qing Min, Ermeng Xiong, Birgitta Heyman, and Ji Yang Wang. 2020. *Regulation of Humoral Immune Responses and B Cell Tolerance by the IgM Fc Receptor (FcμR)*. Vol. 1254.

Liu, Wanli, Tobias Meckel, Pavel Tolar, Hae Won Sohn, and Susan K. Pierce. 2010. "Antigen Affinity Discrimination Is an Intrinsic Function of the B Cell Receptor." *Journal of Experimental Medicine* 207(5):1095–1111.

Liu, Wanli, Tobias Meckel, Pavel Tolar, Hae Won Sohn, and Susan K. Pierce. 2010. "Intrinsic Properties of Immunoglobulin IgG1 Isotype-Switched B Cell Receptors Promote Microclustering and the Initiation of Signaling." *Immunity* 32(6):778–89.

MA, Putnam, Moquin AE, Merrihew M, Outcalt C, Sorge E, Caballero A, Gondré-Lewis TA, and Drake JR. 2003. "Lipid Raft-Independent B Cell Receptor-Mediated Antigen Internalization and Intracellular Trafficking." *Journal of Immunology (Baltimore, Md. : 1950)* 170(2):905–12.

Malinova, Dessislava, Laabiah Wasim, Niklas Engels, and Pavel Tolar. 2020. "Endophilin A2 Regulates B Cell Protein Trafficking and Humoral Responses." *BioRxiv* 2020.04.20.050419.

Marshall, Jean S., Richard Warrington, Wade Watson, and Harold L. Kim. 2018. "An Introduction to Immunology and Immunopathology." *Allergy Asthma Clin Immunol* 14(2):49.

Matsumoto, Masaki, Koji Oyamada, Hidehisa Takahashi, Takamichi Sato, Shigetsugu Hatakeyama, and Keiichi I. Nakayama. 2009. "Large-Scale Proteomic Analysis of Tyrosine-Phosphorylation Induced by T-Cell Receptor or B-Cell Receptor Activation Reveals New

Signaling Pathways." *Proteomics* 9(13):3549–63.

Mattila, Pieta K., Facundo D. Batista, and Bebhinn Treanor. 2016. "Dynamics of the Actin Cytoskeleton Mediates Receptor Cross Talk: An Emerging Concept in Tuning Receptor Signaling." *Journal of Cell Biology* 212(3):267–80.

Mattila, Pieta K., Christoph Feest, David Depoil, Bebhinn Treanor, Beatriz Montaner, Kevin L. Otipoby, Robert Carter, Louis B. Justement, Andreas Bruckbauer, and Facundo D. Batista. 2013. "The Actin and Tetraspanin Networks Organize Receptor Nanoclusters to Regulate B Cell Receptor-Mediated Signaling." *Immunity* 38(3):461–74.

Mazia, Daniel, Gerald Schatten, and Winfield Sale. 1975. "Adhesion of Cells to Surfaces Coated with Polylysine: Applications to Electron Microscopy." *Journal of Cell Biology* 66(1):198–200.

McDonald, W. Hayes, and John R. Yates. 2002. "Shotgun Proteomics and Biomarker Discovery." *Disease Markers* 18(2):99–105.

McGavin, Mary K. H., Karen Badour, Lynne A. Hardy, Terrance J. Kubiseski, Jinyi Zhang, and Katherine A. Siminovitch. 2001. "The Intersectin 2 Adaptor Links Wiskott Aldrich Syndrome Protein (WASp)-Mediated Actin Polymerization to T Cell Antigen Receptor Endocytosis." *The Journal of Experimental Medicine* 194(12):1777.

Mogensen, Trine H. 2009. "Pathogen Recognition and Inflammatory Signaling in Innate Immune Defenses." *Clinical Microbiology Reviews* 22(2):240.

Nagy-Baló, Zsuzsa, Richárd Kiss, Alina Menge, Csaba Bödör, Zsuzsa Bajtay, and Anna Erdei. 2020. "Activated Human Memory B Lymphocytes Use CR4 (CD11c/CD18) for Adhesion, Migration, and Proliferation." *Frontiers in Immunology* 11:565458.

Narita, Akihiro, Toshiro Oda, and Yuichiro Maéda. 2011. "Structural Basis for the Slow Dynamics of the Actin Filament Pointed End." *EMBO Journal* 30(7):1230–37.

Narumlya, Seiji, Yoshiko Abe, Yasumichi Kita, Kensuke Miyake, Kiichiro Nakajima, Takushi X. Watanabe, Yoshihiro Oka, Haruo Sugiyama, Hideo Yagita, Ko Okumura, Toshiyuki Hamaoka, and Hlroml Fujlwara. 1994. "Pre-B Cells Adhere to Fibronectin via Interactions of Integrin A5/Av with RGDS as Well as of Integrin A4 with Two Distinct V Region Sequences at Its Different Binding Sites." *International Immunology* 6(1):139–47.

Neckers, L. M., G. Yenokida, J. B. Trepel, E. Lipford, and S. James. 1985. "Transferrin Receptor Induction Is Required for Human B-lymphocyte Activation but Not for Immunoglobulin Secretion." *Journal of Cellular Biochemistry* 27(4):377–89.

Nicholson, Lindsay B. 2016. "The Immune System." *Essays in Biochemistry* 60:275–301.

Nunes-Santos, Cristiane J., Gulbu Uzel, and Sergio D. Rosenzweig. 2019. "PI3K Pathway Defects Leading to Immunodeficiency and Immune Dysregulation." *Journal of Allergy and Clinical Immunology* 143(5):1676–87.

Okkenhaug, Klaus, and Jan A. Burger. 2015. "PI3K Signaling in Normal B Cells and Chronic Lymphocytic Leukemia (CLL)." *Current Topics in Microbiology and Immunology* 393:123–42.

P, Hou, Araujo E, Zhao T, Zhang M, Massenburg D, Veselits M, Doyle C, Dinner AR, and Clark MR. 2006. "B Cell Antigen Receptor Signaling and Internalization Are Mutually Exclusive Events." *PLoS Biology* 4(7):1147–58.

Pantaloni, D., C. Le Clainche, and M. F. Carlier. 2001. "Mechanism of Actin-Based Motility." *Science* 292(5521):1502–6.

Pchelintsev, Nikolay A., Peter D. Adams, and David M. Nelson. 2016. "Critical Parameters for Efficient Sonication and Improved Chromatin Immunoprecipitation of High Molecular Weight Proteins." *PLoS ONE* 11(1).

Pitt, James J. 2009. "Principles and Applications of Liquid Chromatography-Mass Spectrometry in Clinical Biochemistry." *The Clinical Biochemist. Reviews* 30(1):19–34.

Pollard, Thomas D., and John A. Cooper. 2009. "Actin, a Central Player in Cell Shape and Movement." *Science* 326(5957):1208–12.

Roche, Paul A., and Kazuyuki Furuta. 2015. "The Ins and Outs of MHC Class II-Mediated Antigen Processing and Presentation." *Nature Reviews Immunology* 15(4):203–16.

Satpathy, Shankha, Sebastian A. Wagner, Petra Beli, Rajat Gupta, Trine A. Kristiansen, Dessislava Malinova, Chiara Francavilla, Pavel Tolar, Gail A. Bishop, Bruce S. Hostager, and Chunaram Choudhary. 2015. " Systems-wide Analysis of BCR Signalosomes and Downstream Phosphorylation and Ubiquitylation ." *Molecular Systems Biology* 11(6):810.

Schamel, Wolfgang W. A., and Michael Reth. 2000. "Stability of the B Cell Antigen Receptor Complex." *Molecular Immunology* 37(5):253–59.

Schnyder, Tim, Angelo Castello, Christoph Feest, Naomi E. Harwood, Thomas Oellerich, Henning Urlaub, Michael Engelke, Jürgen Wienands, Andreas Bruckbauer, and Facundo D. Batista. 2011. "B Cell Receptor-Mediated Antigen Gathering Requires Ubiquitin Ligase Cbl and Adaptors Grb2 and Dok-3 to Recruit Dynein to the Signaling Microcluster." *Immunity* 34(6):905–18.

Shaheen, Samina, Zhengpeng Wan, Kabeer Haneef, Yingyue Zeng, Wang Jing, and Wanli Liu. 2019. *B Cell Mechanosensing: A Mechanistic Overview*. Vol. 144. 1st ed. Elsevier Inc.

Shevchenko, Andrej, Henrik Tomas, Jan Havliš, Jesper V. Olsen, and Matthias Mann. 2007. "In-Gel Digestion for Mass Spectrometric Characterization of Proteins and Proteomes." *Nature Protocols* 1(6):2856–60.

Shevchenko, Andrej, Matthias Wilm, Ole Vorm, and Matthias Mann. 1996. "Mass Spectrometric Sequencing of Proteins from Silver-Stained Polyacrylamide Gels." *Analytical Chemistry* 68(5):850–58.

Siegrist, Claire-Anne, and Richard Aspinall. 2009. "B-Cell Responses to Vaccination at the Extremes of Age." *Nature Reviews Immunology 2009 9:3* 9(3):185–94.

Sohn, Hae Won, Susan K. Pierce, and Shiang-Jong Tzeng. 2008. "Live Cell Imaging Reveals That the Inhibitory FcγRIIB Destabilizes B Cell Receptor Membrane-Lipid Interactions and Blocks Immune Synapse Formation." *The Journal of Immunology* 180(2):793–99.

Song, Wenxia, Chaohong Liu, Margaret K. Seeley-Fallen, Heather Miller, Christina Ketchum, and Arpita Upadhyaya. 2013. "Actin-Mediated Feedback Loops in B-Cell Receptor Signaling." *Immunological Reviews* 256(1):177–89.

Song, Wenxia, Chaohong Liu, and Arpita Upadhyaya. 2014. "The Pivotal Position of the Actin Cytoskeleton in the Initiation and Regulation of B Cell Receptor Activation." *Biochimica et Biophysica Acta - Biomembranes* 1838(2):569–78.

Spillane, Katelyn M., and Pavel Tolar. 2018. "Mechanics of Antigen Extraction in the B Cell Synapse." *Molecular Immunology* 101:319–28.

Strzyz, Paulina. 2018. "Breakdancing on Actin." *Nature Reviews Molecular Cell Biology* 19(8):485.

Switzar, Linda, Martin Giera, and Wilfried M. A. Niessen. 2013. "Protein Digestion: An Overview of the Available Techniques and Recent Developments." *Journal of Proteome Research* 12(3):1067–77.

T, Maity, Goswami S, Bhattacharya D, and Roy S. 2015. "Maity et Al. Reply." *Physical Review Letters* 114(9).

Thesis, M. Sc, and Henrik Hammarén. 2012. *SETTING UP METHODS FOR THE STUDY OF INTRACELLULAR MECHANOTRANSDUCTION*.

Tolar, Pavel. 2017. "Cytoskeletal Control of B Cell Responses to Antigens." *Nature Reviews Immunology 2017 17:10* 17(10):621–34.

Tolar, Pavel, Joseph Hanna, Peter D. Krueger, and Susan K. Pierce. 2009. "The Constant Region

of the Membrane Immunoglobulin Mediates B Cell-Receptor Clustering and Signaling in Response to Membrane Antigens." *Immunity* 30(1):44–55.

Tolar, Pavel, and Susan K. Pierce. 2010. "A Conformation-Induced Oligomerization Model for B Cell Receptor Microclustering and Signaling." *Current Topics in Microbiology and Immunology* 340(1):155.

Tolar, Pavel, Hae Won Sohn, and Susan K. Pierce. 2005. "The Initiation of Antigen-Induced B Cell Antigen Receptor Signaling Viewed in Living Cells by Fluorescence Resonance Energy Transfer." *Nature Immunology* 6(11):1168–76.

Treanor, Bebhinn. 2012. "B-Cell Receptor: From Resting State to Activate." *Immunology* 136(1):21–27.

Treanor, Bebhinn, David Depoil, Andreas Bruckbauer, and Facundo D. Batista. 2011. "Dynamic Cortical Actin Remodeling by ERM Proteins Controls BCR Microcluster Organization and Integrity." *Journal of Experimental Medicine* 208(5):1055–68.

Treanor, Bebhinn, David Depoil, Aitor Gonzalez-Granja, Patricia Barral, Michele Weber, Omer Dushek, Andreas Bruckbauer, and Facundo D. Batista. 2010. "The Membrane Skeleton Controls Diffusion Dynamics and Signaling through the B Cell Receptor." *Immunity* 32(2):187–99.

Turvey, Stuart E., David H. Broide, and M. B. Chb. 2009. "Chapter 2: Innate Immunity."

Tyanova, Stefka, Tikira Temu, Pavel Sinitcyn, Arthur Carlson, Marco Y. Hein, Tamar Geiger, Matthias Mann, and Jürgen Cox. 2016. "The Perseus Computational Platform for Comprehensive Analysis of (Prote)Omics Data." *Nature Methods 2016 13:9*13(9):731–40.

Vale, Andre M., Harry W. Schroeder, and Jr. 2010. "Clinical Consequences of Defects in B Cell Development." *The Journal of Allergy and Clinical Immunology* 125(4):778.

Varadé, Jezabel, Susana Magadán, and África González-Fernández. 2020. "Human Immunology and Immunotherapy: Main Achievements and Challenges." *Cellular and Molecular Immunology*.

Vinh, Joelle. 2019. "Proteomics and Proteoforms: Bottom-up or Top-down, How to Use High-Resolution Mass Spectrometry to Reach the Grail." Pp. 529–67 in *Fundamentals and Applications of Fourier Transform Mass Spectrometry*. Elsevier.

Vitetta, Ellen, ELLEN PURÉ, Peter Isakson, Linda Buck, and Jonathan Uhr. 1980. "The Activation of Murine B Cells: The Role of Surface Immunoglobulins." *Immunological Reviews*52(1):211–31.

W, Huang da, Sherman BT, and Lempicki RA. 2009. "Systematic and Integrative Analysis of Large Gene Lists Using DAVID Bioinformatics Resources." *Nature Protocols* 4(1):44–57.

Wang, Ji-Yang, ed. 2020. *B Cells in Immunity and Tolerance*. Vol. 1254. Singapore: Springer Singapore.

Wang, Jia C., Madison Bolger-Munro, and Michael R. Gold. 2018. "Visualizing the Actin and Microtubule Cytoskeletons at the B-Cell Immune Synapse Using Stimulated Emission Depletion (STED) Microscopy." *Journal of Visualized Experiments* 2018(134).

Warrington, Richard, Wade Watson, Harold L. Kim, and Francesca Romana Antonetti. 2011. "An Introduction to Immunology and Immunopathology." *Allergy, Asthma & Clinical Immunology 2011 7:1* 7(1):1–8.

Whiteaker, Jeffrey R., Lei Zhao, Heidi Y. Zhang, Li Chia Feng, Brian D. Piening, Leigh Anderson, and Amanda G. Paulovich. 2007. "Antibody-Based Enrichment of Peptides on Magnetic Beads for Mass-Spectrometry-Based Quantification of Serum Biomarkers." *Analytical Biochemistry* 362(1):44–54.

Wickstead, Bill, and Keith Gull. 2011. "The Evolution of the Cytoskeleton." *Journal of Cell Biology* 194(4):513–25.

Wiesner, Sebastian, Emmanuele Helfer, Dominique Didry, Guylaine Ducouret, Françoise Lafuma, Marie France Carlier, and Dominique Pantaloni. 2003. "A Biomimetic Motility Assay Provides Insight into the Mechanism of Actin-Based Motility." *Journal of Cell Biology* 160(3):387–98.

Wolters, D. A., M. P. Washburn, and J. R. Yates. 2001. "An Automated Multidimensional Protein Identification Technology for Shotgun Proteomics." *Analytical Chemistry* 73(23):5683–90.

Wortis, Henry H., Mark Teutsch, Mindy Higer, Jenny Zheng, and David C. Parkert. 1995. *B-Cell Activation by Crosslinking of Surface IgM or Ligation of CD40 Involves Alternative Signal Pathways and Results in Different B-Cell Phenotypes*. Vol. 92.

Yang, Jianying, and Michael Reth. 2010. "The Dissociation Activation Model of B Cell Antigen Receptor Triggering." *FEBS Letters* 584(24):4872–77.

Yasuda, Tomoharu. 2015. "MAP Kinase Cascades in Antigen Receptor Signaling and Physiology." *Current Topics in Microbiology and Immunology* 393:211–31.

7. Supplementary data

There are:				
1	proteins appearing in 6 lists			
1	proteins appearing in 5 lists			
12	proteins appearing in 4 lists			
88	proteins appearing in 3 lists			
389	proteins appearing in 2 lists			
1420	proteins appearing in 1 lists			
Protein code	Appearances	Lists	Short Name	Full Name
P19070	6	23456	CR2	Complement receptor type 2
Q80U78	5	3467	PUM1	Pumilio homolog 1 {ECO:0000305}
P63260	4	234	ACTG	Actin, cytoplasmic 2
P52332	4	3457	JAK1	Tyrosine-protein kinase JAK1
P11911	4	234	CD79A	B-cell antigen receptor complex-associated protein alpha chain
Q9Z0R6	4	346	ITSN2	Intersectin-2
P48962	4	1356	ADT1	ADP/ATP translocase 1 {ECO:0000305}
Q64518	4	3456	AT2A3	Sarcoplasmic/endoplasmic reticulum calcium ATPase 3
Q8BMK4	4	2467	CKAP4	Cytoskeleton-associated protein 4
P01750	4	234	HVM06	Ig heavy chain V region 102
Q9JJD0	4	3467	THA11	THAP domain-containing protein 11
P01845	4	2346	LAC3	Ig lambda-3 chain C region
Q69Z99	4	1567	ZN512	Zinc finger protein 512
O70503	4	1346	DHB12	Very-long-chain 3-oxoacyl-CoA reductase {ECO:0000305}
Q9Z331	3	345	K2C6B	Keratin, type II cytoskeletal 6B
Q8CGP1	3	245	H2B1K	Histone H2B type 1-K
P10854	3	567	H2B1M	Histone H2B type 1-M
P68368	3	234	TBA4A	Tubulin alpha-4A chain
Q61765	3	145	K1H1	Keratin, type I cuticular Ha1
Q8BFU2	3	136	H2A3	Histone H2A type 3
Q49714	3	245	KRT35	Keratin, type I cuticular Ha5 {ECO:0000250|UniProtKB:Q92764}
Q91W86	3	567	VPS11	Vacuolar protein sorting-associated protein 11 homolog

Q9EQU3	3	46	TLR9	Toll-like receptor 9
P62264	3	36	RS14	40S ribosomal protein S14
Q8CIS0	3	56	CAR11	Caspase recruitment domain-containing protein 11 {ECO:0000303|PubMed:12356734}
Q61033	3	346	LAP2A	Lamina-associated polypeptide 2, isoforms alpha/zeta
Q9WU78	3	234	PDC6I	Programmed cell death 6-interacting protein
Q80U16	3	456	RIPR2	Rho family-interacting cell polarization regulator 2 {ECO:0000250|UniProtKB:Q9Y4F9}
P31001	3	267	DESM	Desmin
P01644	3	234	KV5AB	Ig kappa chain V-V region HP R16.7
Q6IFX3	3	567	K1C40	Keratin, type I cytoskeletal 40
Q3U9G9	3	125	LBR	Delta(14)-sterol reductase LBR
P15530	3	45	CD79B	B-cell antigen receptor complex-associated protein beta chain
Q9WUU7	3	234	CATZ	Cathepsin Z
Q8CDG3	3	56	VCIP1	Deubiquitinating protein VCPIP1 {ECO:0000305}
Q9ERU3	3	135	ZNF22	Zinc finger protein 22
Q6NZN0	3	356	RBM26	RNA-binding protein 26
Q8R550	3	234	SH3K1	SH3 domain-containing kinase-binding protein 1
P41241	3	234	CSK	Tyrosine-protein kinase CSK
P62830	3	45	RL23	60S ribosomal protein L23
Q64727	3	345	VINC	Vinculin
P01631	3	246	KV2A7	Ig kappa chain V-II region 26-10
Q05CL8	3	156	LARP7	La-related protein 7 {ECO:0000303|PubMed:23154982}
Q60902	3	234	EP15R	Epidermal growth factor receptor substrate 15-like 1
Q9CZU6	3	234	CISY	Citrate synthase, mitochondrial
Q8JZU2	3	137	TXTP	Tricarboxylate transport protein, mitochondrial {ECO:0000250|UniProtKB:P53007}
Q9ER69	3	457	FL2D	Pre-mRNA-splicing regulator WTAP {ECO:0000305}
P62317	3	47	SMD2	Small nuclear ribonucleoprotein Sm D2
F7BJB9	3	145	MORC3	MORC family CW-type zinc finger protein 3 {ECO:0000250|UniProtKB:Q14149}
Q9ERL7	3	67	GMFG	Glia maturation factor gamma
Q5SFM8	3	456	RBM27	RNA-binding protein 27
P62245	3	57	RS15A	40S ribosomal protein S15a
O70293	3	45	GRK6	G protein-coupled receptor kinase 6
O08573	3	234	LEG9	Galectin-9
Q9R210	3	567	TFEB	Transcription factor EB {ECO:0000303|PubMed:10036191}

A2AGT5	3	456	CKAP5	Cytoskeleton-associated protein 5
Q9JLF6	3	134	TGM1	Protein-glutamine gamma-glutamyltransferase K
P97789	3	456	XRN1	5'-3' exoribonuclease 1
Q9QXB9	3	67	DRG2	Developmentally-regulated GTP-binding protein 2
Q9CY27	3	134	TECR	Very-long-chain enoyl-CoA reductase {ECO:0000305}
Q9JK81	3	56	MYG1	MYG1 exonuclease {ECO:0000305}
Q9WUM5	3	245	SUCA	Succinate--CoA ligase [ADP/GDP-forming] subunit alpha, mitochondrial {ECO:0000255|HAMAP-Rule:MF_03222}
Q9R0Q6	3	35	ARC1A	Actin-related protein 2/3 complex subunit 1A
O55098	3	234	STK10	Serine/threonine-protein kinase 10
Q3U1G5	3	156	I20L2	Interferon-stimulated 20 kDa exonuclease-like 2
Q8JZQ9	3	34	EIF3B	Eukaryotic translation initiation factor 3 subunit B {ECO:0000255|HAMAP-Rule:MF_03001}
P58462	3	246	FOXP1	Forkhead box protein P1
Q6P9R4	3	456	ARHGI	Rho guanine nucleotide exchange factor 18
Q91YX0	3	56	THMS2	Protein THEMIS2 {ECO:0000305}
P01639	3	246	KV5A7	Ig kappa chain V-V region MOPC 41
Q80U58	3	467	PUM2	Pumilio homolog 2
Q8BJS4	3	124	SUN2	SUN domain-containing protein 2
P83887	3	57	TBG1	Tubulin gamma-1 chain
Q8BYZ1	3	67	ABI3	ABI gene family member 3
Q8C9V1	3	567	TB10C	Carabin
Q9QWV9	3	357	CCNT1	Cyclin-T1
Q9D735	3	267	TRIR	Telomerase RNA component interacting RNase {ECO:0000312|MGI:MGI:1922833}
Q8R0S2	3	457	IQEC1	IQ motif and SEC7 domain-containing protein 1
Q3V3V9	3	346	CARL2	Capping protein, Arp2/3 and myosin-I linker protein 2 {ECO:0000250|UniProtKB:Q6F5E8}
Q924L1	3	345	LTMD1	LETM1 domain-containing protein 1
Q8BHS3	3	125	RBM22	Pre-mRNA-splicing factor RBM22
Q5DTM8	3	156	BRE1A	E3 ubiquitin-protein ligase BRE1A
Q91VI7	3	234	RINI	Ribonuclease inhibitor
Q9ESX5	3	134	DKC1	H/ACA ribonucleoprotein complex subunit DKC1
P12815	3	67	PDCD6	Programmed cell death protein 6
P97379	3	346	G3BP2	Ras GTPase-activating protein-binding protein 2
Q9D2E2	3	156	TOE1	Target of EGR1 protein 1
Q8BY71	3	567	HAT1	Histone acetyltransferase type B catalytic subunit

Q8BJ05	3	146	ZC3HE	Zinc finger CCCH domain-containing protein 14
O35177	3	356	CASL	Enhancer of filamentation 1
Q9CR62	3	156	M2OM	Mitochondrial 2-oxoglutarate/malate carrier protein
Q8K4P0	3	145	WDR33	pre-mRNA 3' end processing protein WDR33
Q9ES28	3	567	ARHG7	Rho guanine nucleotide exchange factor 7
Q6PCM2	3	467	INT6	Integrator complex subunit 6
Q8BKJ9	3	467	SIR7	NAD-dependent protein deacetylase sirtuin-7
Q91W39	3	135	NCOA5	Nuclear receptor coactivator 5
Q9CQM9	3	456	GLRX3	Glutaredoxin-3
Q8CBY8	3	567	DCTN4	Dynactin subunit 4
Q61249	3	567	IGBP1	Immunoglobulin-binding protein 1
Q920Q6	3	467	MSI2H	RNA-binding protein Musashi homolog 2
Q3UMC0	3	456	AFG2H	ATPase family protein 2 homolog {ECO:0000305}
Q8VBV3	3	567	EXOS2	Exosome complex component RRP4
Q8BGZ7	2	15	K2C75	Keratin, type II cytoskeletal 75
Q922F4	2	57	TBB6	Tubulin beta-6 chain
Q64475	2	6	H2B1B	Histone H2B type 1-B
Q9ERE2	2	45	KRT81	Keratin, type II cuticular Hb1 {ECO:0000250|UniProtKB:Q14533}
Q9Z2T6	2	15	KRT85	Keratin, type II cuticular Hb5
Q6NS46	2	56	RRP5	Protein RRP5 homolog
Q9Z0N2	2	47	IF2H	Eukaryotic translation initiation factor 2 subunit 3, Y-linked
P62315	2	67	SMD1	Small nuclear ribonucleoprotein Sm D1
Q9D2U9	2	4	H2B3A	Histone H2B type 3-A
P48678	2	13	LMNA	Prelamin-A/C
P68404	2	24	KPCB	Protein kinase C beta type
Q99P88	2	16	NU155	Nuclear pore complex protein Nup155
Q8VHX6	2	57	FLNC	Filamin-C
P16546	2	24	SPTN1	Spectrin alpha chain, non-erythrocytic 1
Q6IMF0	2	35	KRT87	Keratin, type II cuticular 87
P20444	2	47	KPCA	Protein kinase C alpha type
Q3UMF0	2	4	COBL1	Cordon-bleu protein-like 1 {ECO:0000305}
Q91WM3	2	67	U3IP2	U3 small nucleolar RNA-interacting protein 2
Q61696	2	36	HS71A	Heat shock 70 kDa protein 1A

B1AY13	2	56	UBP24	Ubiquitin carboxyl-terminal hydrolase 24
Q9DAW6	2	14	PRP4	U4/U6 small nuclear ribonucleoprotein Prp4
Q80YV3	2	56	TRRAP	Transformation/transcription domain-associated protein
P01899	2	4	HA11	H-2 class I histocompatibility antigen, D-B alpha chain
Q9Z1N5	2	14	DX39B	Spliceosome RNA helicase Ddx39b
P86048	2	7	RL10L	60S ribosomal protein L10-like
P17156	2	56	HSP72	Heat shock-related 70 kDa protein 2
Q9CYI4	2	37	LUC7L	Putative RNA-binding protein Luc7-like 1
Q9DBG3	2	24	AP2B1	AP-2 complex subunit beta
Q9JHR7	2	37	IDE	Insulin-degrading enzyme
P14438	2	2	HA2U	H-2 class II histocompatibility antigen, A-U alpha chain
Q80VH0	2	34	BANK1	B-cell scaffold protein with ankyrin repeats
P68433	2	57	H31	Histone H3.1
P16277	2	24	BLK	Tyrosine-protein kinase Blk
P41105	2	4	RL28	60S ribosomal protein L28
E9PVA8	2	56	GCN1	eIF-2-alpha kinase activator GCN1 {ECO:0000305}
P14131	2	6	RS16	40S ribosomal protein S16
P10630	2	35	IF4A2	Eukaryotic initiation factor 4A-II
Q99KH8	2	47	STK24	Serine/threonine-protein kinase 24
Q8K3G5	2	34	VRK3	Inactive serine/threonine-protein kinase VRK3
Q61191	2	14	HCFC1	Host cell factor 1
Q8BNW9	2	67	KBTBB	Kelch repeat and BTB domain-containing protein 11
Q69ZN7	2	56	MYOF	Myoferlin
Q8CAQ8	2	14	MIC60	MICOS complex subunit Mic60
P70318	2	4	TIAR	Nucleolysin TIAR
P17427	2	23	AP2A2	AP-2 complex subunit alpha-2
Q9Z277	2	16	BAZ1B	Tyrosine-protein kinase BAZ1B
Q5KU39	2	67	VPS41	Vacuolar protein sorting-associated protein 41 homolog
Q99JX4	2	5	EIF3M	Eukaryotic translation initiation factor 3 subunit M {ECO:0000255|HAMAP-Rule:MF_03012}
Q99KI0	2	24	ACON	Aconitate hydratase, mitochondrial
P27546	2	34	MAP4	Microtubule-associated protein 4
O35218	2	15	CPSF2	Cleavage and polyadenylation specificity factor subunit 2
E9PVX6	2	16	KI67	Proliferation marker protein Ki-67 {ECO:0000305}

Q7TNG5	2	67	EMAL2	Echinoderm microtubule-associated protein-like 2
Q7TMF3	2	7	NDUAC	NADH dehydrogenase [ubiquinone] 1 alpha subcomplex subunit 12
Q5S006	2	56	LRRK2	Leucine-rich repeat serine/threonine-protein kinase 2
Q8BFR5	2	24	EFTU	Elongation factor Tu, mitochondrial
Q80UM7	2	45	MOGS	Mannosyl-oligosaccharide glucosidase
P17742	2	34	PPIA	Peptidyl-prolyl cis-trans isomerase A
Q8JZX4	2	56	SPF45	Splicing factor 45
Q9CQN1	2	35	TRAP1	Heat shock protein 75 kDa, mitochondrial
Q8CG46	2	67	SMC5	Structural maintenance of chromosomes protein 5
Q8JZN5	2	5	ACAD9	Complex I assembly factor ACAD9, mitochondrial {ECO:0000250|UniProtKB:Q9H845}
Q6DIC0	2	16	SMCA2	Probable global transcription activator SNF2L2
Q9WVG6	2	67	CARM1	Histone-arginine methyltransferase CARM1
Q80X90	2	35	FLNB	Filamin-B
P47757	2	24	CAPZB	F-actin-capping protein subunit beta
O08539	2	25	BIN1	Myc box-dependent-interacting protein 1
P59999	2	34	ARPC4	Actin-related protein 2/3 complex subunit 4
A2ASS6	2	47	TITIN	Titin
P68040	2	23	RACK1	Receptor of activated protein C kinase 1
Q99MR6	2	14	SRRT	Serrate RNA effector molecule homolog
Q9WV55	2	45	VAPA	Vesicle-associated membrane protein-associated protein A
P62320	2	6	SMD3	Small nuclear ribonucleoprotein Sm D3
P08113	2	23	ENPL	Endoplasmin
P62962	2	35	PROF1	Profilin-1
Q80X82	2	36	SYMPK	Symplekin
Q9ER64	2	67	OSBL5	Oxysterol-binding protein-related protein 5
E9Q3L2	2	36	PI4KA	Phosphatidylinositol 4-kinase alpha
P09103	2	37	PDIA1	Protein disulfide-isomerase
Q9JHJ0	2	4	TMOD3	Tropomodulin-3
P59326	2	46	YTHD1	YTH domain-containing family protein 1 {ECO:0000305}
Q6ZQ03	2	57	FNBP4	Formin-binding protein 4
Q63932	2	7	MP2K2	Dual specificity mitogen-activated protein kinase kinase 2
Q03141	2	34	MARK3	MAP/microtubule affinity-regulating kinase 3
Q8JZQ2	2	56	AFG32	AFG3-like protein 2 {ECO:0000305}

Q9Z315	2	16	SNUT1	U4/U6.U5 tri-snRNP-associated protein 1
Q9WUM3	2	24	COR1B	Coronin-1B
Q8CCF0	2	34	PRP31	U4/U6 small nuclear ribonucleoprotein Prp31
P80318	2	24	TCPG	T-complex protein 1 subunit gamma
O35286	2	14	DHX15	Pre-mRNA-splicing factor ATP-dependent RNA helicase DHX15 {ECO:0000250|UniProtKB:043143}
Q9ERN0	2	4	SCAM2	Secretory carrier-associated membrane protein 2
P62911	2	67	RL32	60S ribosomal protein L32
O35892	2	14	SP100	Nuclear autoantigen Sp-100
Q8VE37	2	12	RCC1	Regulator of chromosome condensation
Q08879	2	24	FBLN1	Fibulin-1
Q99LX0	2	25	PARK7	Parkinson disease protein 7 homolog {ECO:0000305}
P22682	2	67	CBL	E3 ubiquitin-protein ligase CBL
P61327	2	5	MGN	Protein mago nashi homolog
Q569Z6	2	13	TR150	Thyroid hormone receptor-associated protein 3
Q8BVW3	2	34	TRI14	Tripartite motif-containing protein 14
Q9CVB6	2	23	ARPC2	Actin-related protein 2/3 complex subunit 2
Q91VR5	2	14	DDX1	ATP-dependent RNA helicase DDX1
Q9JMD0	2	1	ZN207	BUB3-interacting and GLEBS motif-containing protein ZNF207 {ECO:0000250|UniProtKB:043670}
P48725	2	56	PCNT	Pericentrin
P35492	2	36	HUTH	Histidine ammonia-lyase
P45481	2	45	CBP	Histone lysine acetyltransferase CREBBP
O35134	2	67	RPA1	DNA-directed RNA polymerase I subunit RPA1
Q3U7R1	2	24	ESYT1	Extended synaptotagmin-1
Q9D287	2	45	SPF27	Pre-mRNA-splicing factor SPF27
P40201	2	67	CHD1	Chromodomain-helicase-DNA-binding protein 1
P57780	2	24	ACTN4	Alpha-actinin-4 {ECO:0000305}
Q7JJ13	2	16	BRD2	Bromodomain-containing protein 2
Q9CYA6	2	57	ZCHC8	Zinc finger CCHC domain-containing protein 8
Q80UW8	2	5	RPAB1	DNA-directed RNA polymerases I, II, and III subunit RPABC1
P80313	2	24	TCPH	T-complex protein 1 subunit eta
Q9EPU4	2	14	CPSF1	Cleavage and polyadenylation specificity factor subunit 1
Q8VH51	2	1	RBM39	RNA-binding protein 39
Q9JLJ2	2	23	AL9A1	4-trimethylaminobutyraldehyde dehydrogenase

Q8C147	2	34	DOCK8	Dedicator of cytokinesis protein 8
Q02053	2	14	UBA1	Ubiquitin-like modifier-activating enzyme 1
P0CG14	2	26	DERPC	Decreased expression in renal and prostate cancer protein {ECO:0000250|UniProtKB:P0CG12}
P0DP26	2	36	CALM1	Calmodulin-1 {ECO:0000250|UniProtKB:P0DP23}
Q3U1J4	2	14	DDB1	DNA damage-binding protein 1
Q6ZQ88	2	57	KDM1A	Lysine-specific histone demethylase 1A
P54276	2	56	MSH6	DNA mismatch repair protein Msh6 {ECO:0000303|PubMed:9390556}
P04627	2	57	ARAF	Serine/threonine-protein kinase A-Raf
P35991	2	24	BTK	Tyrosine-protein kinase BTK
Q9ERU9	2	14	RBP2	E3 SUMO-protein ligase RanBP2
Q62203	2	56	SF3A2	Splicing factor 3A subunit 2
P61027	2	67	RAB10	Ras-related protein Rab-10
P97496	2	14	SMRC1	SWI/SNF complex subunit SMARCC1
Q9QY06	2	36	MYO9B	Unconventional myosin-IXb
P55258	2	25	RAB8A	Ras-related protein Rab-8A
Q8K4B0	2	14	MTA1	Metastasis-associated protein MTA1
Q9D3E6	2	56	STAG1	Cohesin subunit SA-1
Q8VDI1	2	35	ESIP1	Epithelial-stromal interaction protein 1
Q8CI33	2	67	C19L1	CWF19-like protein 1
B2RX14	2	5	TUT4	Terminal uridylyltransferase 4 {ECO:0000305}
Q8CJF7	2	56	ELYS	Protein ELYS
Q6P1F6	2	56	2ABA	Serine/threonine-protein phosphatase 2A 55 kDa regulatory subunit B alpha isoform
P51125	2	56	ICAL	Calpastatin
Q8JZM7	2	14	CDC73	Parafibromin
Q0VGB7	2	6	PP4R2	Serine/threonine-protein phosphatase 4 regulatory subunit 2
Q99MK8	2	34	ARBK1	Beta-adrenergic receptor kinase 1
Q9Z2D6	2	13	MECP2	Methyl-CpG-binding protein 2
Q9QXK7	2	14	CPSF3	Cleavage and polyadenylation specificity factor subunit 3
Q61136	2	56	PRP4B	Serine/threonine-protein kinase PRP4 homolog
Q5SVQ0	2	67	KAT7	Histone acetyltransferase KAT7 {ECO:0000305}
Q9CXT8	2	6	MPPB	Mitochondrial-processing peptidase subunit beta
O08808	2	56	DIAP1	Protein diaphanous homolog 1
P70288	2	46	HDAC2	Histone deacetylase 2 {ECO:0000305}

O08585	2	2	CLCA	Clathrin light chain A
O88942	2	56	NFAC1	Nuclear factor of activated T-cells, cytoplasmic 1
Q99MU3	2	46	DSRAD	Double-stranded RNA-specific adenosine deaminase
Q8CFI7	2	14	RPB2	DNA-directed RNA polymerase II subunit RPB2
Q8K2F0	2	67	BRD3	Bromodomain-containing protein 3
Q62018	2	67	CTR9	RNA polymerase-associated protein CTR9 homolog
Q9JKY0	2	6	CNOT9	CCR4-NOT transcription complex subunit 9 {ECO:0000312|MGI:MGI:1928902}
Q99LH1	2	56	NOG2	Nucleolar GTP-binding protein 2
Q6ZQH8	2	57	NU188	Nucleoporin NUP188 {ECO:0000305}
Q6PDM2	2	14	SRSF1	Serine/arginine-rich splicing factor 1
Q9EQP2	2	34	EHD4	EH domain-containing protein 4 {ECO:0000305}
E9PYH6	2	67	SET1A	Histone-lysine N-methyltransferase SETD1A
Q922B2	2	24	SYDC	Aspartate--tRNA ligase, cytoplasmic
E9Q394	2	34	AKP13	A-kinase anchor protein 13
Q8VC03	2	56	EMAL3	Echinoderm microtubule-associated protein-like 3
Q99J45	2	6	NRBP	Nuclear receptor-binding protein
Q60591	2	56	NFAC2	Nuclear factor of activated T-cells, cytoplasmic 2
Q8CB77	2	17	ELOA1	Elongin-A
Q08093	2	12	CNN2	Calponin-2
Q5SUS0	2	5	FBW10	F-box/WD repeat-containing protein 10
Q9D8N2	2	67	DEN10	DENN domain-containing protein 10 {ECO:0000305}
Q99KJ8	2	6	DCTN2	Dynactin subunit 2
Q6ZQ58	2	45	LARP1	La-related protein 1
O88842	2	67	FGD3	FYVE, RhoGEF and PH domain-containing protein 3
Q8C9B9	2	13	DIDO1	Death-inducer obliterator 1
Q62431	2	46	ARI3A	AT-rich interactive domain-containing protein 3A
P43247	2	56	MSH2	DNA mismatch repair protein Msh2
O08582	2	6	GTPB1	GTP-binding protein 1
P14824	2	24	ANXA6	Annexin A6
Q6A028	2	24	SWP70	Switch-associated protein 70
Q9WUK2	2	35	IF4H	Eukaryotic translation initiation factor 4H
P51150	2	35	RAB7A	Ras-related protein Rab-7a
O54988	2	6	SLK	STE20-like serine/threonine-protein kinase

Q8BK63	2	35	KC1A	Casein kinase I isoform alpha
Q8BHB4	2	56	WDR3	WD repeat-containing protein 3
Q8K363	2	36	DDX18	ATP-dependent RNA helicase DDX18
Q8K124	2	45	PKHO2	Pleckstrin homology domain-containing family O member 2
Q6P069	2	5	SORCN	Sorcin
P35278	2	25	RAB5C	Ras-related protein Rab-5C
Q9R233	2	34	TPSN	Tapasin
Q8R2M2	2	16	TDIF2	Deoxynucleotidyltransferase terminal-interacting protein 2
Q9QZE5	2	56	COPG1	Coatomer subunit gamma-1
Q9Z103	2	16	ADNP	Activity-dependent neuroprotector homeobox protein
Q9R1C7	2	14	PR40A	Pre-mRNA-processing factor 40 homolog A
Q99PP7	2	56	TRI33	E3 ubiquitin-protein ligase TRIM33
P01882	2	26	IGHDM	Ig delta chain C region membrane-bound form
Q8R0X7	2	34	SGPL1	Sphingosine-1-phosphate lyase 1 {ECO:0000305}
P15331	2	67	PERI	Peripherin
Q640N3	2	34	RHG30	Rho GTPase-activating protein 30
Q08122	2	56	TLE3	Transducin-like enhancer protein 3
Q3UHJ0	2	56	AAK1	AP2-associated protein kinase 1
P27601	2	4	GNA13	Guanine nucleotide-binding protein subunit alpha-13
Q8K0V4	2	6	CNOT3	CCR4-NOT transcription complex subunit 3
Q93092	2	14	TALDO	Transaldolase
Q80SW1	2	56	SAHH2	S-adenosylhomocysteine hydrolase-like protein 1
Q9QZK7	2	24	DOK3	Docking protein 3
P67984	2	37	RL22	60S ribosomal protein L22
P62137	2	14	PP1A	Serine/threonine-protein phosphatase PP1-alpha catalytic subunit
Q91YQ5	2	24	RPN1	Dolichyl-diphosphooligosaccharide--protein glycosyltransferase subunit 1
P01864	2	24	GCAB	Ig gamma-2A chain C region secreted form
O70145	2	34	NCF2	Neutrophil cytosol factor 2
P62900	2	7	RL31	60S ribosomal protein L31
Q5SV85	2	56	SYNRG	Synergin gamma
A2AQ19	2	56	RTF1	RNA polymerase-associated protein RTF1 homolog
P00405	2	25	COX2	Cytochrome c oxidase subunit 2
Q99LE6	2	46	ABCF2	ATP-binding cassette sub-family F member 2

Q9QXA5	2	5	LSM4	U6 snRNA-associated Sm-like protein LSm4
Q91WG2	2	6	RABE2	Rab GTPase-binding effector protein 2
Q8K2B3	2	23	SDHA	Succinate dehydrogenase [ubiquinone] flavoprotein subunit, mitochondrial
Q3U319	2	1	BRE1B	E3 ubiquitin-protein ligase BRE1B
Q3UIA2	2	24	RHG17	Rho GTPase-activating protein 17
P17897	2	36	LYZ1	Lysozyme C-1
Q922P9	2	14	GLYR1	Putative oxidoreductase GLYR1
Q9R0P5	2	57	DEST	Destrin
Q6PF93	2	56	PK3C3	Phosphatidylinositol 3-kinase catalytic subunit type 3
P62196	2	34	PRS8	26S proteasome regulatory subunit 8
O55125	2	14	NIPS1	Protein NipSnap homolog 1
P63005	2	56	LIS1	Platelet-activating factor acetylhydrolase IB subunit beta {ECO:0000255|HAMAP-Rule:MF_03141, ECO:0000305}
O54946	2	36	DNJB6	DnaJ homolog subfamily B member 6
Q8CFQ3	2	16	AQR	RNA helicase aquarius
P62488	2	57	RPB7	DNA-directed RNA polymerase II subunit RPB7
Q924K8	2	17	MTA3	Metastasis-associated protein MTA3
Q8BHG9	2	56	CGBP1	CGG triplet repeat-binding protein 1
Q80XP8	2	15	FA76B	Protein FAM76B
Q6NXI6	2	46	RPRD2	Regulation of nuclear pre-mRNA domain-containing protein 2
Q99PS0	2	34	K1C23	Keratin, type I cytoskeletal 23
A2AB59	2	67	RHG27	Rho GTPase-activating protein 27
Q9R1P4	2	34	PSA1	Proteasome subunit alpha type-1
Q8CCJ3	2	67	UFL1	E3 UFM1-protein ligase 1 {ECO:0000305}
Q9ESW4	2	34	AGK	Acylglycerol kinase, mitochondrial {ECO:0000250|UniProtKB:Q53H12}
Q91V81	2	57	RBM42	RNA-binding protein 42
Q8BJL0	2	46	SMAL1	SWI/SNF-related matrix-associated actin-dependent regulator of chromatin subfamily A-like protein 1
O55236	2	67	MCE1	mRNA-capping enzyme
Q8BYW1	2	34	RHG25	Rho GTPase-activating protein 25
Q9WU42	2	46	NCOR2	Nuclear receptor corepressor 2
P59016	2	67	VP33B	Vacuolar protein sorting-associated protein 33B
Q8C2K1	2	45	DEFI6	Differentially expressed in FDCP 6
Q9WVE8	2	67	PACN2	Protein kinase C and casein kinase substrate in neurons protein 2
Q6NV83	2	13	SR140	U2 snRNP-associated SURP motif-containing protein

P70670	2	35	NACAM	Nascent polypeptide-associated complex subunit alpha, muscle-specific form
Q62168	2	45	K1H2	Keratin, type I cuticular Ha2
P61957	2	14	SUMO2	Small ubiquitin-related modifier 2 {ECO:0000305}
Q8CJG0	2	34	AGO2	Protein argonaute-2 {ECO:0000255|HAMAP-Rule:MF_03031}
Q03267	2	14	IKZF1	DNA-binding protein Ikaros
Q9R1P1	2	35	PSB3	Proteasome subunit beta type-3
O35368	2	16	IFI3	Interferon-activable protein 203
Q61595	2	56	KTN1	Kinectin
Q9D0F9	2	67	PGM1	Phosphoglucomutase-1
Q9CX00	2	35	IST1	IST1 homolog
Q9JL61	2	67	RFX5	DNA-binding protein Rfx5
Q9D0B0	2	56	SRSF9	Serine/arginine-rich splicing factor 9
Q61216	2	57	MRE11	Double-strand break repair protein MRE11
Q9ERD6	2	67	RGPS2	Ras-specific guanine nucleotide-releasing factor RalGPS2
O89090	2	13	SP1	Transcription factor Sp1
P63323	2	36	RS12	40S ribosomal protein S12
P11276	2	34	FINC	Fibronectin {ECO:0000305}
Q80VW7	2	56	AKNA	Microtubule organization protein AKNA {ECO:0000305}
Q3TKY6	2	56	CWC27	Spliceosome-associated protein CWC27 homolog {ECO:0000305}
Q8C3P7	2	67	MTA70	N6-adenosine-methyltransferase subunit METTL3
P14148	2	34	RL7	60S ribosomal protein L7
P46061	2	14	RAGP1	Ran GTPase-activating protein 1
Q8BX57	2	67	PXK	PX domain-containing protein kinase-like protein
P46460	2	34	NSF	Vesicle-fusing ATPase
Q3TIX9	2	46	SNUT2	U4/U6.U5 tri-snRNP-associated protein 2
P59729	2	67	RIN3	Ras and Rab interactor 3
Q8R4E9	2	46	CDT1	DNA replication factor Cdt1
Q9CXF4	2	56	TBC15	TBC1 domain family member 15
Q8K2Y9	2	67	CCM2	Cerebral cavernous malformations protein 2 homolog
Q8R4R6	2	13	NUP35	Nucleoporin NUP35 {ECO:0000312|MGI:MGI:1916732}
Q8K212	2	67	PACS1	Phosphofurin acidic cluster sorting protein 1
Q8K2D3	2	67	EDC3	Enhancer of mRNA-decapping protein 3
Q80XI4	2	67	PI42B	Phosphatidylinositol 5-phosphate 4-kinase type-2 beta {ECO:0000305}

Q9D2G2	2	34	ODO2	Dihydrolipoyllysine-residue succinyltransferase component of 2-oxoglutarate dehydrogenase complex, mitochondrial
P70388	2	15	RAD50	DNA repair protein RAD50
Q9CWH6	2	67	PSMA8	Proteasome subunit alpha type-8 {ECO:0000303|PubMed:31358751}
Q6ZQL4	2	16	WDR43	WD repeat-containing protein 43
Q9ERG2	2	57	STRN3	Striatin-3
Q8VDP3	2	34	MICA1	[F-actin]-monooxygenase MICAL1 {ECO:0000305}
Q3UMT1	2	56	PP12C	Protein phosphatase 1 regulatory subunit 12C
Q3TIV5	2	57	ZC3HF	Zinc finger CCCH domain-containing protein 15
Q99KG3	2	16	RBM10	RNA-binding protein 10 {ECO:0000305}
P59997	2	56	KDM2A	Lysine-specific demethylase 2A
Q9WU00	2	57	NRF1	Nuclear respiratory factor 1
P58404	2	67	STRN4	Striatin-4
O54941	2	14	SMCE1	SWI/SNF-related matrix-associated actin-dependent regulator of chromatin subfamily E member 1
Q8BMA6	2	45	SRP68	Signal recognition particle subunit SRP68
Q61466	2	67	SMRD1	SWI/SNF-related matrix-associated actin-dependent regulator of chromatin subfamily D member 1
Q8CGK3	2	56	LONM	Lon protease homolog, mitochondrial {ECO:0000255|HAMAP-Rule:MF_03120}
Q6PGL7	2	56	WASC2	WASH complex subunit 2 {ECO:0000312|MGI:MGI:106463}
Q61751	2	67	Z354A	Zinc finger protein 354A
Q9Z1M8	2	16	RED	Protein Red
Q9DBP5	2	35	KCY	UMP-CMP kinase {ECO:0000255|HAMAP-Rule:MF_03172}
P61514	2	56	RL37A	60S ribosomal protein L37a
Q8CDA1	2	56	SAC2	Phosphatidylinositide phosphatase SAC2
P23611	2	16	IRF8	Interferon regulatory factor 8 {ECO:0000303|PubMed:17579016}
P63154	2	46	CRNL1	Crooked neck-like protein 1
Q9JI44	2	67	DMAP1	DNA methyltransferase 1-associated protein 1
Q640Q5	2	46	PAN3	PAN2-PAN3 deadenylation complex subunit Pan3 {ECO:0000255|HAMAP-Rule:MF_03181}
Q5ND34	2	56	WDR81	WD repeat-containing protein 81 {ECO:0000312|MGI:MGI:2681828}
O88447	2	67	KLC1	Kinesin light chain 1
P01648	2	36	KV5AF	Ig kappa chain V-V region HP 91A3
Q8K3A9	2	56	MEPCE	7SK snRNA methylphosphate capping enzyme {ECO:0000303|PubMed:23154982}
Q8R5L3	2	56	VPS39	Vam6/Vps39-like protein
Q99LI8	2	67	HGS	Hepatocyte growth factor-regulated tyrosine kinase substrate
Q6P2K6	2	56	P4R3A	Serine/threonine-protein phosphatase 4 regulatory subunit 3A {ECO:0000250|UniProtKB:Q6IN85}

Q9DB20	2	34	ATPO	ATP synthase subunit O, mitochondrial {ECO:0000305}
O88291	2	57	ZN326	DBIRD complex subunit ZNF326
Q8BGA5	2	47	KRR1	KRR1 small subunit processome component homolog
Q6PFD9	2	14	NUP98	Nuclear pore complex protein Nup98-Nup96
O88554	2	67	PARP2	Poly [ADP-ribose] polymerase 2
Q9WUK4	2	45	RFC2	Replication factor C subunit 2
Q8BVY0	2	16	RL1D1	Ribosomal L1 domain-containing protein 1
Q8VI36	2	67	PAXI	Paxillin
Q8CGC6	2	16	RBM28	RNA-binding protein 28
Q921G8	2	67	GCP2	Gamma-tubulin complex component 2
Q8CGY8	2	14	OGT1	UDP-N-acetylglucosamine--peptide N-acetylglucosaminyltransferase 110 kDa subunit
Q5SSI6	2	57	UTP18	U3 small nucleolar RNA-associated protein 18 homolog
P97823	2	37	LYPA1	Acyl-protein thioesterase 1
Q922H4	2	34	GMPPA	Mannose-1-phosphate guanyltransferase alpha
Q9QZL0	2	46	RIPK3	Receptor-interacting serine/threonine-protein kinase 3 {ECO:0000303|PubMed:19590578}
Q8BFW4	2	67	TRI65	Tripartite motif-containing protein 65
Q7TNV0	2	14	DEK	Protein DEK
Q6ZWV7	2	56	RL35	60S ribosomal protein L35
Q8CJG1	2	46	AGO1	Protein argonaute-1
Q91X20	2	67	ASH2L	Set1/Ash2 histone methyltransferase complex subunit ASH2
Q8QZY9	2	17	SF3B4	Splicing factor 3B subunit 4
O88286	2	45	WIZ	Protein Wiz
Q3TTA7	2	56	CBLB	E3 ubiquitin-protein ligase CBL-B
O09000	2	56	NCOA3	Nuclear receptor coactivator 3
Q80YV2	2	56	NIPA	Nuclear-interacting partner of ALK
Q8CI51	2	56	PDLI5	PDZ and LIM domain protein 5
Q9JHU9	2	67	INO1	Inositol-3-phosphate synthase 1
Q3TX08	2	56	TRM1	tRNA (guanine(26)-N(2))-dimethyltransferase
Q8BH74	2	16	NU107	Nuclear pore complex protein Nup107
Q9Z2B9	2	47	KS6A4	Ribosomal protein S6 kinase alpha-4
Q8BZ98	2	45	DYN3	Dynamin-3
Q61103	2	16	REQU	Zinc finger protein ubi-d4
Q99M87	2	57	DNJA3	DnaJ homolog subfamily A member 3, mitochondrial

Q80W00	2	56	PP1RA	Serine/threonine-protein phosphatase 1 regulatory subunit 10
Q99LC2	2	67	CSTF1	Cleavage stimulation factor subunit 1
Q8VDS4	2	67	RPR1A	Regulation of nuclear pre-mRNA domain-containing protein 1A
Q9D8M4	2	56	RL7L	60S ribosomal protein L7-like 1
Q8R1Q8	2	46	DC1L1	Cytoplasmic dynein 1 light intermediate chain 1
P62849	2	57	RS24	40S ribosomal protein S24
P18760	2	14	COF1	Cofilin-1
Q6PGH1	2	67	BUD31	Protein BUD31 homolog
Q8K411	2	56	PREP	Presequence protease, mitochondrial {ECO:0000305}
Q8C4B4	2	67	U119B	Protein unc-119 homolog B
B2RUP2	2	56	UN13D	Protein unc-13 homolog D
Q8CHP8	2	67	PGP	Glycerol-3-phosphate phosphatase {ECO:0000305}
Q9QXK3	2	56	COPG2	Coatomer subunit gamma-2
Q9CPS7	2	56	PNO1	RNA-binding protein PNO1
Q8K3H0	2	56	DP13A	DCC-interacting protein 13-alpha {ECO:0000305}
Q8CI08	2	56	SLAI2	SLAIN motif-containing protein 2
Q8VD04	2	56	GRAP1	GRIP1-associated protein 1
P48377	2	56	RFX1	MHC class II regulatory factor RFX1
O54950	2	67	AAKG1	5'-AMP-activated protein kinase subunit gamma-1
Q60841	2	56	RELN	Reelin
P23506	2	67	PIMT	Protein-L-isoaspartate(D-aspartate) O-methyltransferase
Q07417	2	56	ACADS	Short-chain specific acyl-CoA dehydrogenase, mitochondrial
Q8VCN9	2	67	TBCC	Tubulin-specific chaperone C
Q5EG47	2	46	AAPK1	5'-AMP-activated protein kinase catalytic subunit alpha-1
Q9D2M8	2	67	UB2V2	Ubiquitin-conjugating enzyme E2 variant 2
Q04841	2	67	3MG	DNA-3-methyladenine glycosylase
Q9QZH3	2	67	PPIE	Peptidyl-prolyl cis-trans isomerase E
Q924C1	2	56	XPO5	Exportin-5
Q9ER88	2	67	RT29	28S ribosomal protein S29, mitochondrial
Q8CFE2	2	56	HPF1	Histone PARylation factor 1 {ECO:0000305}
Q9JK48	2	67	SHLB1	Endophilin-B1
Q924T2	2	67	RT02	28S ribosomal protein S2, mitochondrial
P62331	2	67	ARF6	ADP-ribosylation factor 6

Q9JLI6	2	67	SCLY	Selenocysteine lyase
P61082	2	67	UBC12	NEDD8-conjugating enzyme Ubc12
Q8BGC4	2	67	PTGR3	Prostaglandin reductase-3 {ECO:0000303|PubMed:23821743}
P62855	2	67	RS26	40S ribosomal protein S26
Q9CY97	2	67	SSU72	RNA polymerase II subunit A C-terminal domain phosphatase SSU72
P36536	2	67	SAR1A	GTP-binding protein SAR1a
Q3UE37	2	67	UBE2Z	Ubiquitin-conjugating enzyme E2 Z
Q9QZQ8	1	1	H2AY	Core histone macro-H2A.1
E9Q555	1	6	RN213	E3 ubiquitin-protein ligase RNF213
P62631	1	7	EF1A2	Elongation factor 1-alpha 2
Q64478	1	0	H2B1H	Histone H2B type 1-H
P68134	1	2	ACTS	Actin, alpha skeletal muscle
P63268	1	6	ACTH	Actin, gamma-enteric smooth muscle
Q61781	1	1	K1C14	Keratin, type I cytoskeletal 14
P0CG49	1	2	UBB	Polyubiquitin-B
Q9R0H5	1	3	K2C71	Keratin, type II cytoskeletal 71
Q6NZJ6	1	4	IF4G1	Eukaryotic translation initiation factor 4 gamma 1
Q6IFZ9	1	6	K2C74	Keratin, type II cytoskeletal 74 {ECO:0000250|UniProtKB:Q7RT57}
P68369	1	0	TBA1A	Tubulin alpha-1A chain
P21619	1	1	LMNB2	Lamin-B2
P05213	1	2	TBA1B	Tubulin alpha-1B chain
P08730	1	3	K1C13	Keratin, type I cytoskeletal 13
Q8BFZ3	1	0	ACTBL	Beta-actin-like protein 2
Q6NXH9	1	1	K2C73	Keratin, type II cytoskeletal 73
P48025	1	2	KSYK	Tyrosine-protein kinase SYK
P11679	1	3	K2C8	Keratin, type II cytoskeletal 8
A2A5R2	1	6	BIG2	Brefeldin A-inhibited guanine nucleotide-exchange protein 2
Q6P4T2	1	1	U520	U5 small nuclear ribonucleoprotein 200 kDa helicase
Q9CZX8	1	0	RS19	40S ribosomal protein S19
Q61414	1	1	K1C15	Keratin, type I cytoskeletal 15
Q7TMM9	1	3	TBB2A	Tubulin beta-2A chain
G3X9K3	1	6	BIG1	Brefeldin A-inhibited guanine nucleotide-exchange protein 1
Q9QWL7	1	0	K1C17	Keratin, type I cytoskeletal 17

Q99M73	1	2	KRT84	Keratin, type II cuticular Hb4
Q61897	1	5	KT33B	Keratin, type I cuticular Ha3-II
Q62383	1	6	SPT6H	Transcription elongation factor SPT6
Q68SN8	1	0	FCRL5	Fc receptor-like protein 5
P63017	1	1	HSP7C	Heat shock cognate 71 kDa protein
Q8R1M2	1	2	H2AJ	Histone H2A.J
Q64523	1	4	H2A2C	Histone H2A type 2-C
P19783	1	0	COX41	Cytochrome c oxidase subunit 4 isoform 1, mitochondrial
Q9CU62	1	1	SMC1A	Structural maintenance of chromosomes protein 1A
P84244	1	2	H33	Histone H3.3
Q9CQV8	1	3	1433B	14-3-3 protein beta/alpha
Q6ZWU9	1	7	RS27	40S ribosomal protein S27
Q9QXS1	1	3	PLEC	Plectin
Q8K0Y2	1	5	KT33A	Keratin, type I cuticular Ha3-I {ECO:0000250|UniProtKB:076009}
O70318	1	6	E41L2	Band 4.1-like protein 2
O55143	1	7	AT2A2	Sarcoplasmic/endoplasmic reticulum calcium ATPase 2 {ECO:0000305}
Q64511	1	1	TOP2B	DNA topoisomerase 2-beta
Q99JY9	1	2	ARP3	Actin-related protein 3
Q8CGP5	1	4	H2A1F	Histone H2A type 1-F
Q7TMY8	1	6	HUWE1	E3 ubiquitin-protein ligase HUWE1
P09405	1	1	NUCL	Nucleolin
G3X987	1	7	GIMA9	GTPase IMAP family member 9
P19001	1	1	K1C19	Keratin, type I cytoskeletal 19
P16627	1	3	HS71L	Heat shock 70 kDa protein 1-like
Q61102	1	7	ABCB7	Iron-sulfur clusters transporter ABCB7, mitochondrial {ECO:0000305}
Q8BHL5	1	0	ELMO2	Engulfment and cell motility protein 2
Q3TEA8	1	1	HP1B3	Heterochromatin protein 1-binding protein 3
P06330	1	2	HVM51	Ig heavy chain V region AC38 205.12
O08638	1	5	MYH11	Myosin-11
Q8VD65	1	6	PI3R4	Phosphoinositide 3-kinase regulatory subunit 4
Q8BT60	1	7	CPNE3	Copine-3 {ECO:0000305}
Q91VM5	1	1	RMXL1	RNA binding motif protein, X-linked-like-1
Q9JHU4	1	3	DYHC1	Cytoplasmic dynein 1 heavy chain 1

P17879	1	5	HS71B	Heat shock 70 kDa protein 1B
Q8C547	1	7	HTR5B	HEAT repeat-containing protein 5B
P35550	1	1	FBRL	rRNA 2'-O-methyltransferase fibrillarin
P70333	1	4	HNRH2	Heterogeneous nuclear ribonucleoprotein H2
P58771	1	5	TPM1	Tropomyosin alpha-1 chain
Q921M3	1	1	SF3B3	Splicing factor 3B subunit 3
Q6P4S8	1	6	INT1	Integrator complex subunit 1
P19246	1	0	NFH	Neurofilament heavy polypeptide
Q8BVK9	1	1	SP110	Sp110 nuclear body protein
P68254	1	3	1433T	14-3-3 protein theta
Q60973	1	4	RBBP7	Histone-binding protein RBBP7
P03911	1	7	NU4M	NADH-ubiquinone oxidoreductase chain 4
Q9CW03	1	1	SMC3	Structural maintenance of chromosomes protein 3
O54824	1	2	IL16	Pro-interleukin-16
Q8VCW2	1	3	K1C25	Keratin, type I cytoskeletal 25
Q8R429	1	7	AT2A1	Sarcoplasmic/endoplasmic reticulum calcium ATPase 1
Q8K4Z5	1	1	SF3A1	Splicing factor 3A subunit 1
Q9D0M3	1	4	CY1	Cytochrome c1, heme protein, mitochondrial
Q8R0W0	1	3	EPIPL	Epiplakin {ECO:0000303|PubMed:12791695}
Q7TT37	1	6	ELP1	Elongator complex protein 1
B2RXC1	1	7	TPC11	Trafficking protein particle complex subunit 11
Q60790	1	0	RASA3	Ras GTPase-activating protein 3
Q8C2Q3	1	1	RBM14	RNA-binding protein 14
Q9R269	1	3	PEPL	Periplakin
P70218	1	4	M4K1	Mitogen-activated protein kinase kinase kinase kinase 1
O08810	1	1	U5S1	116 kDa U5 small nuclear ribonucleoprotein component
P19221	1	2	THRB	Prothrombin
P15105	1	3	GLNA	Glutamine synthetase {ECO:0000303|PubMed:30158707}
O35350	1	4	CAN1	Calpain-1 catalytic subunit {ECO:0000305}
Q99M74	1	5	KRT82	Keratin, type II cuticular Hb2
Q60952	1	7	CP250	Centrosome-associated protein CEP250
Q8R081	1	1	HNRPL	Heterogeneous nuclear ribonucleoprotein L
P70279	1	5	SURF6	Surfeit locus protein 6

Q6PIP5	1	7	NUDC1	NudC domain-containing protein 1
P62880	1	0	GBB2	Guanine nucleotide-binding protein G(I)/G(S)/G(T) subunit beta-2
Q9JIK5	1	1	DDX21	Nucleolar RNA helicase 2 {ECO:0000305}
Q5XG71	1	7	UTP20	Small subunit processome component 20 homolog
Q61390	1	0	TCPW	T-complex protein 1 subunit zeta-2
Q9R190	1	1	MTA2	Metastasis-associated protein MTA2
Q11011	1	3	PSA	Puromycin-sensitive aminopeptidase
P70429	1	4	EVL	Ena/VASP-like protein
Q60710	1	1	SAMH1	Deoxynucleoside triphosphate triphosphohydrolase SAMHD1 {ECO:0000305}
P01897	1	2	HA1L	H-2 class I histocompatibility antigen, L-D alpha chain
Q3UQ44	1	3	IQGA2	Ras GTPase-activating-like protein IQGAP2
Q8BH59	1	4	CMC1	Calcium-binding mitochondrial carrier protein Aralar1
Q6A0D4	1	5	RFTN1	Raftlin
P00397	1	7	COX1	Cytochrome c oxidase subunit 1
Q9D1R9	1	0	RL34	60S ribosomal protein L34
Q8VDW0	1	1	DX39A	ATP-dependent RNA helicase DDX39A
P42227	1	3	STAT3	Signal transducer and activator of transcription 3 {ECO:0000312|MGI:MGI:103038}
P27870	1	4	VAV	Proto-oncogene vav
Q3UH60	1	6	DIP2B	Disco-interacting protein 2 homolog B
Q9D3P8	1	0	PLRKT	Plasminogen receptor (KT)
Q9D6Z1	1	1	NOP56	Nucleolar protein 56
Q02248	1	3	CTNB1	Catenin beta-1
Q2EMV9	1	6	PAR14	Protein mono-ADP-ribosyltransferase PARP14 {ECO:0000305}
P03888	1	7	NU1M	NADH-ubiquinone oxidoreductase chain 1
Q91ZU6	1	0	DYST	Dystonin
O88569	1	1	ROA2	Heterogeneous nuclear ribonucleoproteins A2/B1
P08103	1	3	HCK	Tyrosine-protein kinase HCK
B2RWS6	1	4	EP300	Histone acetyltransferase p300
Q6PAR5	1	6	GAPD1	GTPase-activating protein and VPS9 domain-containing protein 1
Q8VHN7	1	7	AGRV1	Adhesion G-protein coupled receptor V1 {ECO:0000305}
Q9QY81	1	1	PO210	Nuclear pore membrane glycoprotein 210
Q09200	1	2	B4GN1	Beta-1,4 N-acetylgalactosaminyltransferase 1 {ECO:0000305}
P17426	1	4	AP2A1	AP-2 complex subunit alpha-1

Q9DB05	1	5	SNAA	Alpha-soluble NSF attachment protein
Q8VCW4	1	0	UN93B	Protein unc-93 homolog B1 {ECO:0000305}
Q91ZW3	1	1	SMCA5	SWI/SNF-related matrix-associated actin-dependent regulator of chromatin subfamily A member 5
P52480	1	2	KPYM	Pyruvate kinase PKM
Q99KY4	1	6	GAK	Cyclin-G-associated kinase
Q9JJA4	1	7	WDR12	Ribosome biogenesis protein WDR12 {ECO:0000255|HAMAP-Rule:MF_03029}
Q62448	1	0	IF4G2	Eukaryotic translation initiation factor 4 gamma 2
Q6PDG5	1	1	SMRC2	SWI/SNF complex subunit SMARCC2
P03995	1	2	GFAP	Glial fibrillary acidic protein
Q8C2K5	1	6	RASL3	RAS protein activator like-3
Q811P8	1	7	RHG32	Rho GTPase-activating protein 32
F6ZDS4	1	1	TPR	Nucleoprotein TPR
P84091	1	2	AP2M1	AP-2 complex subunit mu
Q80XI3	1	4	IF4G3	Eukaryotic translation initiation factor 4 gamma 3
Q8C052	1	5	MAP1S	Microtubule-associated protein 1S
Q99KK2	1	7	NEUA	N-acylneuraminate cytidylyltransferase
Q8R010	1	0	AIMP2	Aminoacyl tRNA synthase complex-interacting multifunctional protein 2
Q99KP6	1	1	PRP19	Pre-mRNA-processing factor 19 {ECO:0000305}
P84104	1	4	SRSF3	Serine/arginine-rich splicing factor 3
Q8BU30	1	6	SYIC	Isoleucine--tRNA ligase, cytoplasmic
Q8K2C9	1	7	HACD3	Very-long-chain (3R)-3-hydroxyacyl-CoA dehydratase 3 {ECO:0000305}
O55023	1	0	IMPA1	Inositol monophosphatase 1
Q91VC3	1	1	IF4A3	Eukaryotic initiation factor 4A-III
Q9Z320	1	4	K1C27	Keratin, type I cytoskeletal 27
P52431	1	6	DPOD1	DNA polymerase delta catalytic subunit {ECO:0000305}
Q3UUQ7	1	7	PGAP1	GPI inositol-deacylase
Q02257	1	1	PLAK	Junction plakoglobin
P01901	1	2	HA1B	H-2 class I histocompatibility antigen, K-B alpha chain
P30275	1	3	KCRU	Creatine kinase U-type, mitochondrial
Q9Z2E2	1	5	MBD1	Methyl-CpG-binding domain protein 1 {ECO:0000305}
Q689Z5	1	6	SBNO1	Protein strawberry notch homolog 1
P19096	1	0	FAS	Fatty acid synthase
Q9Z2X1	1	1	HNRPF	Heterogeneous nuclear ribonucleoprotein F

Q09014	1	2	NCF1	Neutrophil cytosol factor 1
A2AJI0	1	3	MA7D1	MAP7 domain-containing protein 1
Q61164	1	6	CTCF	Transcriptional repressor CTCF
P49452	1	7	CENPC	Centromere protein C
Q99PV0	1	1	PRP8	Pre-mRNA-processing-splicing factor 8
P57776	1	2	EF1D	Elongation factor 1-delta
Q3TBD2	1	4	HMHA1	Rho GTPase-activating protein 45 {ECO:0000312|MGI:MGI:1917969}
Q8CGF1	1	7	RHG29	Rho GTPase-activating protein 29
Q922Q4	1	0	P5CR2	Pyrroline-5-carboxylate reductase 2
Q8BV49	1	1	IFIX	Pyrin and HIN domain-containing protein 1
Q60865	1	2	CAPR1	Caprin-1
Q9D8W5	1	5	PSD12	26S proteasome non-ATPase regulatory subunit 12
Q6ZPE2	1	6	MTMR5	Myotubularin-related protein 5
Q99K70	1	7	RRAGC	Ras-related GTP-binding protein C
P62889	1	0	RL30	60S ribosomal protein L30
Q3U0V1	1	1	FUBP2	Far upstream element-binding protein 2
Q7TPH6	1	6	MYCB2	E3 ubiquitin-protein ligase MYCBP2 {ECO:0000305}
P61967	1	7	AP1S1	AP-1 complex subunit sigma-1A
Q91YR7	1	1	PRP6	Pre-mRNA-processing factor 6
P62259	1	3	1433E	14-3-3 protein epsilon
A2AF47	1	5	DOC11	Dedicator of cytokinesis protein 11 {ECO:0000312|MGI:MGI:1923224}
Q8K1R7	1	6	NEK9	Serine/threonine-protein kinase Nek9
P53569	1	7	CEBPZ	CCAAT/enhancer-binding protein zeta
Q9JIX8	1	1	ACINU	Apoptotic chromatin condensation inducer in the nucleus
P06328	1	2	HVM49	Ig heavy chain V region 1-72 {ECO:0000312|MGI:MGI:4439633}
Q91WM1	1	4	STRBP	Spermatid perinuclear RNA-binding protein
Q99104	1	5	MYO5A	Unconventional myosin-Va
E9Q4N7	1	6	ARI1B	AT-rich interactive domain-containing protein 1B
Q61425	1	0	HCDH	Hydroxyacyl-coenzyme A dehydrogenase, mitochondrial
Q6PHZ2	1	3	KCC2D	Calcium/calmodulin-dependent protein kinase type II subunit delta
P36371	1	6	TAP2	Antigen peptide transporter 2
Q6P5D8	1	1	SMHD1	Structural maintenance of chromosomes flexible hinge domain-containing protein 1 {ECO:0000303|PubMed:18425126}
Q6IRU2	1	2	TPM4	Tropomyosin alpha-4 chain

Q9CZY3	1	5	UB2V1	Ubiquitin-conjugating enzyme E2 variant 1
Q8C4J7	1	6	TBL3	Transducin beta-like protein 3
Q6ZWQ0	1	7	SYNE2	Nesprin-2
P61089	1	0	UBE2N	Ubiquitin-conjugating enzyme E2 N
D3YXK2	1	1	SAFB1	Scaffold attachment factor B1
P14206	1	2	RSSA	40S ribosomal protein SA {ECO:0000255|HAMAP-Rule:MF_03016}
Q8VDN2	1	6	AT1A1	Sodium/potassium-transporting ATPase subunit alpha-1
Q91W89	1	7	MA2C1	Alpha-mannosidase 2C1
Q8VDD5	1	1	MYH9	Myosin-9
Q9DB77	1	2	QCR2	Cytochrome b-c1 complex subunit 2, mitochondrial
P35821	1	5	PTN1	Tyrosine-protein phosphatase non-receptor type 1
P84089	1	7	ERH	Enhancer of rudimentary homolog
Q7TQ95	1	0	LNP	Endoplasmic reticulum junction formation protein lunapark {ECO:0000305}
Q6PDQ2	1	1	CHD4	Chromodomain-helicase-DNA-binding protein 4
E9QAM5	1	4	HELZ2	Helicase with zinc finger domain 2
Q6PDI5	1	6	ECM29	Proteasome adapter and scaffold protein ECM29 {ECO:0000250|UniProtKB:Q5VYK3}
Q9D8Y1	1	0	T126A	Transmembrane protein 126A
Q99020	1	1	ROAA	Heterogeneous nuclear ribonucleoprotein A/B
P17751	1	3	TPIS	Triosephosphate isomerase
Q6NVF9	1	4	CPSF6	Cleavage and polyadenylation specificity factor subunit 6 {ECO:0000250|UniProtKB:Q16630}
E9PZM4	1	6	CHD2	Chromodomain-helicase-DNA-binding protein 2
O08784	1	1	TCOF	Treacle protein
Q9DCX2	1	2	ATP5H	ATP synthase subunit d, mitochondrial {ECO:0000305}
Q9Z2U0	1	3	PSA7	Proteasome subunit alpha type-7
Q9D7G0	1	5	PRPS1	Ribose-phosphate pyrophosphokinase 1
Q8CGF7	1	1	TCRG1	Transcription elongation regulator 1
Q9JI91	1	3	ACTN2	Alpha-actinin-2
Q9JLV6	1	5	PNKP	Bifunctional polynucleotide phosphatase/kinase
Q9JI78	1	6	NGLY1	Peptide-N(4)-(N-acetyl-beta-glucosaminyl)asparagine amidase
P56391	1	7	CX6B1	Cytochrome c oxidase subunit 6B1
Q6A068	1	1	CDC5L	Cell division cycle 5-like protein
Q80TQ2	1	7	CYLD	Ubiquitin carboxyl-terminal hydrolase CYLD
Q6IME9	1	1	K2C72	Keratin, type II cytoskeletal 72

Q91VD9	1	2	NDUS1	NADH-ubiquinone oxidoreductase 75 kDa subunit, mitochondrial
Q99JY0	1	3	ECHB	Trifunctional enzyme subunit beta, mitochondrial
Q1HFZ0	1	4	NSUN2	RNA cytosine C(5)-methyltransferase NSUN2 {ECO:0000305}
Q8R146	1	5	APEH	Acylamino-acid-releasing enzyme
P70336	1	7	ROCK2	Rho-associated protein kinase 2
Q925I1	1	1	ATAD3	ATPase family AAA domain-containing protein 3
Q6ZPZ3	1	6	ZC3H4	Zinc finger CCCH domain-containing protein 4
Q61036	1	0	PAK3	Serine/threonine-protein kinase PAK 3
Q80ZE3	1	1	SIG10	Sialic acid-binding Ig-like lectin 10
P30681	1	4	HMGB2	High mobility group protein B2
Q9CX34	1	5	SGT1	Protein SGT1 homolog {ECO:0000250|UniProtKB:Q08446}
Q5RJG1	1	7	NOL10	Nucleolar protein 10
Q9CQY5	1	0	MAGT1	Magnesium transporter protein 1
Q9D1J3	1	1	SARNP	SAP domain-containing ribonucleoprotein
Q8BRF7	1	0	SCFD1	Sec1 family domain-containing protein 1
Q6A026	1	1	PDS5A	Sister chromatid cohesion protein PDS5 homolog A
P97807	1	2	FUMH	Fumarate hydratase, mitochondrial {ECO:0000303|PubMed:17418408}
P50396	1	5	GDIA	Rab GDP dissociation inhibitor alpha
Q8CJF8	1	7	AGO4	Protein argonaute-4 {ECO:0000255|HAMAP-Rule:MF_03033}
P01670	1	2	KV3AI	Ig kappa chain V-III region PC 6684
Q8R016	1	3	BLMH	Bleomycin hydrolase
Q6URW6	1	4	MYH14	Myosin-14
B9EJ86	1	6	OSBL8	Oxysterol-binding protein-related protein 8
Q6PAC3	1	5	DCA13	DDB1- and CUL4-associated factor 13
Q2KN98	1	7	CYTSA	Cytospin-A
D0QMC3	1	1	MNDAL	Myeloid cell nuclear differentiation antigen-like protein {ECO:0000303|PubMed:19654412}
P99027	1	3	RLA2	60S acidic ribosomal protein P2
P11881	1	6	ITPR1	Inositol 1,4,5-trisphosphate receptor type 1
Q8BG79	1	7	C19L2	CWF19-like protein 2
P61759	1	0	PFD3	Prefoldin subunit 3
Q8BG05	1	1	ROA3	Heterogeneous nuclear ribonucleoprotein A3
Q9D646	1	4	KRT34	Keratin, type I cuticular Ha4 {ECO:0000250|UniProtKB:O76011}
A2BDX3	1	5	MOCS3	Adenylyltransferase and sulfurtransferase MOCS3 {ECO:0000255|HAMAP-Rule:MF_03049}

Q6KCD5	1	6	NIPBL	Nipped-B-like protein
Q8BK67	1	1	RCC2	Protein RCC2
P58281	1	2	OPA1	Dynamin-like 120 kDa protein, mitochondrial
A2APV2	1	4	FMNL2	Formin-like protein 2
O08900	1	1	IKZF3	Zinc finger protein Aiolos
Q8N7N5	1	7	DCAF8	DDB1- and CUL4-associated factor 8
Q4VA53	1	1	PDS5B	Sister chromatid cohesion protein PDS5 homolog B
P09411	1	2	PGK1	Phosphoglycerate kinase 1
Q922Q1	1	3	MARC2	Mitochondrial amidoxime reducing component 2
Q99LG2	1	5	TNPO2	Transportin-2
Q8CHI8	1	6	EP400	E1A-binding protein p400
Q9WU40	1	7	MAN1	Inner nuclear membrane protein Man1
P17225	1	1	PTBP1	Polypyrimidine tract-binding protein 1
Q8BTV2	1	2	CPSF7	Cleavage and polyadenylation specificity factor subunit 7 {ECO:0000312|MGI:MGI:1917826}
Q99ME2	1	6	WDR6	WD repeat-containing protein 6
Q923G2	1	7	RPAB3	DNA-directed RNA polymerases I, II, and III subunit RPABC3
P11103	1	1	PARP1	Poly [ADP-ribose] polymerase 1
Q60953	1	2	PML	Protein PML
P62852	1	3	RS25	40S ribosomal protein S25
Q8R2N2	1	6	UTP4	U3 small nucleolar RNA-associated protein 4 homolog
E9Q7E2	1	7	ARID2	AT-rich interactive domain-containing protein 2
Q9Z210	1	0	PX11B	Peroxisomal membrane protein 11B
Q9D554	1	1	SF3A3	Splicing factor 3A subunit 3
Q7TN29	1	3	SMAP2	Stromal membrane-associated protein 2
Q3UMU9	1	5	HDGR2	Hepatoma-derived growth factor-related protein 2
A2AKX3	1	7	SETX	Probable helicase senataxin {ECO:0000305}
Q3UVG3	1	0	F91A1	Protein FAM91A1
Q61937	1	1	NPM	Nucleophosmin
Q91V61	1	2	SFXN3	Sideroflexin-3 {ECO:0000303|PubMed:11274051}
Q8BZ03	1	4	KPCD2	Serine/threonine-protein kinase D2
Q9DBC7	1	5	KAP0	cAMP-dependent protein kinase type I-alpha regulatory subunit
A6X8Z5	1	7	RHG31	Rho GTPase-activating protein 31
Q61029	1	1	LAP2B	Lamina-associated polypeptide 2, isoforms beta/delta/epsilon/gamma

P39054	1	2	DYN2	Dynamin-2
B2RRE7	1	3	OTUD4	OTU domain-containing protein 4 {ECO:0000250|UniProtKB:Q01804}
Q8BYK6	1	5	YTHD3	YTH domain-containing family protein 3 {ECO:0000305}
P57784	1	1	RU2A	U2 small nuclear ribonucleoprotein A'
Q66GT5	1	2	PTPM1	Phosphatidylglycerophosphatase and protein-tyrosine phosphatase 1 {ECO:0000305}
Q8K4L4	1	3	POF1B	Protein POF1B
Q571H0	1	7	NPA1P	Nucleolar pre-ribosomal-associated protein 1
O35737	1	1	HNRH1	Heterogeneous nuclear ribonucleoprotein H
Q9WVK4	1	3	EHD1	EH domain-containing protein 1 {ECO:0000305}
Q91XI1	1	5	DUS3L	tRNA-dihydrouridine(47) synthase [NAD(P)(+)]-like
P56382	1	7	ATP5E	ATP synthase subunit epsilon, mitochondrial {ECO:0000305}
P31254	1	2	UBA1Y	Ubiquitin-like modifier-activating enzyme 1 Y
Q6ZQ38	1	3	CAND1	Cullin-associated NEDD8-dissociated protein 1
S4R1M9	1	7	OSB10	Oxysterol-binding protein-related protein 10
Q80YR3	1	0	SKDA1	SKI/DACH domain-containing protein 1
P70372	1	1	ELAV1	ELAV-like protein 1
Q9CWK8	1	2	SNX2	Sorting nexin-2
Q61823	1	3	PDCD4	Programmed cell death protein 4
Q9ERK4	1	5	XPO2	Exportin-2
P11247	1	1	PERM	Myeloperoxidase
P53026	1	2	RL10A	60S ribosomal protein L10a
Q8CDN6	1	3	TXNL1	Thioredoxin-like protein 1
Q91W36	1	4	UBP3	Ubiquitin carboxyl-terminal hydrolase 3
Q8K1M6	1	6	DNM1L	Dynamin-1-like protein
Q6NY15	1	7	TSG10	Testis-specific gene 10 protein
P70290	1	0	EM55	55 kDa erythrocyte membrane protein
P62908	1	1	RS3	40S ribosomal protein S3
P53657	1	2	KPYR	Pyruvate kinase PKLR
Q0VBK2	1	3	K2C80	Keratin, type II cytoskeletal 80
Q8VCW8	1	4	ACSF2	Medium-chain acyl-CoA ligase ACSF2, mitochondrial {ECO:0000305}
P09602	1	5	HMGN2	Non-histone chromosomal protein HMG-17
Q3TES0	1	7	IQEC3	IQ motif and SEC7 domain-containing protein 3
Q91ZV0	1	0	MIA2	Melanoma inhibitory activity protein 2 {ECO:0000305}

Q8BJ71	1	1	NUP93	Nuclear pore complex protein Nup93
Q7TSV4	1	3	PGM2	Phosphoglucomutase-2
P97820	1	6	M4K4	Mitogen-activated protein kinase kinase kinase kinase 4
Q8BQM8	1	7	EMAL5	Echinoderm microtubule-associated protein-like 5
Q9CX56	1	0	PSMD8	26S proteasome non-ATPase regulatory subunit 8
Q91WN4	1	2	KMO	Kynurenine 3-monooxygenase {ECO:0000255|HAMAP-Rule:MF_03018}
P62192	1	3	PRS4	26S proteasome regulatory subunit 4
Q7TT18	1	6	MCAF1	Activating transcription factor 7-interacting protein 1
Q6DFW4	1	1	NOP58	Nucleolar protein 58
Q8QZT1	1	2	THIL	Acetyl-CoA acetyltransferase, mitochondrial
P97386	1	3	DNLI3	DNA ligase 3
O55128	1	5	SAP18	Histone deacetylase complex subunit SAP18
P70335	1	6	ROCK1	Rho-associated protein kinase 1
Q61584	1	7	FXR1	Fragile X mental retardation syndrome-related protein 1
Q9D9R9	1	0	F186A	Protein FAM186A
Q922U1	1	1	PRPF3	U4/U6 small nuclear ribonucleoprotein Prp3
O88967	1	3	YMEL1	ATP-dependent zinc metalloprotease YME1L1
P19253	1	5	RL13A	60S ribosomal protein L13a
Q6GYP7	1	7	RGPA1	Ral GTPase-activating protein subunit alpha-1
P60335	1	1	PCBP1	Poly(rC)-binding protein 1
Q60605	1	3	MYL6	Myosin light polypeptide 6
Q8CIH5	1	4	PLCG2	1-phosphatidylinositol 4,5-bisphosphate phosphodiesterase gamma-2 {ECO:0000305}
P63328	1	5	PP2BA	Serine/threonine-protein phosphatase 2B catalytic subunit alpha isoform
Q9WUN2	1	6	TBK1	Serine/threonine-protein kinase TBK1 {ECO:0000305}
P13542	1	7	MYH8	Myosin-8
P53810	1	0	PIPNA	Phosphatidylinositol transfer protein alpha isoform
Q99NB9	1	1	SF3B1	Splicing factor 3B subunit 1
P84096	1	2	RHOG	Rho-related GTP-binding protein RhoG
Q9CZ13	1	4	QCR1	Cytochrome b-c1 complex subunit 1, mitochondrial
E9Q6J5	1	5	BD1L1	Biorientation of chromosomes in cell division protein 1-like 1 {ECO:0000305}
P28843	1	0	DPP4	Dipeptidyl peptidase 4
P25976	1	1	UBF1	Nucleolar transcription factor 1
P61028	1	2	RAB8B	Ras-related protein Rab-8B

Q99K51	1	3	PLST	Plastin-3
Q8K2F8	1	4	LS14A	Protein LSM14 homolog A
Q6P6L0	1	6	FIL1L	Filamin A-interacting protein 1-like
Q91XS1	1	7	MTMR4	Myotubularin-related protein 4
Q8CJ40	1	0	CROCC	Rootletin
Q8CH25	1	1	SLTM	SAFB-like transcription modulator
P62082	1	3	RS7	40S ribosomal protein S7
P14426	1	4	HA13	H-2 class I histocompatibility antigen, D-K alpha chain
Q9DBG6	1	6	RPN2	Dolichyl-diphosphooligosaccharide--protein glycosyltransferase subunit 2
Q5SUA5	1	1	MYO1G	Unconventional myosin-Ig
P02088	1	2	HBB1	Hemoglobin subunit beta-1
Q7TSH9	1	3	ZN184	Zinc finger protein 184
Q61093	1	6	CY24B	Cytochrome b-245 heavy chain
Q9D0L8	1	0	MCES	mRNA cap guanine-N7 methyltransferase
O89053	1	1	COR1A	Coronin-1A
P49710	1	2	HCLS1	Hematopoietic lineage cell-specific protein
Q8BQ30	1	4	PPR18	Phostensin
Q61884	1	5	MNS1	Meiosis-specific nuclear structural protein 1
Q9CQC7	1	0	NDUB4	NADH dehydrogenase [ubiquinone] 1 beta subcomplex subunit 4
P11499	1	1	HS90B	Heat shock protein HSP 90-beta
Q8BY35	1	4	FGD2	FYVE, RhoGEF and PH domain-containing protein 2
Q9CZ44	1	5	NSF1C	NSFL1 cofactor p47
O88738	1	6	BIRC6	Baculoviral IAP repeat-containing protein 6
Q61214	1	7	DYR1A	Dual specificity tyrosine-phosphorylation-regulated kinase 1A
A2AL36	1	0	CNTRL	Centriolin
Q8VDM6	1	1	HNRL1	Heterogeneous nuclear ribonucleoprotein U-like protein 1
Q8R1S4	1	4	MTSS1	Protein MTSS 1 {ECO:0000305}
Q9JJ28	1	5	FLII	Protein flightless-1 homolog
Q9Z1T1	1	6	AP3B1	AP-3 complex subunit beta-1
P51863	1	0	VA0D1	V-type proton ATPase subunit d 1
Q99LF4	1	2	RTCB	RNA-splicing ligase RtcB homolog {ECO:0000255|HAMAP-Rule:MF_03144}
O35640	1	3	ANXA8	Annexin A8
P11352	1	5	GPX1	Glutathione peroxidase 1 {ECO:0000305}

Q9ET30	1	7	TM9S3	Transmembrane 9 superfamily member 3
Q3TKT4	1	1	SMCA4	Transcription activator BRG1
Q3THE2	1	3	ML12B	Myosin regulatory light chain 12B
Q8C166	1	5	CPNE1	Copine-1 {ECO:0000305}
Q9Z329	1	6	ITPR2	Inositol 1,4,5-trisphosphate receptor type 2
P17012	1	7	ZFX	Zinc finger X-chromosomal protein
Q8BH61	1	0	F13A	Coagulation factor XIII A chain
P63037	1	4	DNJA1	DnaJ homolog subfamily A member1
Q6P1G0	1	7	HEAT6	HEAT repeat-containing protein 6
Q7TPV4	1	1	MBB1A	Myb-binding protein 1A
G3X9C2	1	2	FBX50	F-box only protein 50
P42232	1	5	STA5B	Signal transducer and activator of transcription 5B
A2AR02	1	6	PPIG	Peptidyl-prolyl cis-trans isomerase G
Q3USH5	1	7	SFSWA	Splicing factor, suppressor of white-apricot homolog
P07901	1	1	HS90A	Heat shock protein HSP 90-alpha {ECO:0000305}
O08788	1	6	DCTN1	Dynactin subunit 1
P50096	1	7	IMDH1	Inosine-5'-monophosphate dehydrogenase 1 {ECO:0000255|HAMAP-Rule:MF_03156}
Q9CQE8	1	2	RTRAF	RNA transcription, translation and transport factor protein {ECO:0000312|MGI:MGI:1915295}
Q9QUM9	1	3	PSA6	Proteasome subunit alpha type-6
P83741	1	6	WNK1	Serine/threonine-protein kinase WNK1 {ECO:0000305}
Q6PGB6	1	7	NAA50	N-alpha-acetyltransferase 50
Q9CY50	1	0	SSRA	Translocon-associated protein subunit alpha
Q01853	1	1	TERA	Transitional endoplasmic reticulum ATPase
P70124	1	3	SPB5	Serpin B5
Q9JHI7	1	6	EXOS9	Exosome complex component RRP45
Q6ZPV2	1	7	INO80	Chromatin-remodeling ATPase INO80 {ECO:0000305}
P61965	1	1	WDR5	WD repeat-containing protein 5
Q8BKI2	1	6	TNR6B	Trinucleotide repeat-containing gene 6B protein
Q8R5J9	1	7	PRAF3	PRA1 family protein 3
P20065	1	0	TYB4	Thymosin beta-4
Q60972	1	1	RBBP4	Histone-binding protein RBBP4
P97371	1	2	PSME1	Proteasome activator complex subunit 1
P58774	1	3	TPM2	Tropomyosin beta chain

O54774	1	6	AP3D1	AP-3 complex subunit delta-1
Q3TIU4	1	7	PDE12	2',5'-phosphodiesterase 12
P15508	1	0	SPTB1	Spectrin beta chain, erythrocytic
P62242	1	1	RS8	40S ribosomal protein S8
Q9CRB9	1	2	MIC19	MICOS complex subunit Mic19
P50580	1	3	PA2G4	Proliferation-associated protein 2G4
Q8BL97	1	4	SRSF7	Serine/arginine-rich splicing factor 7
Q8BX17	1	6	GEMI5	Gem-associated protein 5
Q9D4H1	1	7	EXOC2	Exocyst complex component 2
P62311	1	0	LSM3	U6 snRNA-associated Sm-like protein LSm3
P68510	1	4	1433F	14-3-3 protein eta
A2A6A1	1	7	GPTC8	G patch domain-containing protein 8
Q9D0L7	1	0	ARM10	Armadillo repeat-containing protein 10
Q3UKJ7	1	1	SMU1	WD40 repeat-containing protein SMU1
Q9ERI6	1	2	RDH14	Retinol dehydrogenase 14
Q5DU25	1	3	IQEC2	IQ motif and SEC7 domain-containing protein 2
Q91WN1	1	4	DNJC9	DnaJ homolog subfamily C member 9
P35601	1	6	RFC1	Replication factor C subunit 1
P58021	1	7	TM9S2	Transmembrane 9 superfamily member 2
Q8BTX9	1	0	HSDL1	Inactive hydroxysteroid dehydrogenase-like protein 1
Q80YR5	1	1	SAFB2	Scaffold attachment factor B2
P53994	1	7	RAB2A	Ras-related protein Rab-2A
Q9CY57	1	1	CHTOP	Chromatin target of PRMT1 protein
O35129	1	3	PHB2	Prohibitin-2 {ECO:0000305}
Q80TJ7	1	5	PHF8	Histone lysine demethylase PHF8
P13541	1	7	MYH3	Myosin-3
Q9CR61	1	0	NDUB7	NADH dehydrogenase [ubiquinone] 1 beta subcomplex subunit 7
P10711	1	1	TCEA1	Transcription elongation factor A protein 1
P62301	1	4	RS13	40S ribosomal protein S13
Q9Z2N8	1	1	ACL6A	Actin-like protein 6A
P14602	1	3	HSPB1	Heat shock protein beta-1
Q8VDD9	1	6	PHIP	PH-interacting protein
Q3U3D7	1	7	T131L	Transmembrane protein 131-like

P83882	1	0	RL36A	60S ribosomal protein L36a
Q921F2	1	1	TADBP	TAR DNA-binding protein 43
Q61316	1	2	HSP74	Heat shock 70 kDa protein 4
P56399	1	3	UBP5	Ubiquitin carboxyl-terminal hydrolase 5
Q9QXL1	1	7	KI21B	Kinesin-like protein KIF21B
P41317	1	0	MBL2	Mannose-binding protein C
Q6P5F9	1	1	XPO1	Exportin-1
P29452	1	5	CASP1	Caspase-1
Q9WVA3	1	1	BUB3	Mitotic checkpoint protein BUB3
Q05512	1	2	MARK2	Serine/threonine-protein kinase MARK2
Q80U87	1	4	UBP8	Ubiquitin carboxyl-terminal hydrolase 8 {ECO:0000305}
Q8BRN9	1	7	C2D1B	Coiled-coil and C2 domain-containing protein 1B
O55131	1	3	SEPT7	Septin-7
Q09XV5	1	6	CHD8	Chromodomain-helicase-DNA-binding protein 8 {ECO:0000255|HAMAP-Rule:MF_03071}
Q8CBA2	1	7	SLFN5	Schlafen family member 5
Q9D1G1	1	0	RAB1B	Ras-related protein Rab-1B
Q99K48	1	1	NONO	Non-POU domain-containing octamer-binding protein
Q5PSV9	1	6	MDC1	Mediator of DNA damage checkpoint protein 1
Q99LX5	1	7	MMTA2	Multiple myeloma tumor-associated protein 2 homolog
O89086	1	0	RBM3	RNA-binding protein 3
P29351	1	1	PTN6	Tyrosine-protein phosphatase non-receptor type 6
P01029	1	2	CO4B	Complement C4-B
Q60974	1	6	NCOR1	Nuclear receptor corepressor 1
Q6PGF7	1	7	EXOC8	Exocyst complex component 8
Q8BI72	1	1	CARF	CDKN2A-interacting protein
Q62193	1	5	RFA2	Replication protein A 32 kDa subunit
Q80TV8	1	7	CLAP1	CLIP-associating protein 1
P39688	1	0	FYN	Tyrosine-protein kinase Fyn
P20029	1	1	BIP	Endoplasmic reticulum chaperone BiP {ECO:0000305}
Q8K4L0	1	5	DDX54	ATP-dependent RNA helicase DDX54
Q69ZR9	1	6	TASOR	Protein TASOR {ECO:0000305}
P70191	1	7	TRAF5	TNF receptor-associated factor 5
Q9ERS2	1	0	NDUAD	NADH dehydrogenase [ubiquinone] 1 alpha subcomplex subunit 13

Q922V4	1	1	PLRG1	Pleiotropic regulator 1
P50516	1	3	VATA	V-type proton ATPase catalytic subunit A
Q9D753	1	5	EXOS8	Exosome complex component RRP43
Q3UKC1	1	6	TAXB1	Tax1-binding protein 1 homolog
P61021	1	7	RAB5B	Ras-related protein Rab-5B
Q99JI6	1	2	RAP1B	Ras-related protein Rap-1b
Q9D952	1	3	EVPL	Envoplakin
P56960	1	4	EXOSX	Exosome component 10
Q8R0G9	1	6	NU133	Nuclear pore complex protein Nup133
Q8R5H1	1	7	UBP15	Ubiquitin carboxyl-terminal hydrolase 15
Q9Z1X4	1	1	ILF3	Interleukin enhancer-binding factor 3
P35441	1	2	TSP1	Thrombospondin-1
Q9D903	1	5	EBP2	Probable rRNA-processing protein EBP2
Q32M21	1	7	GSDA2	Gasdermin-A2
P70302	1	0	STIM1	Stromal interaction molecule 1
Q9CW46	1	1	RAVR1	Ribonucleoprotein PTB-binding 1
A6X935	1	2	ITIH4	Inter alpha-trypsin inhibitor, heavy chain 4
Q9JLQ2	1	3	GIT2	ARF GTPase-activating protein GIT2
E9Q2M9	1	4	WDFY4	WD repeat- and FYVE domain-containing protein 4 {ECO:0000303|PubMed:30409884}
Q8K224	1	6	NAT10	RNA cytidine acetyltransferase {ECO:0000255|HAMAP-Rule:MF_03211}
Q8CFK6	1	7	DEN1C	DENN domain-containing protein 1C
Q61187	1	0	TS101	Tumor susceptibility gene 101 protein
A2BH40	1	1	ARI1A	AT-rich interactive domain-containing protein 1A
A2ABV5	1	7	MED14	Mediator of RNA polymerase II transcription subunit 14
Q9Z130	1	1	HNRDL	Heterogeneous nuclear ribonucleoprotein D-like
Q9D0I9	1	2	SYRC	Arginine--tRNA ligase, cytoplasmic
Q6ZWV3	1	3	RL10	60S ribosomal protein L10 {ECO:0000305}
Q69ZX6	1	4	MOR2A	ATPase MORC2A {ECO:0000305}
Q8BH69	1	5	SPS1	Selenide, water dikinase 1
Q9D4H2	1	7	GCC1	GRIP and coiled-coil domain-containing protein 1
P32233	1	3	DRG1	Developmentally-regulated GTP-binding protein 1
P61222	1	4	ABCE1	ATP-binding cassette sub-family E member 1
O54879	1	5	HMGB3	High mobility group protein B3

Q2TBA3	1	6	MALT1	Mucosa-associated lymphoid tissue lymphoma translocation protein 1 homolog
Q91WF7	1	7	FIG4	Polyphosphoinositide phosphatase
Q9JKY5	1	3	HIP1R	Huntingtin-interacting protein 1-related protein
Q8BZH4	1	4	POGZ	Pogo transposable element with ZNF domain
Q5SWU9	1	6	ACACA	Acetyl-CoA carboxylase 1 {ECO:0000305}
O70310	1	7	NMT1	Glycylpeptide N-tetradecanoyltransferase 1
P20108	1	0	PRDX3	Thioredoxin-dependent peroxide reductase, mitochondrial
P62702	1	1	RS4X	40S ribosomal protein S4, X isoform
P40630	1	4	TFAM	Transcription factor A, mitochondrial {ECO:0000305}
Q99PP6	1	6	TR34A	Tripartite motif-containing protein 34A
Q9D4H8	1	7	CUL2	Cullin-2
P70268	1	0	PKN1	Serine/threonine-protein kinase N1
Q61210	1	2	ARHG1	Rho guanine nucleotide exchange factor 1
Q91V41	1	3	RAB14	Ras-related protein Rab-14
Q9EQ32	1	4	BCAP	Phosphoinositide 3-kinase adapter protein 1
A2AT37	1	6	RENT2	Regulator of nonsense transcripts 2
P62340	1	7	TBPL1	TATA box-binding protein-like 1
P62754	1	1	RS6	40S ribosomal protein S6
P49312	1	1	ROA1	Heterogeneous nuclear ribonucleoprotein A1
Q921Y0	1	5	MOB1A	MOB kinase activator 1A
Q9DC48	1	6	PRP17	Pre-mRNA-processing factor 17
P53996	1	7	CNBP	Cellular nucleic acid-binding protein
Q9WUP7	1	3	UCHL5	Ubiquitin carboxyl-terminal hydrolase isozyme L5
Q99L45	1	4	IF2B	Eukaryotic translation initiation factor 2 subunit 2
Q9QX47	1	1	SON	Protein SON
Q60932	1	3	VDAC1	Voltage-dependent anion-selective channel protein 1
Q62009	1	4	POSTN	Periostin
P97822	1	5	AN32E	Acidic leucine-rich nuclear phosphoprotein 32 family member E
P39053	1	6	DYN1	Dynamin-1
P17809	1	7	GTR1	Solute carrier family 2, facilitated glucose transporter member 1 {ECO:0000305}
Q62189	1	1	SNRPA	U1 small nuclear ribonucleoprotein A
Q80Z25	1	7	OFD1	Oral-facial-digital syndrome 1 protein homolog
P32067	1	1	LA	Lupus La protein homolog

P05201	1	5	AATC	Aspartate aminotransferase, cytoplasmic
Q9CU65	1	6	ZMYM2	Zinc finger MYM-type protein 2
P63168	1	3	DYL1	Dynein light chain 1, cytoplasmic
Q4LDD4	1	4	ARAP1	Arf-GAP with Rho-GAP domain, ANK repeat and PH domain-containing protein 1
P67871	1	5	CSK2B	Casein kinase II subunit beta
Q5BLK4	1	6	TUT7	Terminal uridylyltransferase 7 {ECO:0000305}
Q9JIB4	1	7	TF2H2	General transcription factor IIH subunit 2
Q6RHW0	1	3	K1C9	Keratin, type I cytoskeletal 9
P24270	1	4	CATA	Catalase
Q04207	1	5	TF65	Transcription factor p65
Q9Z0H1	1	6	WDR46	WD repeat-containing protein 46
Q9CWF2	1	7	TBB2B	Tubulin beta-2B chain
P29341	1	1	PABP1	Polyadenylate-binding protein 1
Q99JF8	1	4	PSIP1	PC4 and SFRS1-interacting protein
Q9D8B7	1	5	JAM3	Junctional adhesion molecule C
Q8BUH8	1	1	SENP7	Sentrin-specific protease 7
Q61510	1	4	TRI25	E3 ubiquitin/ISG15 ligase TRIM25
O88379	1	6	BAZ1A	Bromodomain adjacent to zinc finger domain protein 1A
P60867	1	3	RS20	40S ribosomal protein S20
Q9DBE9	1	7	SPB1	pre-rRNA 2'-O-ribose RNA methyltransferase FTSJ3 {ECO:0000255|HAMAP-Rule:MF_03163}
P14685	1	4	PSMD3	26S proteasome non-ATPase regulatory subunit 3
Q9CSN1	1	1	SNW1	SNW domain-containing protein 1
P08003	1	3	PDIA4	Protein disulfide-isomerase A4
Q8CIN4	1	5	PAK2	Serine/threonine-protein kinase PAK 2
Q69ZA1	1	6	CDK13	Cyclin-dependent kinase 13
P06151	1	1	LDHA	L-lactate dehydrogenase A chain
Q8K4F6	1	4	NSUN5	28S rRNA (cytosine-C(5))-methyltransferase {ECO:0000305}
Q8BU03	1	6	PWP2	Periodic tryptophan protein 2 homolog
P01837	1	1	IGKC	Immunoglobulin kappa constant {ECO:0000250|UniProtKB:P01834}
Q91YP3	1	5	DEOC	Deoxyribose-phosphate aldolase
Q8BG81	1	1	PDIP3	Polymerase delta-interacting protein 3
D3Z1D3	1	3	CEFIP	Cardiac-enriched FHL2-interacting protein {ECO:0000303|PubMed:28717008}
Q00196	1	4	PO2F2	POU domain, class 2, transcription factor 2 {ECO:0000305}

Q6PDK2	1	6	KMT2D	Histone-lysine N-methyltransferase 2D
P57722	1	7	PCBP3	Poly(rC)-binding protein 3
Q9JLI8	1	1	SART3	Squamous cell carcinoma antigen recognized by T-cells 3 {ECO:0000305}
P62821	1	3	RAB1A	Ras-related protein Rab-1A
Q3UMY5	1	4	EMAL4	Echinoderm microtubule-associated protein-like 4
P33175	1	5	KIF5A	Kinesin heavy chain isoform 5A
O09106	1	1	HDAC1	Histone deacetylase 1
Q6DFV5	1	4	HELZ	Probable helicase with zinc finger domain
Q75N62	1	5	GIMA8	GTPase IMAP family member 8
P08775	1	1	RPB1	DNA-directed RNA polymerase II subunit RPB1
Q99388	1	3	CSPRS	Component of Sp100-rs
Q91ZA3	1	5	PCCA	Propionyl-CoA carboxylase alpha chain, mitochondrial {ECO:0000305|PubMed:11461925}
Q8BYH8	1	6	CHD9	Chromodomain-helicase-DNA-binding protein 9
Q8BU11	1	7	TOX4	TOX high mobility group box family member 4
Q920B9	1	1	SP16H	FACT complex subunit SPT16
P49722	1	3	PSA2	Proteasome subunit alpha type-2
Q78PY7	1	4	SND1	Staphylococcal nuclease domain-containing protein 1
Q8CG47	1	6	SMC4	Structural maintenance of chromosomes protein 4
Q8VEM8	1	3	MPCP	Phosphate carrier protein, mitochondrial
Q4FK66	1	6	PR38A	Pre-mRNA-splicing factor 38A
Q91YE6	1	7	IPO9	Importin-9
P63087	1	4	PP1G	Serine/threonine-protein phosphatase PP1-gamma catalytic subunit
Q8C0D5	1	6	EFL1	Elongation factor-like GTPase 1
Q9JJW6	1	7	ALRF2	Aly/REF export factor 2
P63101	1	1	1433Z	14-3-3 protein zeta/delta
Q922D8	1	3	C1TC	C-1-tetrahydrofolate synthase, cytoplasmic
Q3THS6	1	5	METK2	S-adenosylmethionine synthase isoform type-2
P58501	1	6	PAXB1	PAX3- and PAX7-binding protein 1
Q7TQK1	1	7	INT7	Integrator complex subunit 7
Q8R307	1	6	VPS18	Vacuolar protein sorting-associated protein 18 homolog
Q8C129	1	7	LCAP	Leucyl-cystinyl aminopeptidase
Q06890	1	3	CLUS	Clusterin {ECO:0000303|PubMed:8354695}
Q3TJZ6	1	4	FA98A	Protein FAM98A {ECO:0000305}

Q8CBW3	1	7	ABI1	Abl interactor 1
Q8CHY6	1	1	P66A	Transcriptional repressor p66 alpha
P29416	1	4	HEXA	Beta-hexosaminidase subunit alpha {ECO:0000305}
Q9CWJ9	1	5	PUR9	Bifunctional purine biosynthesis protein ATIC
Q8BMC4	1	7	NOP9	Nucleolar protein 9
P70168	1	1	IMB1	Importin subunit beta-1
Q8BMS9	1	3	RASF2	Ras association domain-containing protein 2
E9PYI1	1	5	ZN568	Zinc finger protein 568 {ECO:0000312|MGI:MGI:2142347}
Q99JR8	1	1	SMRD2	SWI/SNF-related matrix-associated actin-dependent regulator of chromatin subfamily D member 2
P08752	1	4	GNAI2	Guanine nucleotide-binding protein G(i) subunit alpha-2
Q11136	1	6	PEPD	Xaa-Pro dipeptidase
Q64213	1	1	SF01	Splicing factor 1
P49718	1	5	MCM5	DNA replication licensing factor MCM5 {ECO:0000250|UniProtKB:P33992}
Q924T7	1	6	RNF31	E3 ubiquitin-protein ligase RNF31
Q8K2V6	1	7	IPO11	Importin-11
Q60520	1	1	SIN3A	Paired amphipathic helix protein Sin3a
Q9D8B3	1	3	CHM4B	Charged multivesicular body protein 4b
Q6NZF1	1	4	ZC11A	Zinc finger CCCH domain-containing protein 11A
Q810D6	1	7	GRWD1	Glutamate-rich WD repeat-containing protein 1
Q924A2	1	6	CIC	Protein capicua homolog
Q80U70	1	7	SUZ12	Polycomb protein Suz12
P23116	1	3	EIF3A	Eukaryotic translation initiation factor 3 subunit A {ECO:0000255|HAMAP-Rule:MF_03000}
P14234	1	4	FGR	Tyrosine-protein kinase Fgr
Q91Z31	1	5	PTBP2	Polypyrimidine tract-binding protein 2
Q61686	1	6	CBX5	Chromobox protein homolog 5
Q91VY9	1	4	ZN622	Zinc finger protein 622
Q9QYI3	1	5	DNJC7	DnaJ homolog subfamily C member 7
Q99L43	1	6	CDS2	Phosphatidate cytidylyltransferase 2 {ECO:0000305}
Q4FZC9	1	7	SYNE3	Nesprin-3
Q5RJH6	1	4	SMG7	Protein SMG7
P62743	1	6	AP2S1	AP-2 complex subunit sigma
Q3ULD5	1	7	MCCB	Methylcrotonoyl-CoA carboxylase beta chain, mitochondrial
Q8BHJ5	1	1	TBL1R	F-box-like/WD repeat-containing protein TBL1XR1

P23492	1	5	PNPH	Purine nucleoside phosphorylase
Q0P678	1	3	ZCH18	Zinc finger CCCH domain-containing protein 18
P17141	1	5	ZFP37	Zinc finger protein 37
Q8CIM8	1	6	INT4	Integrator complex subunit 4
Q8VCY6	1	7	UTP6	U3 small nucleolar RNA-associated protein 6 homolog
Q9CXY6	1	1	ILF2	Interleukin enhancer-binding factor 2
P61205	1	3	ARF3	ADP-ribosylation factor 3
P61982	1	1	1433G	14-3-3 protein gamma
Q69ZR2	1	6	HECD1	E3 ubiquitin-protein ligase HECTD1
Q9R0L6	1	6	PCM1	Pericentriolar material 1 protein
P25425	1	7	PO2F1	POU domain, class 2, transcription factor 1
P22935	1	3	RABP2	Cellular retinoic acid-binding protein 2
Q99LB2	1	4	DHRS4	Dehydrogenase/reductase SDR family member 4
Q924W5	1	6	SMC6	Structural maintenance of chromosomes protein 6
Q6P5B0	1	5	RRP12	RRP12-like protein
Q61703	1	1	ITIH2	Inter-alpha-trypsin inhibitor heavy chain H2
Q7TSH6	1	3	SCAF4	SR-related and CTD-associated factor 4 {ECO:0000305}
Q9D071	1	7	MMS19	MMS19 nucleotide excision repair protein homolog
Q8CH18	1	1	CCAR1	Cell division cycle and apoptosis regulator protein 1
Q5F2E7	1	4	NUFP2	Nuclear fragile X mental retardation-interacting protein 2
Q921H8	1	7	THIKA	3-ketoacyl-CoA thiolase A, peroxisomal {ECO:0000305}
P47911	1	1	RL6	60S ribosomal protein L6
Q9D0T1	1	3	NH2L1	NHP2-like protein 1
Q99N69	1	4	LPXN	Leupaxin
Q80Y81	1	7	RNZ2	Zinc phosphodiesterase ELAC protein 2
A2A4P0	1	6	DHX8	ATP-dependent RNA helicase DHX8
Q91VU7	1	7	PUS7	Pseudouridylate synthase 7 homolog {ECO:0000305}
Q8BX09	1	1	RBBP5	Retinoblastoma-binding protein 5
Q9CR16	1	5	PPID	Peptidyl-prolyl cis-trans isomerase D {ECO:0000250|UniProtKB:Q08752}
Q9JHW9	1	3	AL1A3	Aldehyde dehydrogenase family 1 member A3
Q9DCE5	1	6	PK1IP	p21-activated protein kinase-interacting protein 1
O88939	1	7	ZBT7A	Zinc finger and BTB domain-containing protein 7A {ECO:0000305}
Q60692	1	3	PSB6	Proteasome subunit beta type-6

P54823	1	4	DDX6	Probable ATP-dependent RNA helicase DDX6 {ECO:0000305}
Q9JLV5	1	5	CUL3	Cullin-3
Q3TDD9	1	6	PPR21	Protein phosphatase 1 regulatory subunit 21
Q3UEB3	1	1	PUF60	Poly(U)-binding-splicing factor PUF60
Q8BNV1	1	4	TRM2A	tRNA (uracil-5-)-methyltransferase homolog A
P47941	1	5	CRKL	Crk-like protein
Q91WJ8	1	1	FUBP1	Far upstream element-binding protein 1
Q99J72	1	4	ABEC3	DNA dC->dU-editing enzyme APOBEC-3
Q8BZX4	1	6	SREK1	Splicing regulatory glutamine/lysine-rich protein 1
Q920A7	1	7	AFG31	AFG3-like protein 1
P25206	1	4	MCM3	DNA replication licensing factor MCM3
P21855	1	1	CD72	B-cell differentiation antigen CD72
O55142	1	3	RL35A	60S ribosomal protein L35a
P97484	1	5	LIRB3	Leukocyte immunoglobulin-like receptor subfamily B member 3
Q01965	1	7	LY9	T-lymphocyte surface antigen Ly-9
P80316	1	3	TCPE	T-complex protein 1 subunit epsilon
P14576	1	4	SRP54	Signal recognition particle 54 kDa protein
Q3U821	1	6	WDR75	WD repeat-containing protein 75
Q922J9	1	3	FACR1	Fatty acyl-CoA reductase 1 {ECO:0000305|PubMed:15220348}
Q9Z2C4	1	4	MTMR1	Myotubularin-related protein 1
Q9QY76	1	5	VAPB	Vesicle-associated membrane protein-associated protein B
Q8CHG3	1	6	GCC2	GRIP and coiled-coil domain-containing protein 2
Q8BIH0	1	7	SP130	Histone deacetylase complex subunit SAP130
Q9WV80	1	3	SNX1	Sorting nexin-1
Q921G6	1	4	LRCH4	Leucine-rich repeat and calponin homology domain-containing protein 4
Q9R020	1	6	ZRAB2	Zinc finger Ran-binding domain-containing protein 2
P70403	1	7	CASP	Protein CASP
Q61233	1	1	PLSL	Plastin-2
P06800	1	3	PTPRC	Receptor-type tyrosine-protein phosphatase C {ECO:0000305}
Q64514	1	5	TPP2	Tripeptidyl-peptidase 2
P24549	1	3	AL1A1	Retinal dehydrogenase 1 {ECO:0000305}
A2A432	1	5	CUL4B	Cullin-4B {ECO:0000312|EMBL:CAM17145.1}
Q9Z1R2	1	6	BAG6	Large proline-rich protein BAG6 {ECO:0000305}

P97303	1	6	BACH2	Transcription regulator protein BACH2
Q8C3J5	1	1	DOCK2	Dedicator of cytokinesis protein 2
Q9D6K7	1	7	TTC33	Tetratricopeptide repeat protein 33
P63242	1	3	IF5A1	Eukaryotic translation initiation factor 5A-1
Q9R207	1	5	NBN	Nibrin
Q5SSH7	1	6	ZZEF1	Zinc finger ZZ-type and EF-hand domain-containing protein 1
P01807	1	4	HVM37	Ig heavy chain V region X44
P62918	1	1	RL8	60S ribosomal protein L8
Q99LI7	1	3	CSTF3	Cleavage stimulation factor subunit 3
Q8BG48	1	5	ST17B	Serine/threonine-protein kinase 17B
Q8K2V1	1	7	PP4R1	Serine/threonine-protein phosphatase 4 regulatory subunit 1
Q9CQC6	1	5	BZW1	Basic leucine zipper and W2 domain-containing protein 1
Q6PIU9	1	6	YJ005	Uncharacterized protein FLJ45252 homolog
P46471	1	3	PRS7	26S proteasome regulatory subunit 7
P97313	1	6	PRKDC	DNA-dependent protein kinase catalytic subunit
Q8VI75	1	7	IPO4	Importin-4
P60122	1	1	RUVB1	RuvB-like 1
Q08288	1	5	LYAR	Cell growth-regulating nucleolar protein
Q9Z0H3	1	1	SNF5	SWI/SNF-related matrix-associated actin-dependent regulator of chromatin subfamily B member 1
Q91VL8	1	4	TE2IP	Telomeric repeat-binding factor 2-interacting protein 1
Q6DID3	1	5	SCAF8	SR-related and CTD-associated factor 8 {ECO:0000305}
G5E8P1	1	6	BRD1	Bromodomain-containing protein 1 {ECO:0000303|PubMed:21753189}
O35904	1	7	PK3CD	Phosphatidylinositol 4,5-bisphosphate 3-kinase catalytic subunit delta isoform
Q08943	1	1	SSRP1	FACT complex subunit SSRP1
P54071	1	4	IDHP	Isocitrate dehydrogenase [NADP], mitochondrial
Q6ZPY7	1	5	KDM3B	Lysine-specific demethylase 3B
Q80WJ7	1	6	LYRIC	Protein LYRIC
P26041	1	1	MOES	Moesin {ECO:0000303|PubMed:1429901}
P20060	1	3	HEXB	Beta-hexosaminidase subunit beta {ECO:0000305}
G5E870	1	4	TRIPC	E3 ubiquitin-protein ligase TRIP12
P97742	1	6	CPT1A	Carnitine O-palmitoyltransferase 1, liver isoform
P47857	1	7	PFKAM	ATP-dependent 6-phosphofructokinase, muscle type {ECO:0000255|HAMAP-Rule:MF_03184}
Q61550	1	1	RAD21	Double-strand-break repair protein rad21 homolog

Q9JL62	1	3	GLTP	Glycolipid transfer protein
Q7TPD0	1	6	INT3	Integrator complex subunit 3
Q920E3	1	7	KCNH5	Potassium voltage-gated channel subfamily H member 5
Q8BGH2	1	4	SAM50	Sorting and assembly machinery component 50 homolog
P61963	1	5	DCAF7	DDB1- and CUL4-associated factor 7
Q9JHS4	1	7	CLPX	ATP-dependent Clp protease ATP-binding subunit clpX-like, mitochondrial
Q6PE01	1	1	SNR40	U5 small nuclear ribonucleoprotein 40 kDa protein
P24452	1	3	CAPG	Macrophage-capping protein
P62717	1	4	RL18A	60S ribosomal protein L18a
Q91WQ5	1	5	TAF5L	TAF5-like RNA polymerase II p300/CBP-associated factor-associated factor 65 kDa subunit 5L {ECO:0000305}
Q61990	1	1	PCBP2	Poly(rC)-binding protein 2
Q6GQT1	1	3	A2MG	Alpha-2-macroglobulin-P
Q8BMB0	1	6	EMSY	BRCA2-interacting transcriptional repressor EMSY {ECO:0000250|UniProtKB:Q7Z589}
Q3TW96	1	7	UAP1L	UDP-N-acetylhexosamine pyrophosphorylase-like protein 1
Q62311	1	1	TAF6	Transcription initiation factor TFIID subunit 6
Q8R2Q0	1	3	TRI29	Tripartite motif-containing protein 29
Q8R149	1	6	BUD13	BUD13 homolog
Q80YD1	1	7	SUV3	ATP-dependent RNA helicase SUPV3L1, mitochondrial
O70194	1	3	EIF3D	Eukaryotic translation initiation factor 3 subunit D {ECO:0000255|HAMAP-Rule:MF_03003}
Q810B6	1	4	ANFY1	Rabankyrin-5 {ECO:0000303|PubMed:15328530}
Q99NB1	1	5	ACS2L	Acetyl-coenzyme A synthetase 2-like, mitochondrial
Q8BSQ9	1	6	PB1	Protein polybromo-1
Q80XC6	1	7	NRDE2	Nuclear exosome regulator NRDE2 {ECO:0000305}
Q9Z172	1	1	SUMO3	Small ubiquitin-related modifier 3 {ECO:0000305}
Q9CWZ3	1	5	RBM8A	RNA-binding protein 8A
P05622	1	7	PGFRB	Platelet-derived growth factor receptor beta
Q9CZU3	1	1	MTREX	Exosome RNA helicase MTR4 {ECO:0000305}
P70296	1	3	PEBP1	Phosphatidylethanolamine-binding protein 1
P84084	1	4	ARF5	ADP-ribosylation factor 5
Q61838	1	6	PZP	Pregnancy zone protein
Q3TNL8	1	7	IPRI	Inositol 1,4,5-trisphosphate receptor-interacting protein
Q61171	1	4	PRDX2	Peroxiredoxin-2
P59114	1	5	CAPAM	mRNA (2'-O-methyladenosine-N(6)-)-methyltransferase {ECO:0000250|UniProtKB:Q9H4Z3}

Q8C0I1	1	7	ADAS	Alkyldihydroxyacetonephosphate synthase, peroxisomal
Q61495	1	1	DSG1A	Desmoglein-1-alpha
P35329	1	3	CD22	B-cell receptor CD22
P62267	1	6	RS23	40S ribosomal protein S23
Q8CHP5	1	5	PYM1	Partner of Y14 and mago {ECO:0000250|UniProtKB:P82804}
Q99KQ4	1	3	NAMPT	Nicotinamide phosphoribosyltransferase
O70305	1	4	ATX2	Ataxin-2
P11531	1	6	DMD	Dystrophin
O35900	1	7	LSM2	U6 snRNA-associated Sm-like protein LSm2
B1AZI6	1	1	THOC2	THO complex subunit 2
Q8BH43	1	3	WASF2	Wiskott-Aldrich syndrome protein family member 2
O08677	1	4	KNG1	Kininogen-1
Q8R3G1	1	5	PP1R8	Nuclear inhibitor of protein phosphatase 1
Q61941	1	6	NNTM	NAD(P) transhydrogenase, mitochondrial
O35638	1	1	STAG2	Cohesin subunit SA-2
Q8K0E8	1	3	FIBB	Fibrinogen beta chain
Q9D883	1	4	U2AF1	Splicing factor U2AF 35 kDa subunit
E9Q784	1	6	ZC3HD	Zinc finger CCCH domain-containing protein 13 {ECO:0000305}
Q0VEE6	1	7	ZN800	Zinc finger protein 800
Q9WTM5	1	1	RUVB2	RuvB-like 2
P99026	1	3	PSB4	Proteasome subunit beta type-4
Q8VCH6	1	5	DHC24	Delta(24)-sterol reductase
O35099	1	6	M3K5	Mitogen-activated protein kinase kinase kinase 5
Q9JJF3	1	7	RIOX1	Ribosomal oxygenase 1 {ECO:0000312|MGI:MGI:1919202}
Q5SUF2	1	3	LC7L3	Luc7-like protein 3
Q91VX2	1	4	UBAP2	Ubiquitin-associated protein 2
Q9WTU0	1	5	PHF2	Lysine-specific demethylase PHF2
Q91WG4	1	6	ELP2	Elongator complex protein 2
Q8CFB4	1	7	GBP5	Guanylate-binding protein 5
Q7TMQ7	1	3	WDR91	WD repeat-containing protein 91 {ECO:0000312|MGI:MGI:2141558}
Q8C3R1	1	5	BRAT1	BRCA1-associated ATM activator 1
E9Q5F9	1	6	SETD2	Histone-lysine N-methyltransferase SETD2 {ECO:0000305}
Q5U4D9	1	1	THOC6	THO complex subunit 6 homolog

Q80U93	1	4	NU214	Nuclear pore complex protein Nup214
Q1LZI2	1	5	S35F3	Putative thiamine transporter SLC35F3 {ECO:0000250|UniProtKB:Q8IY50}
Q91YJ5	1	7	IF2M	Translation initiation factor IF-2, mitochondrial
Q61789	1	1	LAMA3	Laminin subunit alpha-3
P08905	1	3	LYZ2	Lysozyme C-2
O35130	1	5	NEP1	Ribosomal RNA small subunit methyltransferase NEP1 {ECO:0000250|UniProtKB:Q92979}
Q8BZR9	1	6	NCBP3	Nuclear cap-binding protein subunit 3 {ECO:0000250|UniProtKB:Q53F19}
Q8CH02	1	7	SUGP1	SURP and G-patch domain-containing protein 1
Q62120	1	3	JAK2	Tyrosine-protein kinase JAK2 {ECO:0000305}
Q8BIK4	1	6	DOCK9	Dedicator of cytokinesis protein 9
Q6SJ95	1	3	TBPL2	TATA box-binding protein-like 2
P00493	1	5	HPRT	Hypoxanthine-guanine phosphoribosyltransferase
A2RSJ4	1	6	UH1BL	UHRF1-binding protein 1-like {ECO:0000312|MGI:MGI:2442888}
Q923B1	1	7	DBR1	Lariat debranching enzyme
P25444	1	1	RS2	40S ribosomal protein S2
P84099	1	3	RL19	60S ribosomal protein L19
Q9DAA6	1	5	EXOS1	Exosome complex component CSL4
Q6P9Q4	1	6	FHOD1	FH1/FH2 domain-containing protein 1
Q9WTV7	1	7	RNF12	E3 ubiquitin-protein ligase RLIM
Q9R0I7	1	1	YLPM1	YLP motif-containing protein 1
P63028	1	5	TCTP	Translationally-controlled tumor protein
O88844	1	3	IDHC	Isocitrate dehydrogenase [NADP] cytoplasmic
Q9JKV1	1	5	ADRM1	Proteasomal ubiquitin receptor ADRM1
Q8BHY2	1	7	NOC4L	Nucleolar complex protein 4 homolog
P14869	1	1	RLA0	60S acidic ribosomal protein P0
P98083	1	6	SHC1	SHC-transforming protein 1
Q9ESU6	1	1	BRD4	Bromodomain-containing protein 4
B2RY56	1	4	RBM25	RNA-binding protein 25
Q9Z0W3	1	6	NU160	Nuclear pore complex protein Nup160
Q9ES64	1	7	USH1C	Harmonin
Q569Z5	1	1	DDX46	Probable ATP-dependent RNA helicase DDX46
P62334	1	3	PRS10	26S proteasome regulatory subunit 10B
Q8C6G8	1	6	WDR26	WD repeat-containing protein 26

Q7TMC8	1	7	FCSK	L-fucose kinase {ECO:0000305}
P58252	1	1	EF2	Elongation factor 2
Q8VDM4	1	3	PSMD2	26S proteasome non-ATPase regulatory subunit 2
O08756	1	5	HCD2	3-hydroxyacyl-CoA dehydrogenase type-2
Q8CAS9	1	6	PARP9	Protein mono-ADP-ribosyltransferase PARP9 {ECO:0000305}
Q8BWQ6	1	7	VP35L	VPS35 endosomal protein-sorting factor-like {ECO:0000305}
Q3U487	1	7	HECD3	E3 ubiquitin-protein ligase HECTD3
Q80XU3	1	6	NUCKS	Nuclear ubiquitous casein and cyclin-dependent kinase substrate 1
Q9CQG2	1	7	MET16	RNA N6-adenosine-methyltransferase METTL16 {ECO:0000305}
Q60749	1	1	KHDR1	KH domain-containing, RNA-binding, signal transduction-associated protein 1
Q78ZA7	1	4	NP1L4	Nucleosome assembly protein 1-like 4
E9QAT4	1	5	SC16A	Protein transport protein Sec16A
Q8CEC0	1	6	NUP88	Nuclear pore complex protein Nup88
Q80UK7	1	7	SAS6	Spindle assembly abnormal protein 6 homolog {ECO:0000305}
Q9EST5	1	1	AN32B	Acidic leucine-rich nuclear phosphoprotein 32 family member B
P50247	1	4	SAHH	Adenosylhomocysteinase
P58929	1	7	GMEB2	Glucocorticoid modulatory element-binding protein 2
Q9CQT2	1	4	RBM7	RNA-binding protein 7 {ECO:0000305}
Q69Z37	1	6	SAM9L	Sterile alpha motif domain-containing protein 9-like
O88351	1	4	IKKB	Inhibitor of nuclear factor kappa-B kinase subunit beta
O70481	1	6	UBR1	E3 ubiquitin-protein ligase UBR1
P97324	1	7	G6PD2	Glucose-6-phosphate 1-dehydrogenase 2
O55201	1	1	SPT5H	Transcription elongation factor SPT5
Q8BFY9	1	4	TNPO1	Transportin-1
Q6P5E6	1	5	GGA2	ADP-ribosylation factor-binding protein GGA2
Q8CG48	1	6	SMC2	Structural maintenance of chromosomes protein 2
P28659	1	7	CELF1	CUGBP Elav-like family member 1
P58871	1	6	TB182	182 kDa tankyrase-1-binding protein
Q9D906	1	7	ATG7	Ubiquitin-like modifier-activating enzyme ATG7
Q9Z1Q9	1	1	SYVC	Valine--tRNA ligase
Q9WV70	1	7	NOC2L	Nucleolar complex protein 2 homolog
P35235	1	7	PTN11	Tyrosine-protein phosphatase non-receptor type 11
Q9DBR1	1	1	XRN2	5'-3' exoribonuclease 2

O88627	1	6	S28A2	Sodium/nucleoside cotransporter 2
Q91YE7	1	7	RBM5	RNA-binding protein 5
Q9JI13	1	5	SAS10	Something about silencing protein 10
Q3UHC2	1	6	LRRK1	Leucine-rich repeat serine/threonine-protein kinase 1
Q8BGC0	1	7	HTSF1	HIV Tat-specific factor 1 homolog
P80314	1	4	TCPB	T-complex protein 1 subunit beta
P39749	1	5	FEN1	Flap endonuclease 1 {ECO:0000255|HAMAP-Rule:MF_03140}
P63166	1	1	SUMO1	Small ubiquitin-related modifier 1
Q9WTK5	1	6	NFKB2	Nuclear factor NF-kappa-B p100 subunit
Q8CGB3	1	7	UACA	Uveal autoantigen with coiled-coil domains and ankyrin repeats
Q60668	1	1	HNRPD	Heterogeneous nuclear ribonucleoprotein D0
Q3TWF6	1	6	WDR70	WD repeat-containing protein 70
Q9QUK6	1	7	TLR4	Toll-like receptor 4
Q9ET01	1	5	PYGL	Glycogen phosphorylase, liver form
Q8BHZ4	1	6	ZN592	Zinc finger protein 592
P63158	1	1	HMGB1	High mobility group protein B1
Q9WVQ5	1	5	MTNB	Methylthioribulose-1-phosphate dehydratase {ECO:0000255|HAMAP-Rule:MF_03116}
P55937	1	6	GOGA3	Golgin subfamily A member 3
Q9D0R4	1	7	DDX56	Probable ATP-dependent RNA helicase DDX56
Q9JKP5	1	1	MBNL1	Muscleblind-like protein 1
Q9R0G6	1	4	COMP	Cartilage oligomeric matrix protein
P97452	1	5	BOP1	Ribosome biogenesis protein BOP1 {ECO:0000255|HAMAP-Rule:MF_03027}
E9Q8T7	1	6	DYH1	Dynein axonemal heavy chain 1
O08967	1	7	CYH3	Cytohesin-3
Q5SYD0	1	4	MYO1D	Unconventional myosin-Id
Q07802	1	5	COE1	Transcription factor COE1
A2BE28	1	6	LAS1L	Ribosomal biogenesis protein LAS1L
Q64287	1	7	IRF4	Interferon regulatory factor 4
Q9EQU5	1	1	SET	Protein SET
Q9CZN7	1	4	GLYM	Serine hydroxymethyltransferase, mitochondrial {ECO:0000305}
Q9D1A2	1	5	CNDP2	Cytosolic non-specific dipeptidase
Q8VDG3	1	6	PARN	Poly(A)-specific ribonuclease PARN
Q8R3C0	1	5	MCMBP	Mini-chromosome maintenance complex-binding protein

P68373	1	6	TBA1C	Tubulin alpha-1C chain
Q6P9R1	1	7	DDX51	ATP-dependent RNA helicase DDX51
Q9CXW3	1	5	CYBP	Calcyclin-binding protein
Q6ZWY9	1	6	H2B1C	Histone H2B type 1-C/E/G
Q9DBY8	1	1	NVL	Nuclear valosin-containing protein-like
P35979	1	4	RL12	60S ribosomal protein L12
P26043	1	6	RADI	Radixin
Q62280	1	7	SSXT	Protein SSXT
Q8BIQ5	1	4	CSTF2	Cleavage stimulation factor subunit 2
Q60664	1	7	IRAG2	Inositol 1,4,5-triphosphate receptor associated 2 {ECO:0000305}
P47915	1	4	RL29	60S ribosomal protein L29
P35922	1	5	FMR1	Synaptic functional regulator FMR1 {ECO:0000305}
Q3TFD2	1	7	PCAT1	Lysophosphatidylcholine acyltransferase 1
Q61464	1	1	ZN638	Zinc finger protein 638 {ECO:0000303|PubMed:21602272}
Q8K4I3	1	4	ARHG6	Rho guanine nucleotide exchange factor 6
Q9D824	1	5	FIP1	Pre-mRNA 3'-end-processing factor FIP1
Q6GSS7	1	6	H2A2A	Histone H2A type 2-A
Q9JIF0	1	1	ANM1	Protein arginine N-methyltransferase 1
Q8BP67	1	4	RL24	60S ribosomal protein L24
Q9DCD2	1	6	SYF1	Pre-mRNA-splicing factor SYF1
Q810V0	1	7	MPP10	U3 small nucleolar ribonucleoprotein protein MPP10
P26369	1	4	U2AF2	Splicing factor U2AF 65 kDa subunit
Q8BKT7	1	7	THOC5	THO complex subunit 5 homolog
Q8R4U7	1	1	LUZP1	Leucine zipper protein 1
P62270	1	4	RS18	40S ribosomal protein S18
O09130	1	5	NF2IP	NFATC2-interacting protein
Q9WTX6	1	7	CUL1	Cullin-1
P28656	1	4	NP1L1	Nucleosome assembly protein 1-like 1
Q810A7	1	6	DDX42	ATP-dependent RNA helicase DDX42
Q8VDD8	1	7	WASH1	WASH complex subunit 1 {ECO:0000312|MGI:MGI:1916017}
P19973	1	1	LSP1	Lymphocyte-specific protein 1
Q8C7R4	1	6	UBA6	Ubiquitin-like modifier-activating enzyme 6
Q9CWK3	1	7	CD2B2	CD2 antigen cytoplasmic tail-binding protein 2

P23198	1	1	CBX3	Chromobox protein homolog 3
P28352	1	4	APEX1	DNA-(apurinic or apyrimidinic site) endonuclease
P68033	1	7	ACTC	Actin, alpha cardiac muscle 1
Q922K7	1	1	NOP2	Probable 28S rRNA (cytosine-C(5))-methyltransferase
P70122	1	5	SBDS	Ribosome maturation protein SBDS
Q99JT2	1	4	STK26	Serine/threonine-protein kinase 26 {ECO:0000305}
P63085	1	5	MK01	Mitogen-activated protein kinase 1
Q99NH0	1	4	ANR17	Ankyrin repeat domain-containing protein 17
Q9CWL8	1	5	CTBL1	Beta-catenin-like protein 1
P97376	1	1	FRG1	Protein FRG1
Q8CI11	1	6	GNL3	Guanine nucleotide-binding protein-like 3
Q9JKB3	1	7	YBOX3	Y-box-binding protein 3
Q921N6	1	5	DDX27	Probable ATP-dependent RNA helicase DDX27
Q00422	1	6	GABPA	GA-binding protein alpha chain
Q8BVI4	1	7	DHPR	Dihydropteridine reductase
O88512	1	6	AP1G2	AP-1 complex subunit gamma-like 2
Q9Z2E1	1	1	MBD2	Methyl-CpG-binding domain protein 2 {ECO:0000305}
P47811	1	7	MK14	Mitogen-activated protein kinase 14
Q9QYE3	1	1	BC11A	B-cell lymphoma/leukemia 11A
O54734	1	5	OST48	Dolichyl-diphosphooligosaccharide--protein glycosyltransferase 48 kDa subunit
Q3TIR3	1	6	RIC8A	Synembryn-A
P62827	1	1	RAN	GTP-binding nuclear protein Ran
Q3TUH1	1	5	TAM41	Phosphatidate cytidylyltransferase, mitochondrial
P15532	1	7	NDKA	Nucleoside diphosphate kinase A
Q62376	1	1	RU17	U1 small nuclear ribonucleoprotein 70 kDa
O70494	1	4	SP3	Transcription factor Sp3
Q8R0A0	1	7	T2FB	General transcription factor IIF subunit 2
Q8VHD8	1	1	HORN	Hornerin
Q922Q8	1	4	LRC59	Leucine-rich repeat-containing protein 59
P27641	1	5	XRCC5	X-ray repair cross-complementing protein 5
Q8R3N6	1	6	THOC1	THO complex subunit 1
Q3U2S8	1	7	HVCN1	Voltage-gated hydrogen channel 1
O88532	1	1	ZFR	Zinc finger RNA-binding protein

Q01320	1	6	TOP2A	DNA topoisomerase 2-alpha
Q921T2	1	1	TOIP1	Torsin-1A-interacting protein 1
Q9EP89	1	6	LACTB	Serine beta-lactamase-like protein LACTB, mitochondrial {ECO:0000305}
Q9JL26	1	1	FMNL1	Formin-like protein 1
Q9DBR7	1	4	MYPT1	Protein phosphatase 1 regulatory subunit 12A
Q9QUG9	1	6	GRP2	RAS guanyl-releasing protein 2
Q9D1Q6	1	7	ERP44	Endoplasmic reticulum resident protein 44
Q8BFQ4	1	1	WDR82	WD repeat-containing protein 82
Q8BGD9	1	4	IF4B	Eukaryotic translation initiation factor 4B
Q9R0N0	1	7	GALK1	Galactokinase
P08226	1	1	APOE	Apolipoprotein E
Q8BLR5	1	5	PSD4	PH and SEC7 domain-containing protein 4
Q8CE96	1	6	TRM6	tRNA (adenine(58)-N(1))-methyltransferase non-catalytic subunit TRM6
P05132	1	4	KAPCA	cAMP-dependent protein kinase catalytic subunit alpha
Q8BHZ0	1	5	CYRIA	CYFIP-related Rac1 interactor A
P60670	1	6	NPL4	Nuclear protein localization protein 4 homolog
Q8BZN6	1	4	DOC10	Dedicator of cytokinesis protein 10 {ECO:0000305}
Q80US4	1	5	ARP5	Actin-related protein 5
P18468	1	7	HB2I	H-2 class II histocompatibility antigen, I-A beta chain
Q08761	1	4	PROS	Vitamin K-dependent protein S
Q8VI33	1	5	TAF9	Transcription initiation factor TFIID subunit 9
Q99KN9	1	6	EPN4	Clathrin interactor 1
P50295	1	5	ARY2	Arylamine N-acetyltransferase 2
Q6P1B1	1	6	XPP1	Xaa-Pro aminopeptidase 1
Q3TDN2	1	7	FAF2	FAS-associated factor 2
Q61687	1	1	ATRX	Transcriptional regulator ATRX
Q9CT10	1	4	RANB3	Ran-binding protein 3
Q8C854	1	6	MYEF2	Myelin expression factor 2
P40142	1	1	TKT	Transketolase
P21550	1	4	ENOB	Beta-enolase
Q9QZD4	1	5	XPF	DNA repair endonuclease XPF
Q9CQF6	1	7	ADPPT	L-aminoadipate-semialdehyde dehydrogenase-phosphopantetheinyl transferase
Q0VBL3	1	1	RBM15	RNA-binding protein 15 {ECO:0000303|PubMed:17376872}

O70439	1	4	STX7	Syntaxin-7
P49117	1	6	NR2C2	Nuclear receptor subfamily 2 group C member 2
Q99M51	1	7	NCK1	Cytoplasmic protein NCK1
Q61211	1	6	EIF2D	Eukaryotic translation initiation factor 2D
P56135	1	7	ATPK	ATP synthase subunit f, mitochondrial {ECO:0000305}
O88559	1	6	MEN1	Menin
Q9DCJ5	1	7	NDUA8	NADH dehydrogenase [ubiquinone] 1 alpha subcomplex subunit 8
Q01405	1	5	SC23A	Protein transport protein Sec23A {ECO:0000305}
Q922D4	1	6	PP6R3	Serine/threonine-protein phosphatase 6 regulatory subunit 3
P08228	1	7	SODC	Superoxide dismutase [Cu-Zn]
Q8BKZ9	1	5	ODPX	Pyruvate dehydrogenase protein X component, mitochondrial
Q01730	1	7	RSU1	Ras suppressor protein 1
Q69Z38	1	4	PEAK1	Inactive tyrosine-protein kinase PEAK1 {ECO:0000305}
Q91VJ5	1	5	PQBP1	Polyglutamine-binding protein 1
P56477	1	6	IRF5	Interferon regulatory factor 5 {ECO:0000303|PubMed:15665823, ECO:0000303|PubMed:18824541}
P63276	1	4	RS17	40S ribosomal protein S17
Q8K2A7	1	5	INT10	Integrator complex subunit 10
Q80XC2	1	7	TRM61	tRNA (adenine(58)-N(1))-methyltransferase catalytic subunit TRMT61A
Q6ZQF7	1	5	JADE2	E3 ubiquitin-protein ligase Jade-2 {ECO:0000303|PubMed:25018020}
O88874	1	6	CCNK	Cyclin-K
Q3TGF2	1	5	F107B	Protein FAM107B {ECO:0000305}
Q3UHX2	1	7	HAP28	28 kDa heat- and acid-stable phosphoprotein
O35522	1	7	PSB9	Proteasome subunit beta type-9
P62751	1	4	RL23A	60S ribosomal protein L23a
P24527	1	5	LKHA4	Leukotriene A-4 hydrolase
Q9CQI3	1	7	GMFB	Glia maturation factor beta
P47962	1	4	RL5	60S ribosomal protein L5
Q9Z1F9	1	5	SAE2	SUMO-activating enzyme subunit 2
Q3U308	1	6	CTU2	Cytoplasmic tRNA 2-thiolation protein 2 {ECO:0000255|HAMAP-Rule:MF_03054}
Q9QZB7	1	7	ARP10	Actin-related protein 10
Q64433	1	5	CH10	10 kDa heat shock protein, mitochondrial
Q9R1E0	1	6	FOXO1	Forkhead box protein O1
Q8R123	1	7	FAD1	FAD synthase

Q8BIY3	1	4	ZC12D	Probable ribonuclease ZC3H12D
Q9EQK5	1	5	MVP	Major vault protein
Q9CQT1	1	7	MTNA	Methylthioribose-1-phosphate isomerase {ECO:0000255|HAMAP-Rule:MF_03119}
Q9CQR2	1	7	RS21	40S ribosomal protein S21
Q80VD1	1	4	FA98B	Protein FAM98B
Q6P9R2	1	5	OXSR1	Serine/threonine-protein kinase OSR1
Q2NL51	1	6	GSK3A	Glycogen synthase kinase-3 alpha
P46414	1	7	CDN1B	Cyclin-dependent kinase inhibitor 1B
P54822	1	4	PUR8	Adenylosuccinate lyase
Q8BFQ8	1	7	GALD1	Glutamine amidotransferase-like class 1 domain-containing protein 1 {ECO:0000305}
Q6A0A2	1	4	LAR4B	La-related protein 4B
Q58A65	1	5	JIP4	C-Jun-amino-terminal kinase-interacting protein 4
Q8K2K6	1	6	AGFG1	Arf-GAP domain and FG repeat-containing protein 1
Q8R0J7	1	7	VP37B	Vacuolar protein sorting-associated protein 37B
Q8VEE4	1	4	RFA1	Replication protein A 70 kDa DNA-binding subunit
O35613	1	5	DAXX	Death domain-associated protein 6
Q9JHW4	1	6	SELB	Selenocysteine-specific elongation factor
Q8K4Z3	1	7	NNRE	NAD(P)H-hydrate epimerase {ECO:0000255|HAMAP-Rule:MF_03159}
Q9CRA8	1	5	EXOS5	Exosome complex component RRP46
Q8BGB5	1	7	LIMD2	LIM domain-containing protein 2 {ECO:0000305}
P28867	1	4	KPCD	Protein kinase C delta type {ECO:0000305}
Q9R0L7	1	5	AKP8L	A-kinase anchor protein 8-like
P18653	1	6	KS6A1	Ribosomal protein S6 kinase alpha-1
Q9D110	1	7	MTHFS	5-formyltetrahydrofolate cyclo-ligase
Q60930	1	4	VDAC2	Voltage-dependent anion-selective channel protein 2
Q7TSI3	1	5	PP6R1	Serine/threonine-protein phosphatase 6 regulatory subunit 1
Q80TE0	1	7	RPAP1	RNA polymerase II-associated protein 1
P31266	1	5	SUH	Recombining binding protein suppressor of hairless
Q9JHW2	1	7	NIT2	Omega-amidase NIT2 {ECO:0000303|PubMed:19596042}
Q8R0H9	1	6	GGA1	ADP-ribosylation factor-binding protein GGA1
O54962	1	7	BAF	Barrier-to-autointegration factor
Q9JI11	1	4	STK4	Serine/threonine-protein kinase 4
P50544	1	6	ACADV	Very long-chain specific acyl-CoA dehydrogenase, mitochondrial {ECO:0000305|Ref.1}

Q8K1E0	1	7	STX5	Syntaxin-5
P97465	1	6	DOK1	Docking protein 1
O08992	1	4	SDCB1	Syntenin-1
P99029	1	7	PRDX5	Peroxiredoxin-5, mitochondrial
Q922R5	1	6	P4R3B	Serine/threonine-protein phosphatase 4 regulatory subunit 3B {ECO:0000250|UniProtKB:Q5MIZ7}
Q8K268	1	6	ABCF3	ATP-binding cassette sub-family F member 3
Q8K2T1	1	7	NMRL1	NmrA-like family domain-containing protein 1
Q9EPB4	1	7	ASC	Apoptosis-associated speck-like protein containing a CARD
Q9JIG7	1	5	CCD22	Coiled-coil domain-containing protein 22
P70303	1	6	PYRG2	CTP synthase 2
Q9CR00	1	7	PSMD9	26S proteasome non-ATPase regulatory subunit 9
Q91Y97	1	5	ALDOB	Fructose-bisphosphate aldolase B
Q9D0D3	1	6	PAPD1	Poly(A) RNA polymerase, mitochondrial
Q60864	1	4	STIP1	Stress-induced-phosphoprotein 1
Q9DBS5	1	6	KLC4	Kinesin light chain 4
Q9CWS4	1	4	INT11	Integrator complex subunit 11
Q61543	1	6	GSLG1	Golgi apparatus protein 1
P80317	1	4	TCPZ	T-complex protein 1 subunit zeta
Q68FH4	1	5	GALK2	N-acetylgalactosamine kinase
Q99KV1	1	7	DJB11	DnaJ homolog subfamily B member 11
Q9WV54	1	4	ASAH1	Acid ceramidase {ECO:0000305}
Q3B7Z2	1	5	OSBP1	Oxysterol-binding protein 1
Q6P2L6	1	6	NSD3	Histone-lysine N-methyltransferase NSD3
Q8CCX5	1	5	KT222	Keratin-like protein KRT222
Q3TCJ1	1	6	ABRX2	BRISC complex subunit Abraxas 2 {ECO:0000312|MGI:MGI:1926116}
Q9D0D4	1	7	DIM1	Probable dimethyladenosine transferase
Q8BPZ8	1	5	ABRX1	BRCA1-A complex subunit Abraxas 1 {ECO:0000312|MGI:MGI:1917931}
Q9D8T2	1	6	GSDMD	Gasdermin-D {ECO:0000303|PubMed:26611636}
Q9CPT5	1	7	NOP16	Nucleolar protein 16
Q9D773	1	7	RM02	39S ribosomal protein L2, mitochondrial
Q7TPN9	1	5	PRR14	Proline-rich protein 14
B1AZP2	1	7	DLGP4	Disks large-associated protein 4
Q9QX60	1	7	DGUOK	Deoxyguanosine kinase, mitochondrial

P26645	1	4	MARCS	Myristoylated alanine-rich C-kinase substrate
Q8VDJ3	1	5	VIGLN	Vigilin
Q9D2H6	1	6	SP2	Transcription factor Sp2
Q01147	1	7	CREB1	Cyclic AMP-responsive element-binding protein 1
Q9CWX9	1	4	DDX47	Probable ATP-dependent RNA helicase DDX47
Q8K114	1	5	INT9	Integrator complex subunit 9
A2AQP0	1	6	MYH7B	Myosin-7B
Q8BX10	1	7	PGAM5	Serine/threonine-protein phosphatase PGAM5, mitochondrial
P54103	1	4	DNJC2	DnaJ homolog subfamily C member 2
Q6PAM1	1	5	TXLNA	Alpha-taxilin
Q9CYH6	1	7	RRS1	Ribosome biogenesis regulatory protein homolog
Q9ES74	1	5	NEK7	Serine/threonine-protein kinase Nek7
Q62432	1	6	SMAD2	Mothers against decapentaplegic homolog 2
Q80UU9	1	7	PGRC2	Membrane-associated progesterone receptor component 2 {ECO:0000305}
O35841	1	4	API5	Apoptosis inhibitor 5
Q14C51	1	6	PTCD3	Pentatricopeptide repeat domain-containing protein 3, mitochondrial
P52912	1	7	TIA1	Nucleolysin TIA-1
Q91VR2	1	4	ATPG	ATP synthase subunit gamma, mitochondrial {ECO:0000305}
Q8C863	1	6	ITCH	E3 ubiquitin-protein ligase Itchy
Q8CDI6	1	5	CD158	Coiled-coil domain-containing protein 158
Q6P3D0	1	7	NUD16	U8 snoRNA-decapping enzyme
Q8BRT1	1	5	CLAP2	CLIP-associating protein 2
Q6ZQK5	1	6	ACAP2	Arf-GAP with coiled-coil, ANK repeat and PH domain-containing protein 2
Q9JIY5	1	7	HTRA2	Serine protease HTRA2, mitochondrial
Q8K370	1	7	ACD10	Acyl-CoA dehydrogenase family member 10
Q9CPW4	1	5	ARPC5	Actin-related protein 2/3 complex subunit 5
Q8BGA7	1	7	CG026	Uncharacterized protein C7orf26 homolog
Q9QUR6	1	6	PPCE	Prolyl endopeptidase
Q91VW3	1	7	SH3L3	SH3 domain-binding glutamic acid-rich-like protein 3
Q9Z2I9	1	5	SUCB1	Succinate--CoA ligase [ADP-forming] subunit beta, mitochondrial {ECO:0000255|HAMAP-Rule:MF_03220}
P62843	1	7	RS15	40S ribosomal protein S15
P30416	1	5	FKBP4	Peptidyl-prolyl cis-trans isomerase FKBP4
Q99K95	1	7	RTF2	Replication termination factor 2 {ECO:0000305}

P63318	1	5	KPCG	Protein kinase C gamma type
Q61161	1	6	M4K2	Mitogen-activated protein kinase kinase kinase kinase 2
O55126	1	5	NIPS2	Protein NipSnap homolog 2
P70697	1	7	DCUP	Uroporphyrinogen decarboxylase
Q9WTL4	1	5	INSRR	Insulin receptor-related protein
Q9Z2I0	1	6	LETM1	Mitochondrial proton/calcium exchanger protein {ECO:0000305}
Q9CQZ5	1	7	NDUA6	NADH dehydrogenase [ubiquinone] 1 alpha subcomplex subunit 6 {ECO:0000305}
Q9D4J7	1	5	PHF6	PHD finger protein 6
P70677	1	7	CASP3	Caspase-3
P54728	1	6	RD23B	UV excision repair protein RAD23 homolog B
Q9QXL8	1	7	NDK7	Nucleoside diphosphate kinase 7
Q9D0I8	1	5	MRT4	mRNA turnover protein 4 homolog {ECO:0000250|UniProtKB:P33201}
Q8C092	1	6	TAF5	Transcription initiation factor TFIID subunit 5
Q9R0Q7	1	7	TEBP	Prostaglandin E synthase 3
Q5EBH1	1	7	RASF5	Ras association domain-containing protein 5
Q7TSG2	1	5	CTDP1	RNA polymerase II subunit A C-terminal domain phosphatase
Q9CZW5	1	6	TOM70	Mitochondrial import receptor subunit TOM70 {ECO:0000305}
O54788	1	5	DFFB	DNA fragmentation factor subunit beta
Q9D832	1	7	DNJB4	DnaJ homolog subfamily B member 4
A2ADY9	1	5	DDI2	Protein DDI1 homolog 2 {ECO:0000305}
Q78IK4	1	5	MIC27	MICOS complex subunit Mic27
Q7TT50	1	7	MRCKB	Serine/threonine-protein kinase MRCK beta
Q8BG67	1	6	EFR3A	Protein EFR3 homolog A {ECO:0000305}
Q8C3X2	1	7	CC90B	Coiled-coil domain-containing protein 90B, mitochondrial
Q9Z110	1	6	P5CS	Delta-1-pyrroline-5-carboxylate synthase
Q9QYR6	1	7	MAP1A	Microtubule-associated protein 1A
Q9WU01	1	5	KHDR2	KH domain-containing, RNA-binding, signal transduction-associated protein 2
P59325	1	6	IF5	Eukaryotic translation initiation factor 5
Q9CPX6	1	7	ATG3	Ubiquitin-like-conjugating enzyme ATG3
Q8BMI3	1	6	GGA3	ADP-ribosylation factor-binding protein GGA3
Q9D7M1	1	7	GID8	Glucose-induced degradation protein 8 homolog
Q8CCS6	1	6	PABP2	Polyadenylate-binding protein 2
Q9CPP6	1	7	NDUA5	NADH dehydrogenase [ubiquinone] 1 alpha subcomplex subunit 5

P58854	1	6	GCP3	Gamma-tubulin complex component 3
Q640M1	1	6	UT14A	U3 small nucleolar RNA-associated protein 14 homolog A
Q8BGS0	1	7	MAK16	Protein MAK16 homolog
Q9ESZ8	1	6	GTF2I	General transcription factor II-I
Q9QXV1	1	7	CBX8	Chromobox protein homolog 8
Q9D5T0	1	7	ATAD1	Outer mitochondrial transmembrane helix translocase {ECO:0000305}
P26450	1	6	P85A	Phosphatidylinositol 3-kinase regulatory subunit alpha
P63139	1	7	NFYB	Nuclear transcription factor Y subunit beta
Q9JKR6	1	6	HYOU1	Hypoxia up-regulated protein 1
O54984	1	7	GET3	ATPase GET3 {ECO:0000255|HAMAP-Rule:MF_03112}
Q8R3F9	1	6	STPAP	Speckle targeted PIP5K1A-regulated poly(A) polymerase
Q9CWZ7	1	7	SNAG	Gamma-soluble NSF attachment protein
P08043	1	6	ZFP2	Zinc finger protein 2
Q9CQS8	1	7	SC61B	Protein transport protein Sec61 subunit beta
P10078	1	6	ZFP28	Zinc finger protein 28
Q810U5	1	7	CCD50	Coiled-coil domain-containing protein 50
A3KMP2	1	7	TTC38	Tetratricopeptide repeat protein 38
Q8R344	1	7	CCD12	Coiled-coil domain-containing protein 12
Q9JIH2	1	6	NUP50	Nuclear pore complex protein Nup50
Q6PDL0	1	7	DC1L2	Cytoplasmic dynein 1 light intermediate chain 2
Q99K28	1	6	ARFG2	ADP-ribosylation factor GTPase-activating protein 2
Q8CIG9	1	7	FBXL8	F-box/LRR-repeat protein 8
Q80XQ2	1	6	TBCD5	TBC1 domain family member 5
Q6ZQB6	1	6	VIP2	Inositol hexakisphosphate and diphosphoinositol-pentakisphosphate kinase 2
O70252	1	7	HMOX2	Heme oxygenase 2
O35382	1	6	EXOC4	Exocyst complex component 4
Q9QZ08	1	7	NAGK	N-acetyl-D-glucosamine kinase
Q99MN9	1	6	PCCB	Propionyl-CoA carboxylase beta chain, mitochondrial {ECO:0000305|PubMed:11245989}
Q9JJU8	1	7	SH3L1	SH3 domain-binding glutamic acid-rich-like protein
Q8K2X3	1	7	STN1	CST complex subunit STN1 {ECO:0000250|UniProtKB:Q9H668}
Q9CZ91	1	6	SRFB1	Serum response factor-binding protein 1
Q3U0V2	1	7	TRADD	Tumor necrosis factor receptor type 1-associated DEATH domain protein {ECO:0000305}
Q9Z1J3	1	7	NFS1	Cysteine desulfurase, mitochondrial

Q6P5G6	1	6	UBXN7	UBX domain-containing protein 7
Q9D880	1	7	TIM50	Mitochondrial import inner membrane translocase subunit TIM50
Q99MR8	1	6	MCCA	Methylcrotonoyl-CoA carboxylase subunit alpha, mitochondrial
Q9D6T0	1	7	NOSIP	Nitric oxide synthase-interacting protein
Q78JT3	1	7	3HAO	3-hydroxyanthranilate 3,4-dioxygenase {ECO:0000255|HAMAP-Rule:MF_03019}
Q3TCX3	1	6	KHDC4	KH homology domain-containing protein 4 {ECO:0000250|UniProtKB:Q7Z7F0}
Q6ZPR5	1	6	NSMA3	Sphingomyelin phosphodiesterase 4
P83870	1	7	PHF5A	PHD finger-like domain-containing protein 5A
Q9ES00	1	6	UBE4B	Ubiquitin conjugation factor E4 B {ECO:0000305}
Q61733	1	7	RT31	28S ribosomal protein S31, mitochondrial
Q9R0P6	1	7	SC11A	Signal peptidase complex catalytic subunit SEC11A
Q9R088	1	7	KITM	Thymidine kinase 2, mitochondrial
Q9CRD0	1	7	OCAD1	OCIA domain-containing protein 1
P13439	1	6	UMPS	Uridine 5'-monophosphate synthase
Q99MI6	1	7	GIMA3	GTPase IMAP family member 3
Q9JHN8	1	7	STK19	Serine/threonine-protein kinase 19
Q8C2E7	1	6	WASC5	WASH complex subunit 5 {ECO:0000312|MGI:MGI:2146110}
Q8BYL4	1	7	SYYM	Tyrosine--tRNA ligase, mitochondrial
P50136	1	7	ODBA	2-oxoisovalerate dehydrogenase subunit alpha, mitochondrial
Q9ERA6	1	6	TFP11	Tuftelin-interacting protein 11
P70671	1	7	IRF3	Interferon regulatory factor 3
Q8C0T5	1	6	SI1L1	Signal-induced proliferation-associated 1-like protein 1
Q9D0Q7	1	7	RM45	39S ribosomal protein L45, mitochondrial
Q9EQC5	1	6	SCYL1	N-terminal kinase-like protein
Q9CQA1	1	7	TPPC5	Trafficking protein particle complex subunit 5
P63254	1	7	CRIP1	Cysteine-rich protein 1
Q99LS3	1	7	SERB	Phosphoserine phosphatase {ECO:0000250|UniProtKB:P78330}
Q9CPP0	1	7	NPM3	Nucleoplasmin-3
Q99LC8	1	7	EI2BA	Translation initiation factor eIF-2B subunit alpha
P54310	1	6	LIPS	Hormone-sensitive lipase
Q99N94	1	7	RM09	39S ribosomal protein L9, mitochondrial
Q8BIJ6	1	6	SYIM	Isoleucine--tRNA ligase, mitochondrial
Q6DID5	1	6	PWP3A	PWWP domain-containing DNA repair factor 3A {ECO:0000305}

Q3V132	1	6	ADT4	ADP/ATP translocase 4 {ECO:0000305}
O88545	1	7	CSN6	COP9 signalosome complex subunit 6
P27046	1	6	MA2A1	Alpha-mannosidase 2
Q91VA6	1	7	PDIP2	Polymerase delta-interacting protein 2 {ECO:0000250|UniProtKB:Q9Y2S7}
Q8C9H6	1	6	STRP2	Striatin-interacting proteins 2
Q8R4X3	1	6	RBM12	RNA-binding protein 12
Q8R4N0	1	7	CLYBL	Citramalyl-CoA lyase, mitochondrial
Q8BG15	1	6	CTSL2	CTD small phosphatase-like protein 2
P35737	1	7	DMB	Class II histocompatibility antigen, M beta 1 chain
Q923T9	1	6	KCC2G	Calcium/calmodulin-dependent protein kinase type II subunit gamma
Q9CRA9	1	7	FGOP2	FGFR1 oncogene partner 2 homolog
P28271	1	6	ACOC	Cytoplasmic aconitate hydratase
Q9DBS1	1	7	TMM43	Transmembrane protein 43
Q8BVW0	1	6	GANC	Neutral alpha-glucosidase C
P48024	1	7	EIF1	Eukaryotic translation initiation factor 1
P27512	1	7	TNR5	Tumor necrosis factor receptor superfamily member 5
Q9JL35	1	6	HMGN5	High mobility group nucleosome-binding domain-containing protein 5
B1AVZ0	1	7	UPP	Uracil phosphoribosyltransferase homolog
Q80V86	1	6	INT8	Integrator complex subunit 8
Q91ZJ5	1	7	UGPA	UTP--glucose-1-phosphate uridylyltransferase
O54897	1	7	GPR27	Probable G-protein coupled receptor 27
Q8K245	1	6	UVRAG	UV radiation resistance-associated protein
Q8VCH8	1	6	UBXN4	UBX domain-containing protein 4
Q8CD15	1	7	RIOX2	Ribosomal oxygenase 2 {ECO:0000312|MGI:MGI:1914264}
P59708	1	7	SF3B6	Splicing factor 3B subunit 6
P07742	1	6	RIR1	Ribonucleoside-diphosphate reductase large subunit
Q60676	1	6	PPP5	Serine/threonine-protein phosphatase 5
P57746	1	7	VATD	V-type proton ATPase subunit D
Q3UMB9	1	6	WASC4	WASH complex subunit 4 {ECO:0000312|MGI:MGI:2441787}
Q9CPU0	1	7	LGUL	Lactoylglutathione lyase
P06537	1	6	GCR	Glucocorticoid receptor
Q60759	1	7	GCDH	Glutaryl-CoA dehydrogenase, mitochondrial
Q99KK9	1	7	SYHM	Histidine--tRNA ligase, mitochondrial

Q64152	1	7	BTF3	Transcription factor BTF3
Q8CBE3	1	6	WDR37	WD repeat-containing protein 37
Q9CYX7	1	7	RRP15	RRP15-like protein
A2A8Z1	1	6	OSBL9	Oxysterol-binding protein-related protein 9
Q8BMG7	1	6	RBGPR	Rab3 GTPase-activating protein non-catalytic subunit
Q9JM14	1	7	NT5C	5'(3')-deoxyribonucleotidase, cytosolic type
Q9QWY8	1	6	ASAP1	Arf-GAP with SH3 domain, ANK repeat and PH domain-containing protein 1
P12787	1	7	COX5A	Cytochrome c oxidase subunit 5A, mitochondrial
Q8R480	1	6	NUP85	Nuclear pore complex protein Nup85
P56671	1	6	MAZ	Myc-associated zinc finger protein
Q9QZ73	1	7	DCNL1	DCN1-like protein 1 {ECO:0000305}
Q8BGZ4	1	6	CDC23	Cell division cycle protein 23 homolog
Q9ER38	1	7	TOR3A	Torsin-3A
Q80XH1	1	7	KXDL1	KxDL motif-containing protein 1
Q62192	1	6	CD180	CD180 antigen
P22366	1	7	MYD88	Myeloid differentiation primary response protein MyD88
Q8CAY6	1	7	THIC	Acetyl-CoA acetyltransferase, cytosolic
Q99LU0	1	7	CH1B1	Charged multivesicular body protein 1b-1
P81069	1	6	GABP2	GA-binding protein subunit beta-2
Q8VCF0	1	6	MAVS	Mitochondrial antiviral-signaling protein {ECO:0000305}
Q99J47	1	7	DRS7B	Dehydrogenase/reductase SDR family member 7B
Q91V64	1	7	ISOC1	Isochorismatase domain-containing protein 1
Q9ERS5	1	6	PKHA2	Pleckstrin homology domain-containing family A member 2
Q99LR1	1	7	ABD12	Lysophosphatidylserine lipase ABHD12 {ECO:0000305}
P42128	1	6	FOXK1	Forkhead box protein K1 {ECO:0000303|PubMed:12446708}
Q8C7E9	1	6	CSTFT	Cleavage stimulation factor subunit 2 tau variant
Q6R891	1	6	NEB2	Neurabin-2
Q8VD75	1	6	HIP1	Huntingtin-interacting protein 1 {ECO:0000250|UniProtKB:O00291}
Q91WC0	1	6	SETD3	Actin-histidine N-methyltransferase {ECO:0000305}
P97770	1	6	THUM3	THUMP domain-containing protein 3
O88746	1	6	TOM1	Target of Myb protein 1
Q5SWD9	1	6	TSR1	Pre-rRNA-processing protein TSR1 homolog
Q91YU8	1	6	SSF1	Suppressor of SWI4 1 homolog

Q8K3X4	1	6	I2BPL	Probable E3 ubiquitin-protein ligase IRF2BPL {ECO:0000250|UniProtKB:Q9H1B7}
Q99MD9	1	6	NASP	Nuclear autoantigenic sperm protein
P48193	1	6	EPB41	Protein 4.1
Q8BTZ4	1	6	APC5	Anaphase-promoting complex subunit 5
Q9JM13	1	6	RABX5	Rab5 GDP/GTP exchange factor
Q9CRC8	1	6	LRC40	Leucine-rich repeat-containing protein 40
Q921M4	1	6	GOGA2	Golgin subfamily A member 2
P46935	1	6	NEDD4	E3 ubiquitin-protein ligase NEDD4
Q922L6	1	6	NELFD	Negative elongation factor D
Q99M31	1	6	HSP7E	Heat shock 70 kDa protein 14
P54731	1	6	FAF1	FAS-associated factor 1
Q8CHW4	1	6	EI2BE	Translation initiation factor eIF-2B subunit epsilon
Q61183	1	6	PAPOA	Poly(A) polymerase alpha
Q68FF6	1	6	GIT1	ARF GTPase-activating protein GIT1
Q8VBW6	1	6	ULA1	NEDD8-activating enzyme E1 regulatory subunit
P70698	1	6	PYRG1	CTP synthase 1 {ECO:0000305}
Q7SIG6	1	6	ASAP2	Arf-GAP with SH3 domain, ANK repeat and PH domain-containing protein 2
Q91YN5	1	6	UAP1	UDP-N-acetylhexosamine pyrophosphorylase
Q80UJ7	1	6	RB3GP	Rab3 GTPase-activating protein catalytic subunit
Q8K1C0	1	6	ANGE2	Protein angel homolog 2
Q9D787	1	6	PPIL2	RING-type E3 ubiquitin-protein ligase PPIL2 {ECO:0000305}
Q9EPL8	1	6	IPO7	Importin-7
P35980	1	6	RL18	60S ribosomal protein L18
Q64522	1	6	H2A2B	Histone H2A type 2-B
O89079	1	6	COPE	Coatomer subunit epsilon
O70456	1	6	1433S	14-3-3 protein sigma
Q3TBT3	1	6	STING	Stimulator of interferon genes protein {ECO:0000303|PubMed:18724357, ECO:0000303|PubMed:19776740}
Q921I9	1	6	EXOS4	Exosome complex component RRP41
Q9D3D0	1	6	TTPAL	Alpha-tocopherol transfer protein-like
Q9CPW7	1	6	ZMAT2	Zinc finger matrin-type protein 2
Q91VE6	1	6	MK67I	MKI67 FHA domain-interacting nucleolar phosphoprotein
P70404	1	6	IDHG1	Isocitrate dehydrogenase [NAD] subunit gamma 1, mitochondrial
Q8R5C5	1	6	ACTY	Beta-centractin

Q9CQC9	1	6	SAR1B	GTP-binding protein SAR1b
P58321	1	6	UCHL4	Ubiquitin carboxyl-terminal hydrolase isozyme L4
P09671	1	6	SODM	Superoxide dismutase [Mn], mitochondrial
P19437	1	6	CD20	B-lymphocyte antigen CD20
Q9D1C9	1	6	RRP7A	Ribosomal RNA-processing protein 7 homolog A
Q921W4	1	6	QORL1	Quinone oxidoreductase-like protein 1
P70224	1	6	GIMA1	GTPase IMAP family member 1
Q9D8X1	1	6	CUTC	Copper homeostasis protein cutC homolog
Q9D6J6	1	6	NDUV2	NADH dehydrogenase [ubiquinone] flavoprotein 2, mitochondrial
Q99LC3	1	6	NDUAA	NADH dehydrogenase [ubiquinone] 1 alpha subcomplex subunit 10, mitochondrial
Q9D937	1	6	CK098	Uncharacterized protein C11orf98 homolog {ECO:0000250|UniProtKB:E9PRG8}
O08579	1	6	EMD	Emerin
Q8BFV2	1	6	PCID2	PCI domain-containing protein 2
P61202	1	6	CSN2	COP9 signalosome complex subunit 2
P35293	1	6	RAB18	Ras-related protein Rab-18
Q8BYP3	1	6	RHOF	Rho-related GTP-binding protein RhoF
Q80WW9	1	6	DDRGK	DDRGK domain-containing protein 1 {ECO:0000305}
Q9QX11	1	6	CYH1	Cytohesin-1
P47226	1	6	TES	Testin
Q9CX11	1	6	UTP23	rRNA-processing protein UTP23 homolog
Q9CQE1	1	6	NPS3B	Protein NipSnap homolog 3B
Q8BMJ3	1	6	IF1AX	Eukaryotic translation initiation factor 1A, X-chromosomal
Q91XD6	1	6	VPS36	Vacuolar protein-sorting-associated protein 36
Q6IE21	1	6	OTU6A	OTU domain-containing protein 6A
Q9JK38	1	6	GNA1	Glucosamine 6-phosphate N-acetyltransferase
Q9ERD8	1	6	PARVG	Gamma-parvin
Q8R3D1	1	6	TBC13	TBC1 domain family member 13
Q3TWL2	1	6	PP4P1	Type 1 phosphatidylinositol 4,5-bisphosphate 4-phosphatase
Q8BVQ5	1	6	PPME1	Protein phosphatase methylesterase 1
P49443	1	6	PPM1A	Protein phosphatase 1A
Q9EQN3	1	6	T22D4	TSC22 domain family protein 4
Q9CRA5	1	6	GOLP3	Golgi phosphoprotein 3
Q8BTU1	1	6	XOF20	Cilia- and flagella-associated protein 20

Q8VHZ7	1	6	IMP4	U3 small nucleolar ribonucleoprotein protein IMP4
Q99PM3	1	6	TF2AA	Transcription initiation factor IIA subunit 1
Q99N87	1	6	RT05	28S ribosomal protein S5, mitochondrial
Q9WTP6	1	6	KAD2	Adenylate kinase 2, mitochondrial {ECO:0000255|HAMAP-Rule:MF_03168}
Q60766	1	6	IRGM1	Immunity-related GTPase family M protein 1
P23591	1	6	FCL	GDP-L-fucose synthase {ECO:0000305}
Q9CX99	1	6	GRAP	GRB2-related adapter protein {ECO:0000305}
Q9JIK9	1	6	RT34	28S ribosomal protein S34, mitochondrial
Q61176	1	6	ARGI1	Arginase-1
Q8C7Q4	1	6	RBM4	RNA-binding protein 4
P01657	1	6	KV3A5	Ig kappa chain V-III region PC 2413
Q3UM45	1	6	PP1R7	Protein phosphatase 1 regulatory subunit 7
Q8BUM3	1	6	PTN7	Tyrosine-protein phosphatase non-receptor type 7
O54825	1	6	BYST	Bystin
Q9CY21	1	6	BUD23	Probable 18S rRNA (guanine-N(7))-methyltransferase {ECO:0000305}
Q9Z0H7	1	6	BCL10	B-cell lymphoma/leukemia 10
Q01768	1	6	NDKB	Nucleoside diphosphate kinase B
Q9D0G0	1	6	RT30	28S ribosomal protein S30, mitochondrial
O88522	1	6	NEMO	NF-kappa-B essential modulator
Q8K0H5	1	6	TAF10	Transcription initiation factor TFIID subunit 10
Q8BHL8	1	6	PSMF1	Proteasome inhibitor PI31 subunit
Q91XB0	1	6	TREX1	Three-prime repair exonuclease 1 {ECO:0000250|UniProtKB:Q9NSU2}
Q80XN0	1	6	BDH	D-beta-hydroxybutyrate dehydrogenase, mitochondrial {ECO:0000305}
Q99J99	1	6	THTM	3-mercaptopyruvate sulfurtransferase
Q9JKX6	1	6	NUDT5	ADP-sugar pyrophosphatase {ECO:0000250|UniProtKB:Q9UKK9}
C0HKD8	1	6	MFA1A	Microfibrillar-associated protein 1A {ECO:0000312|MGI:MGI:1914782}
P49615	1	6	CDK5	Cyclin-dependent-like kinase 5
Q9DB15	1	6	RM12	39S ribosomal protein L12, mitochondrial
Q9DB34	1	6	CHM2A	Charged multivesicular body protein 2a
Q9Z2X2	1	6	PSD10	26S proteasome non-ATPase regulatory subunit 10
Q9CZ30	1	6	OLA1	Obg-like ATPase 1 {ECO:0000255|HAMAP-Rule:MF_03167}
Q6NZQ6	1	6	ZN740	Zinc finger protein 740
Q9D358	1	6	PPAC	Low molecular weight phosphotyrosine protein phosphatase

Q9QXT1	1	6	DAPP1	Dual adapter for phosphotyrosine and 3-phosphotyrosine and 3-phosphoinositide
Q8C6B9	1	6	AROS	Active regulator of SIRT1
Q9D7H3	1	6	RTCA	RNA 3'-terminal phosphate cyclase
Q91Z49	1	6	UIF	UAP56-interacting factor
O88271	1	6	CFDP1	Craniofacial development protein 1
Q3U5Q7	1	6	CMPK2	UMP-CMP kinase 2, mitochondrial
P60762	1	6	MO4L1	Mortality factor 4-like protein 1
Q8BYK4	1	6	RDH12	Retinol dehydrogenase 12